

NORTHWESTERN UNIVERSITY

**Striato-Nigro-Striatal Circuits for Dopamine Disinhibition**

A DISSERTATION

SUBMITTED TO THE GRADUATE SCHOOL  
IN PARTIAL FULFILLMENT OF THE REQUIREMENTS

for the degree

**DOCTOR OF PHILOSOPHY**

Interdepartmental Neuroscience Program (NUIN)

By

**Priscilla Ambrosi**

EVANSTON, ILLINOIS

June 2023

© Copyright by Priscilla Ambrosi, 2023

All Rights Reserved

## Abstract

The basal ganglia operate largely in *closed* parallel loops, including an associative circuit for goal-directed behavior originating from the dorsomedial striatum (DMS) and a somatosensory circuit important for habit formation originating from the dorsolateral striatum (DLS). An exception to this parallel circuit organization was proposed to explain how information is transferred between striatal subregions, for example from DMS to DLS during habit formation. The “ascending spiral hypothesis” proposes that DMS disinhibits dopamine signaling in DLS through an *open* loop involving substantia nigra pars reticulata (SNr) and compacta (SNc). Specifically, this hypothesis predicts the existence of a tri-synaptic striato-nigro-striatal circuit, DMS→SNr→SNc→DLS. Despite deeply influencing the habit and addiction literature, this hypothesis rests on weak anatomical evidence and lacks functional support. I tested the ascending spiral hypothesis using electrophysiology, optogenetics, and new tools available for circuit interrogation in mice. Using transsynaptic and intersectional genetic tools, I labeled SNr and SNc cells based on their inputs and outputs, respectively. Together, these tools allowed me to investigate both closed- and open-loop striato-nigro-striatal circuits *ex vivo*. I found strong evidence for closed loops (e.g., DLS→SNr→SNc→DLS), which would allow striatal subregions to self-regulate their dopamine signaling. I also found evidence for functional synapses in open loops, including a descending spiral (DLS→SNr→SNc→DMS). However, the synapses in open loops were unable to modulate dopamine neuron firing, questioning their ability to mediate crosstalk between striatal subregions through disinhibition of dopamine neurons. These findings challenge key predictions from the ascending spiral hypothesis and call for alternative mechanisms of habit formation.

## Acknowledgments

The PhD was a long journey, and I am extremely grateful to all who helped along the way.

Thank you to Talia N. Lerner, my advisor, who trusted me when my confidence was at its lowest, and provided a lab environment where I could thrive. Thank you for being a role model of a caring, knowledgeable, and productive PI who also goes on vacations and protects her time with her family!

Thank you to my thesis committee, Mark Bevan, Rajeshwar “Raj” Awatramani, and Dalton James “Jim” Surmeier, for their feedback, advice, and support during all these years. Thank you for welcoming me into the basal ganglia world and for helping me make a significant contribution to the field. And thank you to Indira Raman for her thorough feedback on our manuscript sent to Cell Reports.

I am also deeply indebted to my labmates in the Lerner Lab, who made me feel safe to be myself, and helped me remember my favorite thing about science: learning together. Thank you for being mentors, mentees, supportive peers, cheerleaders, sponsors, and friends. Thank you for teaching me so much and for indulging my love for white boards (RIP mouse board in the break room). Special thanks to Gabriela “Gaby” Lopez for founding the *noms club* with me, and for being a relentless source of joy and support in this very confusing (and often cruel) academic world. Many thanks to Ashley Holloway, for nicknaming patchable dopamine neurons with me (pregnant bois, sweet potato bois, triangle bois...) and for our (very healing, much therapeutic) PAAH chats. Thank you to Ellen “Ellie” Coleman for being an exceptional mentee and collecting some key data

in this dissertation. Thank you to Venus Sherathiya for writing the mIPSC detection code and inspiring me to use convolutions in my own code. Thank you to Gates Palissery, Sean Pawelko, and Loius Van Camp for keeping our mice happy and saving me from getting lost in the Lurie tunnels countless times.

Thank you to Sage Morison, Maite Azcorra and Raj Awatramani for sharing precious mice that made so many of the findings in this dissertation possible.

Thank you to David McLean, Sandeep Kishore, and Evi Menelaou for getting me started in the motor control field and helping me become an expert electrophysiologist.

Thank you to so many wonderful people who helped me through the hardest parts of my PhD, including Raj Awatramani, Anis Contractor, John “Jack” Kessler, Gayle E. Woloschak, Sally McIver, Indira Raman, and Alicia Guemez-Gamboa. Your unwavering support helped me keep going. Special thanks to Toni Gutierrez and Mona Dugo, who helped me make my most important decision during graduate school, and to Wei-Jen Huang, Monika Gutkowska, Sara Walz, and Eleanor Annan, who helped me heal and get to the finish line of the PhD.

Thank you to current and past members of the Science in Society leadership, including Michael Kennedy, Rabiah Mayas, Sarina McBride, Ashley Jennings, Tania Burns, and Emily Mathews. Joining Science Club was one of the most rewarding and growth-inducing decisions I made in graduate school. I am forever indebted to you, to the Pedersen-McCormick Boys & Girls Club, and to the kids.

Thank you to my friends and peers, including Oscar Maurício Arenas, Anant Jain, Namratha Sastry, Asha Lahiri, Ryan Kovalski, Maggie Swerdloff, Kevin Murnan, Cristiane Bahi dos

Santos, and Cintia Kozonoi Vezzani, who made me feel at home so far away from home. Your kindness and generosity have forever changed me.

Thank you to previous teachers and mentors in Brazil, Switzerland and in the US for going out of your way to train and support me. Thank you to Nara Sobczack, my middle school science teacher, who let me borrow her Scientific American magazines and taught me that there is plenty unknown about the world. Thank you to the faculty of my alma mater, UFRGS, especially Denise Maria Zancan, Guido Lenz, Maria Cristina Faccioni Heuser, Fábio Klamt, Vera Lucia da Silva Valente Gaiesky, Jose Claudio Fonseca Moreira, and Carmem Gottfried, who taught me the fundamentals of doing science. Thank you to Claudia Mieko Mizutani and Hillel Chiel, my advisors at CWRU, who helped me publish my first first-author paper and taught me to be skeptically bold. Thank you to Ralf Schneggenburger for welcoming me into the world of electrophysiology at EPFL and to Evan Dean Vickers for letting me use his rig (I now realize what an incredibly generous thing that is) and teaching me how to patch.

Thank you to my family, who instilled in me this daring attitude that makes me look past the obstacles and focus on my goals (“foca no trabalho”). Thank you for pushing me to dream big and to advocate for myself without questioning if I should. Thank you for your patience, love, and support as I dove deep into these uncertain academic waters and almost drowned a few times. Thank you to my dad, for always being eager to help in any way you can. I still remember you teaching me sines and cosines back in middle school to help me prepare for the high school entrance exam. Look how far I’ve come! Obrigada pela minha mãe, pelo seu amor incondicional. Você me ensinou a manter minha cabeça erguida em todos os momentos, mesmo no meio da tempestade. Eu sei que não importa o que aconteça, o jardineiro da rosa está sempre ali, pronto pra

espantar as pragas e para um abraço do tamanho do universo. Thank you to my brother, for teaching me that I am stronger than I think (i.e., I will carry you on my arms for many flights of stairs if you “accidentally” kick a glass door and cut your foot in half). Thank you to my aunt and late grandparents, who never let me forget how proud they were of me.

Thank you to my husband and personal mathematician, Vinícius Ambrosi, for your love, patience, and unconditional support. Thank you for being the best company in this crazy adventure we embarked on together. And thank you to my cats, Felix and Fluff, for filling our daily life with chaos and reminding us that food, play and sleep are *very urgent* necessities.

Finally, thank you to the funding sources that supported this work, including the NIH-NINDS T32 award (T32NS041234) to P.A, the Houk Scholar Award to P.A., the NIH K99/R00 award (R00MH109569) to T.N.L. and the Aligning Science Across Parkinson’s award through the Michael J. Fox Foundation for Parkinson’s Research (ASAP-020529) to T.N.L.

## List of Abbreviations

### Neurotransmitters

DA	Dopamine
GABA	$\gamma$ -AminoButyric Acid

### Anatomy

DMS	DorsoMedial Striatum
DLS	DorsoLateral Striatum
Cd	Caudate
Pu	Putamen
SN	Substantia Nigra
SNc	Substantia Nigra pars compacta
SNr	Substantia Nigra pars reticulata
VMS	VentroMedial Striatum
VTA	Ventral Tegmental Area

### Genes and Proteins

DAT	Dopamine Transporter
TH	Tyrosine Hydroxylase
VGAT	Vesicular GABA Transporter

### Opsins and Fluorophores

ChR2	ChannelRhodopsin 2
EYFP	Enhanced Yellow Fluorescent Protein
NpHR	HaloRhodopsin

**Behavior**

NP	Nosepoke
FR	Fixed Ratio
VI	Variable Interval

**Electrophysiology**

oIPSC	optogenetically-evoked Inhibitory Post-Synaptic Current
mIPSC	miniature Inhibitory Post-Synaptic Current
GBZ	Gabazine
TTX	Tetrodotoxin
4-AP	4-aminopyridine
NBQX	2,3-dioxo-6-nitro-1,2,3,4-tetrahydrobenzo[f]quinoxaline-7-sulfonamide
D-AP5	D-(-)-2-Amino-5-phosphonopentanoic acid

**Neurons**

FSI	Fast Spiking Interneuron
LTSI	Low-Threshold Spiking Interneuron
SPN	Spiny Projection Neuron (aka MSN, Medium Spiny Neuron)

**Other**

AAV	Adeno-Associated Virus
scAAV	self-complementary Adeno-Associated Virus
Con	CreON
Foff	FlpOFF
WT	Wildtype
SD	Standard Deviation
SEM	Standard Error of Mean

*To my inner child – “eles passarão, eu passarinho”*

## Table of Contents

<b>Abstract.....</b>	<b>3</b>
<b>Acknowledgments .....</b>	<b>4</b>
<b>List of Abbreviations .....</b>	<b>8</b>
<b>Table of Contents .....</b>	<b>11</b>
<b>List of Figures.....</b>	<b>13</b>
<b>List of Supplementary Figures .....</b>	<b>15</b>
<b>Chapter 1 – Introduction .....</b>	<b>16</b>
1.1 Why Study Striato-Nigro-Striatal Circuits? .....	16
1.2 Habit Formation as the Transition from Flexible to Inflexible Behavior.....	17
1.3 A Striato-Nigro-Striatal Circuit Called Ascending Spiral was Hypothesized to Drive Habit Formation. ....	21
1.4 Dissertation Aims and Next Chapters .....	23
<b>Chapter 2 – Closed, But Not Open, Striato-Nigro-Striatal Circuits Support Dopamine         Disinhibition .....</b>	<b>26</b>
2.1 DLS- and DMS-Projecting Dopamine Neurons Are Robustly Inhibited by SNr .....	26
2.2 Dissection of Polysynaptic Striato-Nigro-Striatal Circuits Using a Transsynaptic Cre Virus and Intersectional Genetics .....	32
2.3 Characterization of Closed Striato-Nigro-Striatal Loops.....	37
2.4 Open Spiral Striato-Nigro-Striatal Circuits Are Unlikely to Support Robust Dopamine Disinhibition.....	41
2.5 Strong GABAergic SNr Inputs Onto DA Neurons Do Not Predict Inhibition of Tonic Firing.....	46
2.6 Differences Between Closed Loops and Open Spirals Are Not Explained by Differences in Short-Term Plasticity .....	49
2.7 Discussion .....	51
2.8 Methods.....	58

	12
2.9 Additional Data Sent to Reviewers .....	68
<b>Chapter 3 – Dopamine Disinhibition Cannot be Directly Assessed in Midbrain Slices.....</b>	<b>74</b>
3.1 Activation of DMS Terminals in Substantia Nigra Does NOT Disinhibit DLS-projecting Dopamine Neurons.....	74
3.2 Activation of DMS Terminals in Substantia Nigra Inhibits VGAT+ SNr Neurons. ....	75
3.3 Silencing of SNr Neurons Does NOT Disinhibit DLS-projecting Dopamine Neurons.	75
3.4 Blockage of Inhibitory Transmission Does NOT Disinhibit Dopamine Neurons in Midbrain Slices. ....	76
3.5 Discussion .....	81
3.6 Methods.....	82
<b>Chapter 4 – <i>in vivo</i> Assessment of Open and Closed Striato-Nigro-Striatal Circuits .....</b>	<b>83</b>
4.1 Activation of Dopamine Neurons in SNc Leads to Dopamine Release in DLS .....	83
4.2 Inhibition of SNr Neurons Leads to Dopamine Release in DMS and DLS .....	84
4.3 Activation of DMS Terminals in Substantia Nigra is Not Sufficient to Cause Dopamine Release in DLS.....	84
4.4 Discussion .....	87
4.5 Methods.....	89
<b>Chapter 5 – Conclusions and Future Directions.....</b>	<b>90</b>
<b>References .....</b>	<b>96</b>
<b>Short Vita.....</b>	<b>104</b>

## List of Figures

Figure 1. Habit formation paradigm and probes.....	19
Figure 2. A striato-nigro-striatal circuit called Ascending Spiral was hypothesized to drive habit formation.....	24
Figure 3. Anatomical data supporting the Ascending Spiral.....	25
Figure 4. VGAT+ cells in SNr monosynaptically inhibit DLS- and DMS-projecting DA neurons in SNc and suppress their tonic firing.....	30
Figure 5. Viral strategy used for polysynaptic circuit dissection.....	35
Figure 6. DLS-targeted and DMS-targeted GABAergic cells in SNr monosynaptically inhibit DLS-projecting and DMS-projecting DA neurons in SNc, respectively, and suppress their tonic firing.....	39
Figure 7. DMS-targeted and DLS-targeted GABAergic cells in SNr monosynaptically inhibit DLS-projecting and DMS-projecting DA neurons in SNc, respectively, but do not suppress their tonic firing. ....	44
Figure 8. Closed loops are supported by monosynaptic connectivity and suppression of tonic firing, while open spirals are supported by monosynaptic connectivity only. ....	48
Figure 9. Pre-synaptic release probability does not explain differences between closed loops and open spirals. ....	50
Figure 10. oIPSC kinetics are not consistently different between open and closed loops (CsCl recordings). ....	71

Figure 11. oIPSC kinetics are not consistently different between open and closed loops (CsMeSO3 recordings). .....	72
Figure 12. A GABAAR-mediated slow hyperpolarizing current was found in a subset of cells in all circuit configurations. ....	73
Figure 13. Optogenetic activation of DMS terminals in midbrain slices suppresses the tonic firing of VGAT+ cells in SNr, but does not disinhibit DLS-projecting SNc neurons.....	78
Figure 14. Optogenetic silencing of VGAT+ SNr cells in midbrain slices does not disinhibit DLS-projecting SNc neurons.....	79
Figure 15. Pharmacological blockage of inhibitory transmission does not disinhibit dopamine neurons in midbrain slices. ....	80
Figure 16. <i>in vivo</i> fiber photometry controls and test of the ascending spiral hypothesis.....	86
Figure 17. Testing if synapse location explains the differences between closed and open striato-nigro-striatal circuits using sCRACM. ....	94
Figure 18. Testing closed and open striato-nigro-striatal circuits <i>in vivo</i> . ....	95

## List of Supplementary Figures

Supplementary Figure 1. Injection spread in striatum and location of patched cells in midbrain slices for experiments with VGAT-IRES-Cre mice. ....	31
Supplementary Figure 2. Similar results from Figure 5 are obtained using a Con/Foff-ChR2-EYFP virus.....	36
Supplementary Figure 3. Injection spread in striatum and location of patched cells in midbrain slices for closed loop experiments. ....	40
Supplementary Figure 4. Injection spread in striatum and location of patched cells in midbrain slices for open spiral experiments.....	45

## Chapter 1– Introduction

### 1.1 Why Study Striato-Nigro-Striatal Circuits?

The short answer is that a striato-nigro-striatal circuit called *ascending spiral* was implicated in motor learning and habit formation, but unambiguous evidence supporting the existence of this circuit was lacking. As I collected data on the ascending spiral, the need for comparison to other striato-nigro-striatal circuits became increasingly apparent. Conveniently, the original work that proposed the existence of the ascending spiral also had predictions about three other striato-nigro-striatal circuits (Haber et al. 2000). By comparing the functional evidence supporting these four striato-nigro-striatal circuits, I aimed to situate my findings in the larger context of basal ganglia circuits and critically evaluate the role of the ascending spiral as the key driver of habit formation.

Besides satisfying a basic science curiosity, there is vast clinical significance to studying the neural circuits of habit formation. First, the same circuits that underlie the behavioral inflexibility observed during habit formation are thought to underlie the pathophysiology of addiction and obsessive-compulsive disorders (Lipton et al. 2019; Lüscher et al. 2020). Second, the dopamine circuits studied in this dissertation are thought to (or in some cases known to) contribute to the motor and cognitive symptoms of neurodegenerative diseases like Parkinson’s disease and neurodevelopmental disorders like autism spectrum disorder. Thus, a rigorous study of striato-nigro-striatal circuits will not only help answer a fundamental question in neuroscience – what is the mechanism of habit formation? – but also provide a foundation for future translational studies.

In this introduction, I will provide a short, non-exhaustive overview of the habit formation literature, followed by a summary of the evidence behind the ascending spiral hypothesis of habit formation. Finally, I will outline the aims of my dissertation and the contents of the next chapters.

## **1.2 Habit Formation as the Transition from Flexible to Inflexible Behavior.**

The word “habit” can have many meanings (Robbins and Costa 2017), so it is important to clarify its definition. In this dissertation (and much of the habit formation literature), habit is defined as a stimulus-response behavior that is insensitive to contingency degradation and/or outcome devaluation (Dickinson 1985; Lerner 2020). **Figure 1** illustrates the habit formation paradigm used in the Lerner Lab, as well as classic behavioral probes used to assess habitual behavior. In our lab, food restricted mice are placed in an operant chamber and trained to nosepoke for food rewards. Contingency degradation happens when the causal relationship between action and outcome is reduced (e.g. nosepoking no longer triggers a food reward), while outcome devaluation happens when the outcome becomes less valuable (e.g. nosepoking still triggers a reward, but the mouse had free access to this reward a few moments ago and is satiated). In other words, habitual behaviors persist even if they no longer lead to rewarding outcomes.

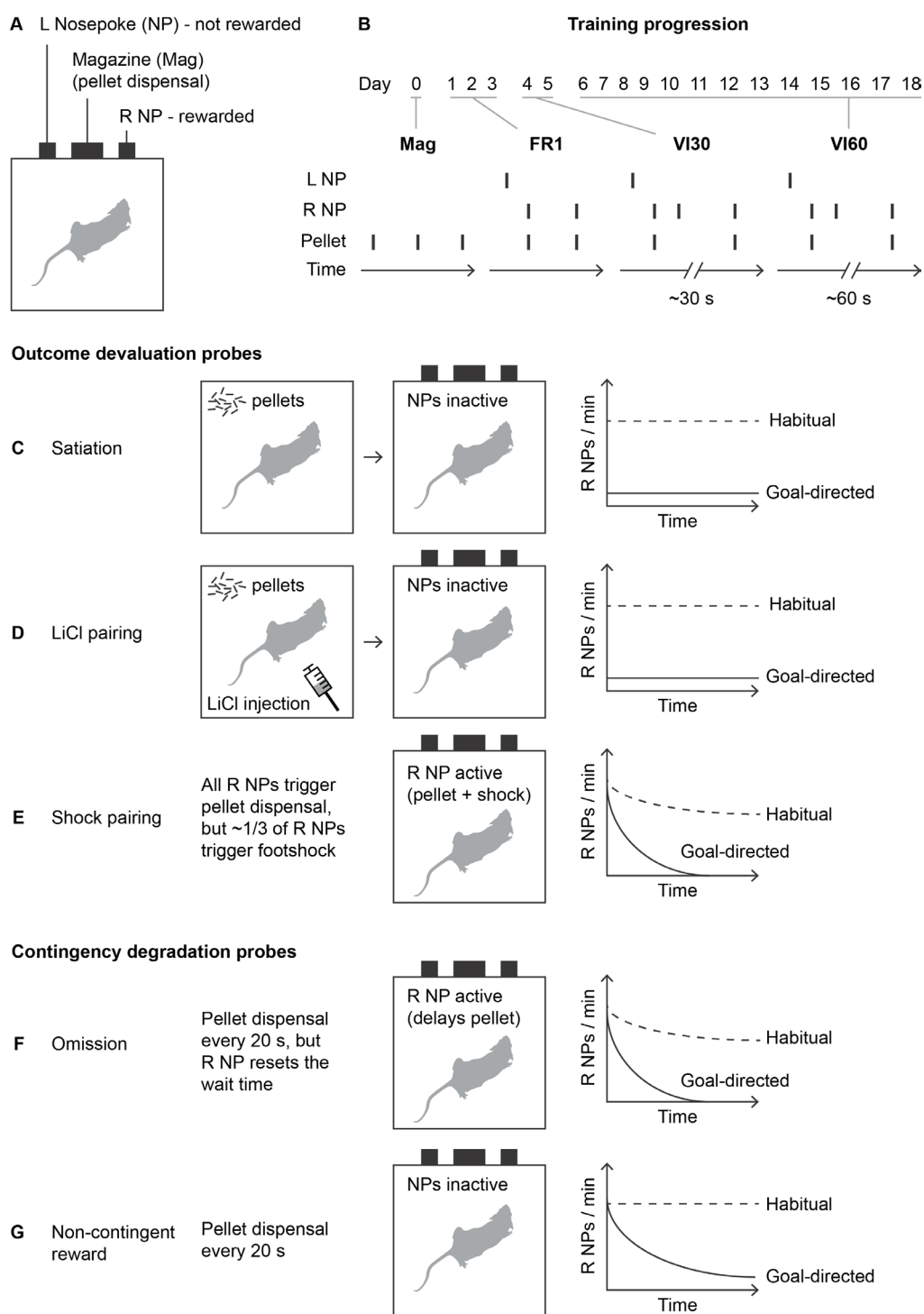
In the Lerner Lab, we use operant conditioning under a Variable Interval (VI) schedule of reinforcement to promote habit formation. In this task, mice have to nosepoke to get a food reward (sucrose pellet), but nosepoking *per se* does not guarantee a reward. After a pellet is dispensed, there is a variable time interval during which nosepoking no longer triggers a reward. In the VI30 task, the average wait time is 30 s (range: 15-45 s), while in the VI60 task the average wait time is 60 s (range: 30-90 s). This uncertainty in the action-outcome contingency leads to an escalation of the rate of nosepoking (Seiler et al. 2022), which is thought to strengthen the stimulus-response

association required for habit formation (Derusso et al. 2010). Before mice go through the VI tasks, they are first trained to (1) retrieve pellets from the magazine, and (2) nosepoke for pellets in a Fixed Ratio 1 (FR1) schedule of reinforcement, in which every nosepoke triggers a reward.

Variable Interval schedules of reinforcement were first developed by Ferster and Skinner (Ferster and Skinner 1957) using pigeons and were shown to promote habit formation in rats in the 80s (Dickinson et al. 1983; Dickinson 1985). A key discovery from experimental psychologists was that over-training is *necessary* but not *sufficient* to promote habits: over-training in Variable Interval tasks, but not in Fixed Ratio or Fixed Interval tasks, leads to outcome devaluation-resistant behavior (Dickinson 1985; Derusso et al. 2010). There is vast speculation in the literature as to why that is the case (**Box 1**), but the exact mechanisms underlying habit formation remain unknown.

A prominent hypothesis in the field suggests that animal behavior starts out goal-directed (*i.e.* sensitive to outcome devaluation and to changes in action-outcome contingencies), but neural plasticity in basal ganglia circuits promotes the emergence of habitual behaviors (Yin and Knowlton 2006). This hypothesis assumes that two parallel brain circuits are in constant competition for control: one promoting behaviors based on continually updated action-outcome contingencies (goal-directed) and the other promoting behaviors based on previously learned stimulus-response associations (habitual). A key prediction of this hypothesis is that these two parallel circuits are connected via a striato-nigro-striatal circuit called the “ascending spiral”. The main goal of my PhD work was to test this prediction.

**Figure 1. Habit formation paradigm and probes.**



(A) Illustration of the operant chamber. (B) Training progression used in the Lerner Lab to promote habit formation. (C-G) Behavioral probes used to assess habit formation after training. Plots on the right represent the expected behavior for habitual and goal-directed mice. L: left. R: right.

**Box 1. What Controls Animal Behavior?**

Skinner's work inspired a long-standing debate about the definition and origin of behavior. Are all behaviors *responses* to a stimulus (reflex-like) or motivated *actions* (goal-directed)? One way that neuroscientists have approached this question is to experimentally test whether animals have an internal model of the behavioral tasks they are trained in (Drummond and Niv 2020). Do animals understand the rules governing their action-outcome contingencies? If they do, their behavior is labeled *model-based action*; if not, their behavior is labeled *model-free response*.

One caveat of the model-free vs model-based approach is that understanding the rules is not sufficient to demonstrate such understanding. This problem reminds me of classic cerebellum experiments attempting to identify circuits required for learning vs expression of a behavior (Thompson 2005). When you rely on a behavioral output to assess learning (or understanding), it can be challenging to interpret the loss of the expected behavior after an intervention. This caveat is also highlighted in human behavior. For instance, individuals with substance use disorder or obsessive-compulsive disorder have difficulties disengaging from self-destructive behaviors despite understanding their negative consequences. On the other hand, complex behavior can emerge from simple mechanisms that do not necessarily encode "meaning" or action-outcome contingencies (Oyama 1985; Braitenberg 1986).

The ontogeny of behaviors is a key open question in neuroscience. Are the circuits controlling flexible and inflexible behavior truly parallel or are they hierarchically organized? How do these circuits interact with internal states? Answering these questions is far beyond the scope of this dissertation, but this is a topic of great interest to me.

### **1.3 A Striato-Nigro-Striatal Circuit Called Ascending Spiral was Hypothesized to Drive Habit Formation.**

The striatum is well-known for its roles in motor control and reinforcement learning. The dorsomedial striatum (DMS) is thought to be involved in goal-directed learning, while the dorsolateral striatum (DLS) is thought to be involved in motor skill acquisition and habit formation (Yin and Knowlton 2006; Lipton et al. 2019). As animals are overtrained in a motor skill task (e.g., accelerating rotarod) or in an instrumental task designed to elicit habit (e.g., variable interval training), their behavior becomes more stereotyped and less flexible, and dependence of the behavior shifts from DMS to DLS (Yin et al. 2004; Yin et al. 2005a; Yin et al. 2005b; Yin et al. 2006; Yin et al. 2009; Derusso et al. 2010; Thorn et al. 2010; Corbit et al. 2012; Gremel and Costa 2013; Sommer et al. 2014).

Both DMS and DLS are richly innervated by dopamine (DA) neurons from the substantia nigra pars compacta (SNc). Although DA axonal fields in striatum are broad (Matsuda et al. 2009), there is topography within the nigrostriatal system that can allow for separate control of DA release in DMS and DLS (Joel and Weiner 2000; Ikemoto 2007; Lerner et al. 2015; Farassat et al. 2019). Indeed, DA neurons projecting to DMS and those projecting to DLS display distinct *in vivo* activity patterns (Brown et al. 2011; Lerner et al. 2015; Tsutsui-Kimura et al. 2020; Hamid et al. 2021; Seiler et al. 2022).

How distinct activity in DMS-projecting and DLS-projecting DA neurons arises is a key question. One possibility is that these cells receive distinct inputs (Lerner et al. 2015). In particular, it has been widely hypothesized that DMS-DLS transitions observed during habit formation are regulated by an input circuit to DLS-projecting DA neurons termed the “ascending spiral” (Haber

et al. 2000; Yin and Knowlton 2006; Lerner 2020; Lüscher et al. 2020). The premise of the ascending spiral hypothesis is that DMS and DLS are connected by a tri-synaptic circuit involving GABAergic neurons in substantia nigra pars reticulata (SNr) and DA neurons in SNc (**Figure 2**). More specifically, DA neurons are thought to be under tonic inhibition from GABAergic neurons in SNr; spiny projection neurons (SPNs) from DMS can inhibit these SNr GABA cells, and thus disinhibit DLS-projecting DA neurons, allowing for DA release in DLS. The individual steps in this polysynaptic circuit (DMS→SNr, SNr→SNc, and SNc→DLS) are well-established (Chevalier et al. 1985; Tepper et al. 1995; Tepper and Lee 2007; Freeze et al. 2013). However, it is not necessarily the case that the individual connections link into a continuous polysynaptic circuit (DMS→SNr→SNc→DLS). Indeed, anatomical and electrophysiological work in other basal ganglia circuits supports a largely parallel organization of DMS and DLS subcircuits (Alexander et al. 1986; Mandelbaum et al. 2019; Lee et al. 2020). The idea that an ascending spiral through the midbrain DA system could be a major route of crosstalk between otherwise parallel circuits has been appealing to behavioral neuroscientists, but evidence of a functional circuit at the synaptic level is lacking.

Evidence for the ascending spiral circuit stems primarily from anatomical work done in non-human primates (Haber et al. 2000). Following the injection of retrograde and anterograde tracers in striatum, Haber and colleagues uncovered a medio-lateral organization of striato-nigro-striatal circuits. Namely, axon terminals from medial striatum are medially located in SN and overlap with the cell bodies of neurons that project to medial and lateral striatum (**Figure 3**). Axons from lateral striatum, on the other hand, are laterally located in SN and overlap with cells that project to lateral, but not medial striatum. Thus, there is a proposed asymmetry in which medial striatum could

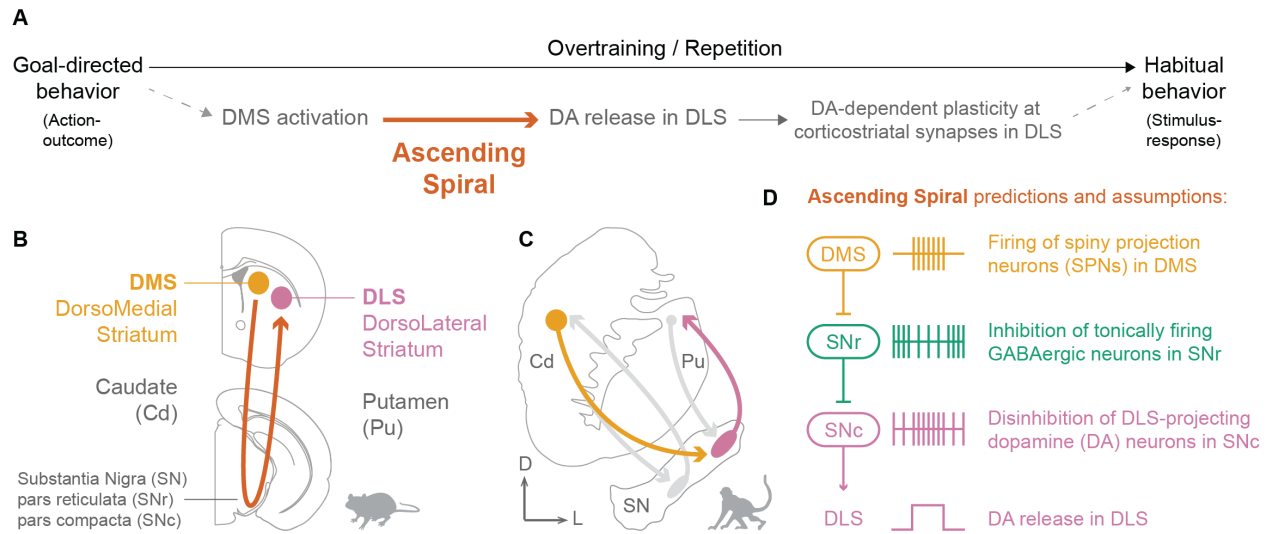
influence DA release in lateral striatum, but lateral striatum would not influence DA release in medial striatum. Critically, however, the overlap of axon terminals and cell bodies is neither necessary nor sufficient for the existence of a functional circuit, especially a polysynaptic circuit involving an intermediary GABAergic connection as proposed. Therefore, despite its continuing appeal, the ascending spiral hypothesis rests on weak evidence.

A direct test of the tri-synaptic circuit proposed by the ascending spiral hypothesis has been lacking in part because of technological limitations that prevented selective targeting of projection-specific circuit components. We took advantage of recent developments in transsynaptic tracing (Zingg et al. 2017; Zingg et al. 2020) and intersectional genetics (Fenno et al. 2014; Poulin et al. 2018) to solve this problem. Our findings have important implications for *in vivo* DA circuit function and should prompt a reevaluation of the ascending spiral hypothesis.

#### **1.4 Dissertation Aims and Next Chapters**

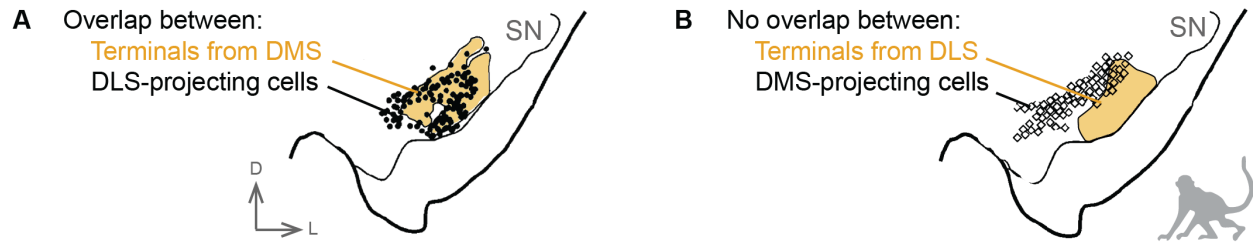
The main goal of this dissertation was to answer the following question: is there a polysynaptic circuit of disinhibition from DMS to DLS-projecting dopamine neurons in naïve mice? Chapter 2 describes the answer to this question and places our findings in the larger context of basal ganglia circuits. Chapter 3 describes unpublished *ex vivo* findings that helped us refine our main experimental approach. Chapter 4 describes unpublished *in vivo* findings regarding the following question: does DMS activation lead to dopamine release in DLS? Chapter 5 summarizes our findings and describes outstanding questions, on-going experiments, and future directions.

**Figure 2. A striato-nigro-striatal circuit called Ascending Spiral was hypothesized to drive habit formation.**



**(A)** Hypothesized mechanism underlying the transition from goal-directed to habitual behavior. **(B)** Cartoon showing the mouse striatum and substantia nigra. **(C)** Cartoon showing the primate striatum and substantia nigra. **(D)** Ascending spiral predictions and assumptions. D: dorsal. L: lateral.

**Figure 3. Anatomical data supporting the Ascending Spiral.**



(**A**) Anatomical data supporting the ascending spiral. (**B**) Anatomical data against the descending spiral. Modified from (Haber et al. 2000). DMS and DLS were used instead of caudate and putamen for the sake of clarity. D: dorsal. L: lateral.

## Chapter 2 – Closed, But Not Open, Striato-Nigro-Striatal Circuits

### Support Dopamine Disinhibition

This chapter is a partial reproduction of my published first-author paper titled “Striatonigrostriatal Circuit Architecture for Disinhibition of Dopamine Signaling” (Ambrosi and Lerner 2022). Some unpublished data was also included in the last section of this chapter.

#### 2.1 DLS- and DMS-Projecting Dopamine Neurons Are Robustly Inhibited by SNr

To test whether there is a synaptic basis for the ascending spiral hypothesis, and to understand the organization of disinhibitory striato-nigro-striatal circuits more generally, we designed a series of experiments using synaptic physiology in combination with carefully targeted optogenetic stimulation. We began by assessing the connectivity of GABAergic SNr cells to DLS- and DMS-projecting DA neurons. Although SNr is a well-known source of inhibitory input onto SNc DA neurons in general (Tepper et al. 1995; Tepper and Lee 2007), it was unclear whether the likelihood of receiving GABAergic inputs varied depending on the downstream projection target of the DA neuron.

We labeled projection-defined DA neurons by injecting red retrobeads into DLS or DMS (**Figure 4**). These fluorescently labeled latex beads travel retrogradely from axon terminals to cell bodies and allow for targeted patching of DLS- or DMS-projecting DA neurons in midbrain slices. We are confident that bead-labeled cells are dopaminergic given that (1) bead-labeled cells in SNc were previously shown to be TH<sup>+</sup> (Lerner et al. 2015) and (2) all bead-labeled cells recorded in a

loose seal configuration in this study (143/143 cells from 24 mice) had wide action potential waveforms (total duration > 2 ms) characteristic of DA neurons (Grace and Bunney 1983).

To allow for optogenetic stimulation of GABAergic neurons in SNr, we injected an adeno-associated virus (AAV) carrying a Cre-dependent channelrhodopsin-2 (ChR2) construct into the SNr of VGAT-IRES-Cre mice. The specific virus used (AAV5-hSyn-Con/Foff-ChR2-EYFP) also contains a feature by which ChR2 expression is turned off by Flp recombinase. In these initial experiments (Figure 4), the Flp-dependent feature is irrelevant. However, it was crucial for later experiments and so we decided to use the same virus throughout this study.

We began by examining SNr inputs to DLS-projecting DA neurons (**Figure 4A-B**). We verified that all retrobead injections were contained within the DLS (**Supplementary Figure 1A-B**). As expected from previous findings (Haber et al. 2000; Ikemoto 2007; Lerner et al. 2015; Farassat et al. 2019), the resulting bead-labeled DLS-projecting DA cells were located in mid to lateral SNc (**Figure 4D, Supplementary Figure 1C-D**). We first evaluated the proportion of DLS-projecting DA neurons that were monosynaptically inhibited by GABAergic SNr cells. Our goal was to maximize the detection of inhibitory post-synaptic currents (IPSCs) and minimize false negative results. Therefore, we recorded from bead-labeled cells in whole-cell mode using a high chloride internal solution ( $E_{Cl} = 0$  mV) and held the cells at -70 mV. In addition, we used a pharmacological approach to isolate monosynaptic connections (Petreanu et al. 2009) – we added tetrodotoxin (TTX, 1 $\mu$ M) to the bath to block action potentials, and 4-aminopyridine (4-AP, 100 $\mu$ M) to boost the neurotransmitter release probability from ChR2-expressing terminals. To isolate inhibitory synapses, we added NBQX (5 $\mu$ M) and D-AP5 (50 $\mu$ M) to the bath to block AMPA and NMDA receptor currents, respectively. A 5 ms light pulse (475 nm, ~10 mW/mm<sup>2</sup>) was delivered to the

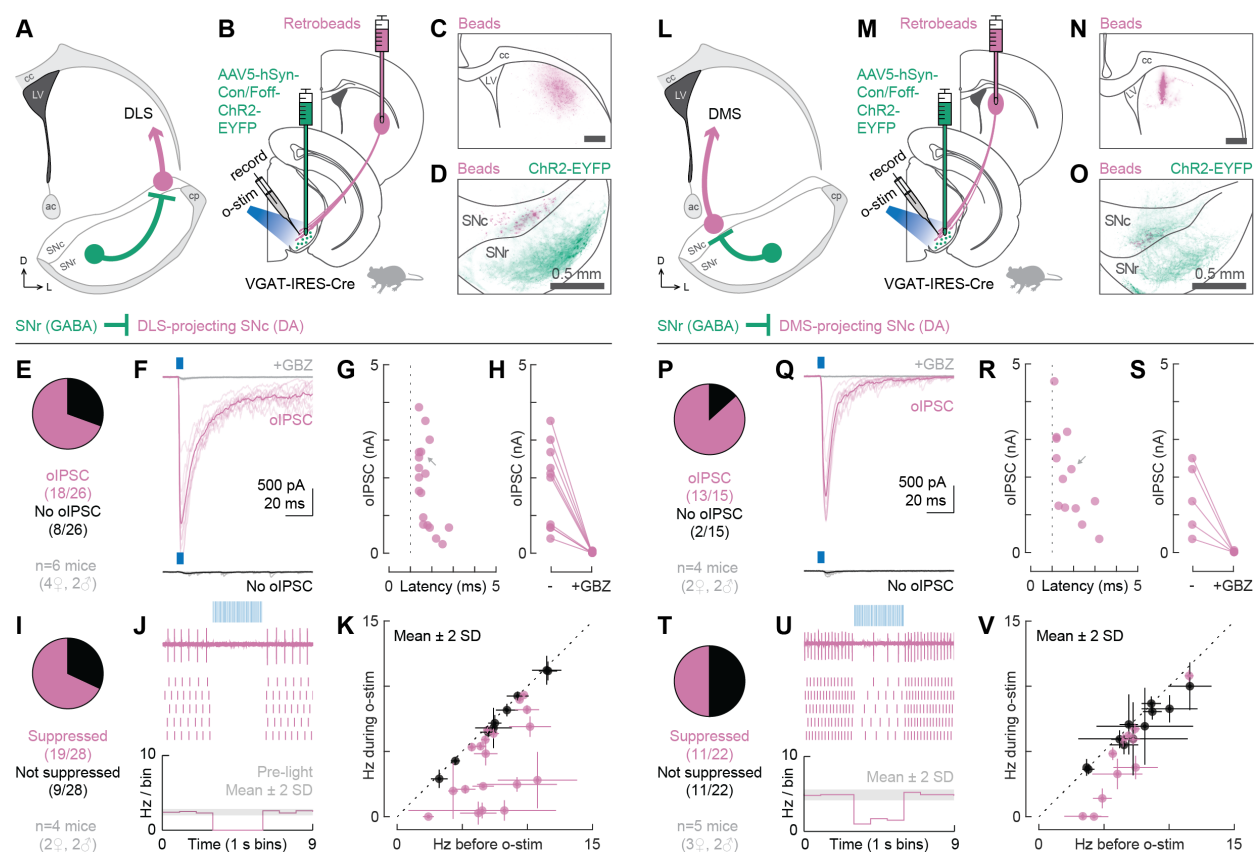
slice to stimulate ChR2-expressing terminals. Under this configuration, we found that 69% (18/26) of the recorded DLS-projecting neurons were monosynaptically inhibited by GABAergic SNr cells (**Figure 4E-F**). The amplitude of the optogenetically-evoked IPSCs (oIPSCs) ranged from 0.2 to 3.9 nA (mean $\pm$ SD: 1.8 $\pm$ 1.1 nA) and the onset latencies were within 5 ms (range: 1.4-2.8 ms; mean $\pm$ SD: 1.7 $\pm$ 0.4 ms), consistent with the isolation of monosynaptic connections (**Figure 4G**). For all tested cells, the oIPSC was blocked by the GABA<sub>A</sub> receptor antagonist gabazine (GBZ, 10 $\mu$ M; **Figure 4H**).

These experiments established a robust synaptic connectivity between SNr and DLS-projecting SNc DA neurons, but the measurements were performed under non-physiological conditions (large chloride driving force and high neurotransmitter release probability). Therefore, we additionally wanted to assess whether the observed GABAergic inputs could suppress the tonic firing of DA cells under more physiological conditions. To avoid manipulating intracellular chloride, we recorded from bead-labeled cells in a loose seal configuration. NBQX and D-AP5 were again added to bath, but not TTX and 4-AP. For these experiments, we used a 3 s-long light train consisting of 5 ms pulses delivered at 20 Hz (475 nm,  $\sim$ 10 mW/mm<sup>2</sup>). A cell was considered inhibited if the light train reduced its firing rate by more than 2 standard deviations (SD) from the mean (**Figure 4J-K**). Suppression of tonic firing was observed in 68% (19/28) of the recorded DLS-projecting cells (**Figure 4I**). The percentage of cells whose firing was inhibited by SNr inputs closely matched the percentage in which oIPSCs were observed, arguing that the GABAergic connections detected onto DLS-projecting DA neurons are effective at controlling their firing rates.

We next examined SNr inputs to DMS-projecting DA neurons (**Figure 4L-M**). We verified that all retrobead injections were contained within the DMS (**Figure 4N, Supplementary Figure 1E-F**) and that, as expected (Lerner et al. 2015), bead-labeled DMS-projecting DA cells were medially located in SNc (**Figure 4O, Supplementary Figure 1G-H**). Under recording conditions used to isolate monosynaptic inhibitory connections, we found that 87% (13/15) of the recorded DMS-projecting neurons were monosynaptically inhibited by GABAergic SNr cells (**Figure 4P-Q**). The oIPSC amplitude ranged from 0.4 to 4.5 nA (mean±SD: 2.0±1.2 nA) and the onset latencies were within 5 ms (range: 1.1-3.2 ms; mean±SD: 1.8±0.7 ms; **Figure 4R**). For all tested cells, the oIPSC was blocked by GBZ (**Figure 4S**). Under a loose seal configuration, suppression of tonic firing was observed in 50% (11/22) of the recorded DMS-projecting cells (**Figure 4T-V**). In contrast to our findings for DLS-projecting DA neurons, we found a higher percentage of DMS-projecting cells receiving monosynaptic inputs from SNr (87% vs 69%), but a lower percentage of DMS-projecting cells whose tonic firing was inhibited by SNr (50% vs 68%).

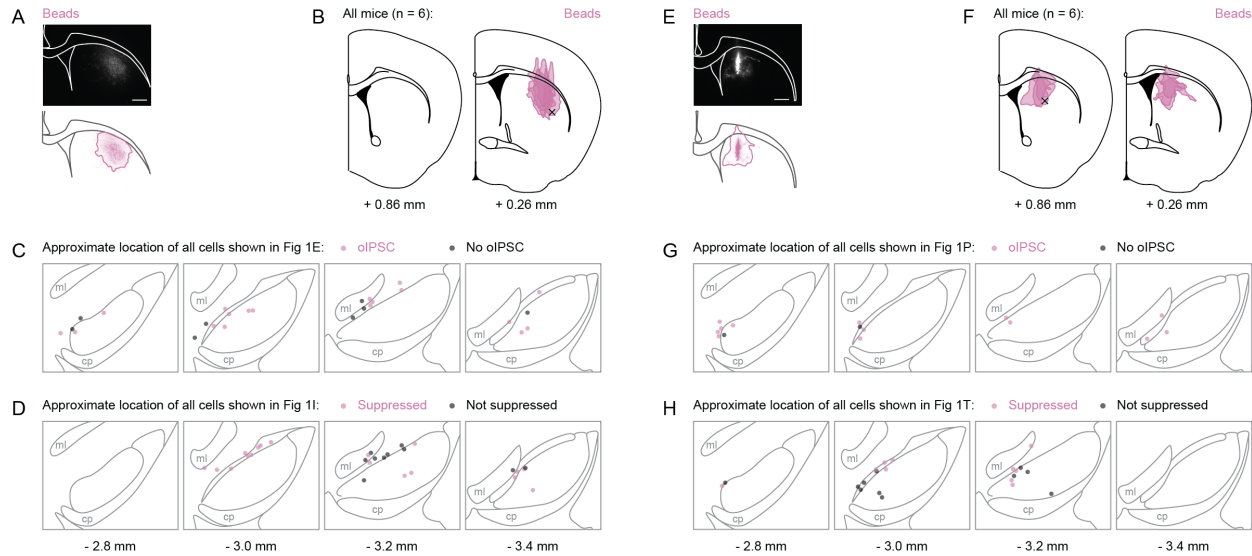
Collectively, these findings suggest that both DLS- and DMS-projecting DA neurons in SNc receive robust inhibition from GABAergic SNr cells. Although we did not assess disinhibition directly, such robust inhibition indicates that a decrease in the tonic firing rate of GABAergic SNr cells would be sufficient to disinhibit DLS- and DMS-projecting DA cells. Moreover, our results hint at a dissociation between optogenetically-defined synaptic connectivity and effective suppression of tonic firing. Asymmetries in the proportion of connected versus effectively inhibited cells may indicate fundamental differences between sub-circuits involving DLS- and DMS-projecting DA neurons.

**Figure 4. VGAT+ cells in SNr monosynaptically inhibit DLS- and DMS-projecting DA neurons in SNc and suppress their tonic firing.**



(A) Schematic of the tested circuit. Anatomical landmarks: corpus callosum (cc), lateral ventricle (LV), anterior commissure (ac), cerebral peduncle (cp). (B) Experimental design for probing the connection between VGAT+ cells in SNr and DLS-projecting DA neurons in SNc. In VGAT-IRES-Cre mice, AAV5-hSyn-Con/Foff-ChR2-EYFP was injected into SNr to deliver the excitatory opsin ChR2 to VGAT+ cells. Retrobeads were injected into DLS to label DLS-projecting DA neurons in SNc for recording. Optogenetic stimulation (o-stim) was delivered via the objective (475 nm, ~10 mW/mm<sup>2</sup>). (C) Distribution of retrobeads (magenta) in a representative striatum slice. Scale bar: 0.5mm. (D) Distribution of bead-labeled somas (magenta) and ChR2-EYFP-labeled neuropil (green) in a representative midbrain slice. SNc was outlined based on TH immunolabeling. (E) Proportion of DLS-projecting neurons that did (magenta) or did not (black) respond to o-stim with an optogenetically-evoked inhibitory postsynaptic current (oIPSC). (F) Example cells for E. The oIPSC was absent after gabazine (GBZ) perfusion (gray). Thin lines: individual sweeps. Thick lines: average across sweeps. (G) oIPSC amplitude and onset latency for all responding cells (dotted line = 1ms). Gray arrow: oIPSC shown in F. (H) oIPSC amplitude before and after GBZ perfusion for all tested cells. (I) Proportion of DLS-projecting neurons that did (magenta) or did not (black) have their tonic firing suppressed by o-stim. (J) Example recordings for I. Top: data from a single sweep. Middle: raster plot showing action potentials from 5 sweeps. Bottom: histogram of the average firing rate across all sweeps. The gray shaded area indicates mean±2SD of the baseline firing rate. (K) Average firing rate during vs before o-stim for all cells from I (suppressed cells: magenta; not suppressed: black). Error bars represent ±2SD. Dotted line: unity. (L-V) Same as A-K but for testing the connection between VGAT+ cells in SNr and DMS-projecting DA neurons in SNc. See also Supplementary Figure 1.

### Supplementary Figure 1. Injection spread in striatum and location of patched cells in midbrain slices for experiments with VGAT-IRES-Cre mice.



**(A)** Example striatum slice. Scale bar: 0.5 mm. **(B)** Approximate spread of retrobeads in the striatum of all mice used for Figure 1 A-K. A black x marks the approximate target location for DLS injections. The numbers below the atlas images indicate their AP position relative to bregma. **(C)** Approximate location of all DLS-projecting cells recorded in whole-cell mode used for Figure 1 E-H. Each dot is a cell, color-coded in magenta (oIPSC) or black (no oIPSC). **(D)** Approximate location of all DLS-projecting cells recorded in loose seal mode used for Figure 1 I-K. Each dot is a cell, color-coded in magenta (inhibited) or black (not inhibited). The numbers below the atlas images indicate their AP position relative to bregma. **(E-H)** Same as A-D but relative to experiments shown in Figure 1 L-V with DMS-projecting cells instead of DLS-projecting.

## 2.2 Dissection of Polysynaptic Striato-Nigro-Striatal Circuits Using a Transsynaptic Cre Virus and Intersectional Genetics

The previous experiments assessed two nigrostriatal circuits: SNr→SNc→DLS and SNr→SNc→DMS (**Figure 4**). We next wanted to layer on to our assessment of these circuits the contributions of striatal inputs to SNr, which would allow either for striatal neurons to control disinhibition of their own dopaminergic input (through closed loops such as DLS→SNr→SNc→DLS) or for one striatal region to regulate dopaminergic transmission in a neighboring region (e.g., DMS→SNr→SNc→DLS) as proposed in the ascending spiral hypothesis (Haber et al. 2000; Yin and Knowlton 2006). While hypotheses about DA neuron disinhibition through striato-nigro-striatal circuits are often incorporated into theory (e.g., Lüscher et al., 2020), the difficulty of tracing synaptic connectivity through a polysynaptic circuit has impeded their testability. Therefore, hypotheses about the structure and function of these circuits have remained highly speculative. We realized that new anterograde tracing (Zingg et al. 2017; Zingg et al. 2020) and combinatorial targeting tools (Fenno et al. 2014) would – for the first time – allow highly-specific tests of the structure and function of striato-nigro-striatal circuits.

To label SNr cells by their striatal inputs, we used scAAV1-hSyn-Cre as a transsynaptic anterograde Cre vector (Zingg et al. 2020). When injected into DLS or DMS, this virus will transduce SPNs at the injection site and the post-synaptic targets of these SPNs throughout the brain. Thus, cells that receive a monosynaptic input from DLS or DMS will also carry Cre. We refer to these anterogradely-labeled cells as “DLS-targeted” and “DMS-targeted,” respectively. Before continuing our electrophysiology experiments, we examined the resulting histology in striatum and substantia nigra (SN) after injection of scAAV1-hSyn-Cre into striatum (**Figure 5**).

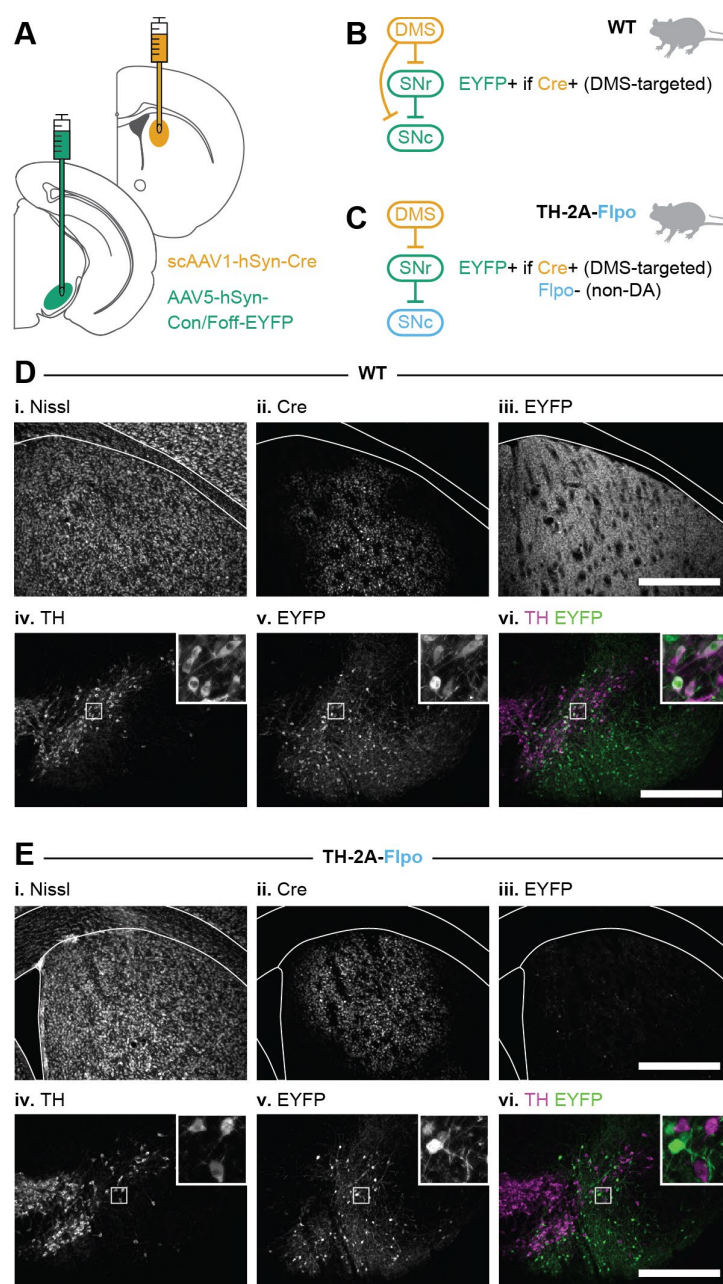
First, we injected wildtype (WT) mice (**Figure 5B**). We verified that scAAV1-hSyn-Cre did not lesion the striatum, as evidenced by healthy Nissl staining (**Figure 5D-i**), and observed that Cre expression was restricted to the targeted region (**Figure 5D-ii**). Next, we looked for Cre expression in SNr. To do so, we injected a Cre-dependent EYFP construct (AAV5-hSyn-Con/Foff-EYFP) into SNr. EYFP<sup>+</sup> cells were observed in SNr (**Figure 5D-v**), but EYFP<sup>+</sup> fibers were also observed in the striatum (**Figure 5D-iii**). GABAergic SNr cells receive monosynaptic inputs from striatum but do not project directly to striatum, whereas dopaminergic SNc neurons do both (Matsuda et al. 2009; Watabe-Uchida et al. 2012; Lerner et al. 2015; Zingg et al. 2020; Evans et al. 2020). Thus, EYFP<sup>+</sup> fibers observed within the striatum indicate that DA neurons received Cre. Indeed, after immunostaining for the DA marker tyrosine hydroxylase (TH), we confirmed that EYFP-labeled cells in SN included both TH<sup>-</sup> and TH<sup>+</sup> cells (**Figure 5D-vi**). It is also possible that some DA neurons received Cre through unintended retrograde movement of the transsynaptic Cre virus (Hollis et al. 2008; Zingg et al. 2017; Zingg et al. 2020). However, any retrograde movement of the virus does not affect the labeling of SNr neurons, since these cells do not project to striatum (McElvain et al. 2021)

While not surprising, the finding that SNc DA neurons were labeled with Cre by injection of scAAV1-hSyn-Cre in the striatum presented a problem for our experimental design, which required that we limit ChR2 expression to GABAergic SNr neurons. Therefore, we used an intersectional Cre/Flp recombinase expression strategy to exclude expression of EYFP/ChR2 from DA neurons. Namely, we injected scAAV1-hSyn-Cre into the DMS of TH-2A-Flpo mice, which express Flp recombinase in DA neurons (Poulin et al. 2018). We then injected the same EYFP virus as above (AAV5-hSyn-Con/Foff-EYFP) into SNr. The Con/Foff construct allows expression

of EYFP in cells that express Cre, but not Flp. Therefore, we could positively label non-DA SNr neurons identified as receiving input from a particular striatal subregion (**Figure 5C**). Using this strategy, we did not find evidence of overlapping EYFP and TH expression in SN (**Figure 5E-vi**). In addition, we did not observe EYFP+ fibers in the striatum (**Figure 5E-iii**). The success of this strategy is more easily visualized with an EYFP virus, which labels the cytoplasm of neurons, but this strategy was equally successful when we used a ChR2 virus (AAV5-hSyn-Con/Foff-ChR2-EYFP, **Supplementary Figure 2**).

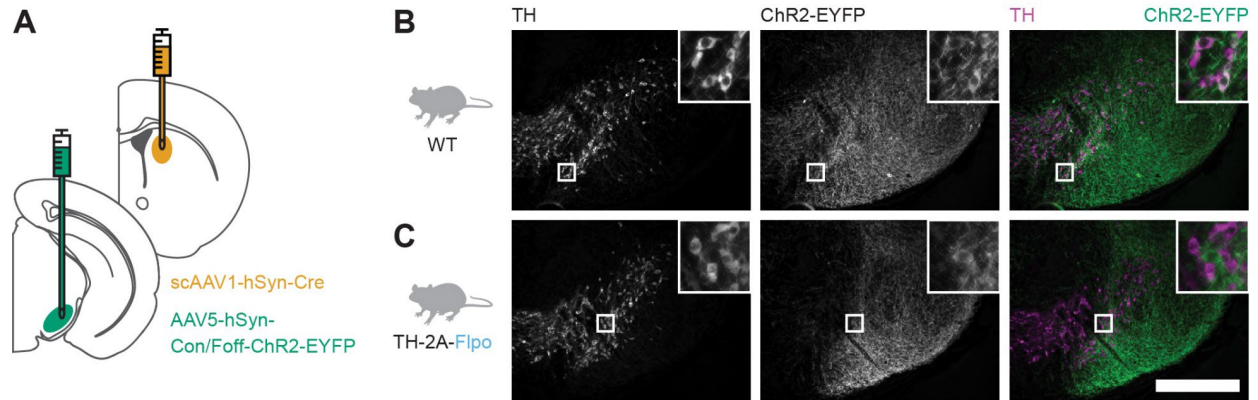
In sum, we can deliver ChR2 to DMS- and DLS-targeted non-DA cells in SN with two viral injections in a TH-2A-Flpo mouse: a transsynaptic anterograde Cre virus in striatum (DMS or DLS) and a Con/Foff-ChR2 virus in SNr.

**Figure 5. Viral strategy used for polysynaptic circuit dissection.**



(A) Experimental design for labeling DMS-targeted non-dopaminergic neurons in SNr. scAAV1-hSyn-Cre injected into DMS moves transsynaptically in the anterograde direction to deliver Cre to DMS-targeted neurons. AAV5-hSyn-Con/Foff-EYFP is injected into SNr to deliver EYFP to cells that are both Cre+ and Flp-. (B) Schematic of the resulting EYFP labeling in a WT mouse (all cells are Flp-; both GABA and DA cells may be Cre+). (C) Schematic of the resulting EYFP labeling in a TH-2A-Flpo mouse (DA cells are Flp+; only DMS-targeted, non-DA cells are Flp- and Cre+). (D-E) Example histology from the striatum (top row) and SN (bottom row) after injections in WT (D) and TH-2A-Flpo (E) mice. Scale bar: 0.5 mm. See also Supplementary Figure 2.

**Supplementary Figure 2. Similar results from Figure 5 are obtained using a Con/Foff-ChR2-EYFP virus.**



**(A)** Experimental design for labeling DMS-targeted, non-dopaminergic neurons in SNr with ChR2-EYFP. **(B-C)** Example SN histology after injections in WT (B) and TH-2A-Flpo (C) mice. Scale bar: 0.5 mm.

### 2.3 Characterization of Closed Striato-Nigro-Striatal Loops

By combining retrobead injections in striatum with our viral strategy in TH-2A-Flpo mice, we could investigate the structure and function of multiple striato-nigro-striatal circuits. Because basal ganglia circuits are thought to operate primarily in parallel closed loops (Alexander et al. 1986; Haber et al. 2000; Yin and Knowlton 2006; Mandelbaum et al. 2019; Lee et al. 2020), we began by testing closed striato-nigro-striatal loops through which DLS and DMS could regulate their own dopaminergic drive.

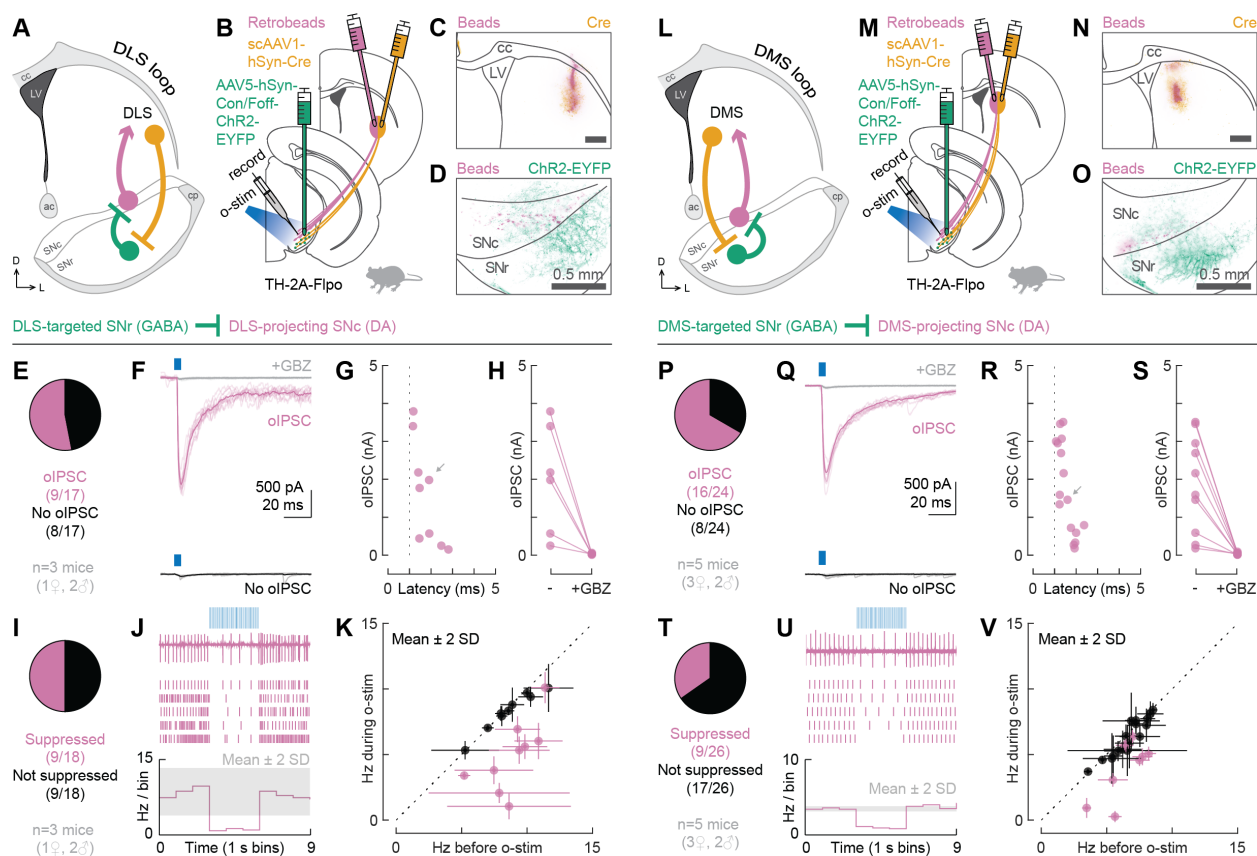
To test a closed DLS loop (**Figure 6A**), we injected both the transsynaptic Cre virus (scAAV1-hSyn-Cre) and red retrobeads into the DLS of TH-2A-Flpo mice. We also injected AAV5-hSyn-Con/Foff-ChR2-EYFP into SNr. With this design, we could record from bead-labeled DLS-projecting DA neurons in SNc while optogenetically stimulating DLS-targeted GABAergic neurons in SNr (**Figure 6B**). We verified that all DLS injections were contained within the DLS (**Figure 6C**, **Supplementary Figure 3A-B**). We also observed that both bead-labeled somas and ChR2-EYFP<sup>+</sup> neuropil were located in mid-lateral SN (**Figure 6D**). Under recording conditions used to isolate monosynaptic inhibitory connections, we found that 53% (9/17) of the recorded DLS-projecting neurons were monosynaptically inhibited by DLS-targeted GABAergic cells in SNr (**Figure 6E-F**). The oIPSC amplitude ranged from 0.2 to 3.8 nA (mean±SD: 1.6±1.3 nA) and the onset latencies were 1.2-2.8 ms (mean±SD: 1.7±0.5 ms; **Figure 6G**). For all tested cells, the oIPSC was blocked by GBZ (**Figure 6H**). Under a loose seal configuration, suppression of tonic firing was observed in 50% (9/18) of the recorded DLS-projecting cells (**Figure 6I-K**). The percentage of cells whose firing was suppressed closely matched the percentage in which oIPSCs were observed (50% vs 53%), recapitulating the correlation between effective inhibition and

synaptic connectivity observed for DLS-projecting DA neurons previously (**Figure 6E-K**, 68% vs 69%).

We next examined a closed DMS loop by injecting both the transsynaptic Cre virus (scAAV1-hSyn-Cre) and red retrobeads into the DMS of TH-2A-Flpo mice and injecting AAV5-hSyn-Con/Foff-ChR2-EYFP into SNr. We recorded from bead-labeled DMS-projecting DA neurons in SNc while optogenetically stimulating DMS-targeted GABAergic neurons in SNr (**Figure 6L-M**). We verified that all DMS injections were contained within the DMS (**Figure 6N**, **Supplementary Figure 3E-F**). We also observed that both bead-labeled somas and ChR2-EYFP<sup>+</sup> neuropil were medially located in SN (**Figure 6O**). Under recording conditions used to isolate monosynaptic inhibitory connections, we found that 67% (16/24) of the recorded DMS-projecting neurons were monosynaptically inhibited by DMS-targeted GABAergic cells in SNr (**Figure 6P-Q**). The oIPSC amplitude ranged from 0.2 to 3.5 nA (mean±SD: 1.8±1.2 nA) and the onset latencies were 1.1-2.4 ms (mean±SD: 1.6±0.4 ms; **Figure 6R**). For all tested cells, the oIPSC was blocked by GBZ (**Figure 6S**). Under a loose seal configuration, suppression of tonic firing was observed in 35% (9/26) of the recorded DMS-projecting cells (**Figure 6T-V**). The percentage of cells whose firing was inhibited was approximately half of the percentage in which oIPSCs were observed (35% versus 67%), corroborating the dissociation between effective inhibition and synaptic connectivity observed for DMS-projecting DA neurons previously (**Figure 4P-V**, 50% vs 87%).

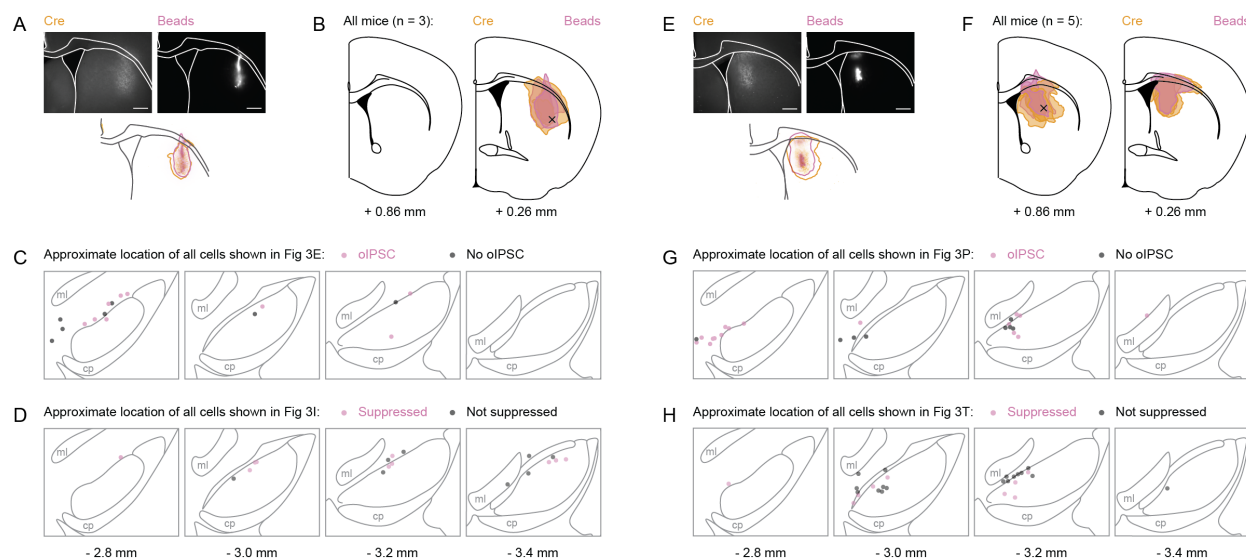
Collectively, these findings confirm the existence of closed striato-nigro-striatal loops through which DLS and DMS could alter their own dopaminergic drive via inhibition of GABAergic cells in SNr and disinhibition of DA cells in SNc. Moreover, our findings suggest that DLS would be more effective at such disinhibition than DMS.

**Figure 6. DLS-targeted and DMS-targeted GABAergic cells in SNr monosynaptically inhibit DLS-projecting and DMS-projecting DA neurons in SNc, respectively, and suppress their tonic firing.**



**(A)** Schematic of the DLS Loop. **(B)** Experimental design for probing the connection between DLS-targeted GABAergic cells in SNr and DLS-projecting DA neurons in SNc. In TH-2A-Flpo mice, scAAV1-hSyn-Cre was injected into DLS to label DLS-targeted cells with Cre. AAV5-hSyn-Con/Foff-ChR2-EYFP was injected into SNr to deliver ChR2 to cells carrying Cre but not Flp. Retrobeads were injected into DLS to label DLS-projecting DA neurons in SNc for recording. **(C)** Distribution of retrobeads (magenta) and Cre (yellow) in a representative striatum slice. Scale bar: 0.5 mm. **(D)** Distribution of bead-labeled somas (magenta) and ChR2-EYFP-labeled neuropil (green) in a representative midbrain slice. **(E)** Proportion of DLS-projecting neurons that did (magenta) or did not (black) respond to o-stim with an oIPSC. **(F)** Example cells for E. **(G)** oIPSC amplitude and onset latency for all responding cells. Gray arrow: oIPSC shown in F. **(H)** oIPSC amplitude before and after GBZ perfusion. **(I)** Proportion of DLS-projecting neurons that did (magenta) or did not (black) have their tonic firing suppressed by o-stim. **(J)** Example cell for I. Top: data from a single sweep. Middle: raster plot showing action potentials from 5 sweeps. Bottom: average firing rate across all sweeps. The gray shaded area indicates mean±2SD of the baseline firing rate. **(K)** Average firing rate during vs before o-stim for all cells from I. Error bars represent ±2SD. Dotted line: unity. **(L-V)** Same as A-K but for testing the DMS Loop. See also Supplementary Figure 3.

### Supplementary Figure 3. Injection spread in striatum and location of patched cells in midbrain slices for closed loop experiments.



**(A)** Example striatum slice. Scale bar: 0.5 mm. **(B)** Approximate spread of retrobeads in the striatum of all mice used for Figure 3A-K. A black x marks the approximate target location for DLS injections. The numbers below the atlas images indicate their AP position relative to bregma. **(C)** Approximate location of all DLS-projecting cells recorded in whole-cell mode used for Figure 3E-H. Each dot is a cell, color-coded in magenta (oIPSC) or black (no oIPSC). **(D)** Approximate location of all DLS-projecting cells recorded in loose seal mode used for Figure 3I-K. Each dot is a cell, color-coded in magenta (inhibited) or black (not inhibited). The numbers below the atlas images indicate their AP position relative to bregma. **(E-H)** Same as A-D but relative to experiments shown in Figure 3L-V with DMS-projecting cells instead of DLS-projecting.

## 2.4 Open Spiral Striato-Nigro-Striatal Circuits Are Unlikely to Support Robust Dopamine Disinhibition

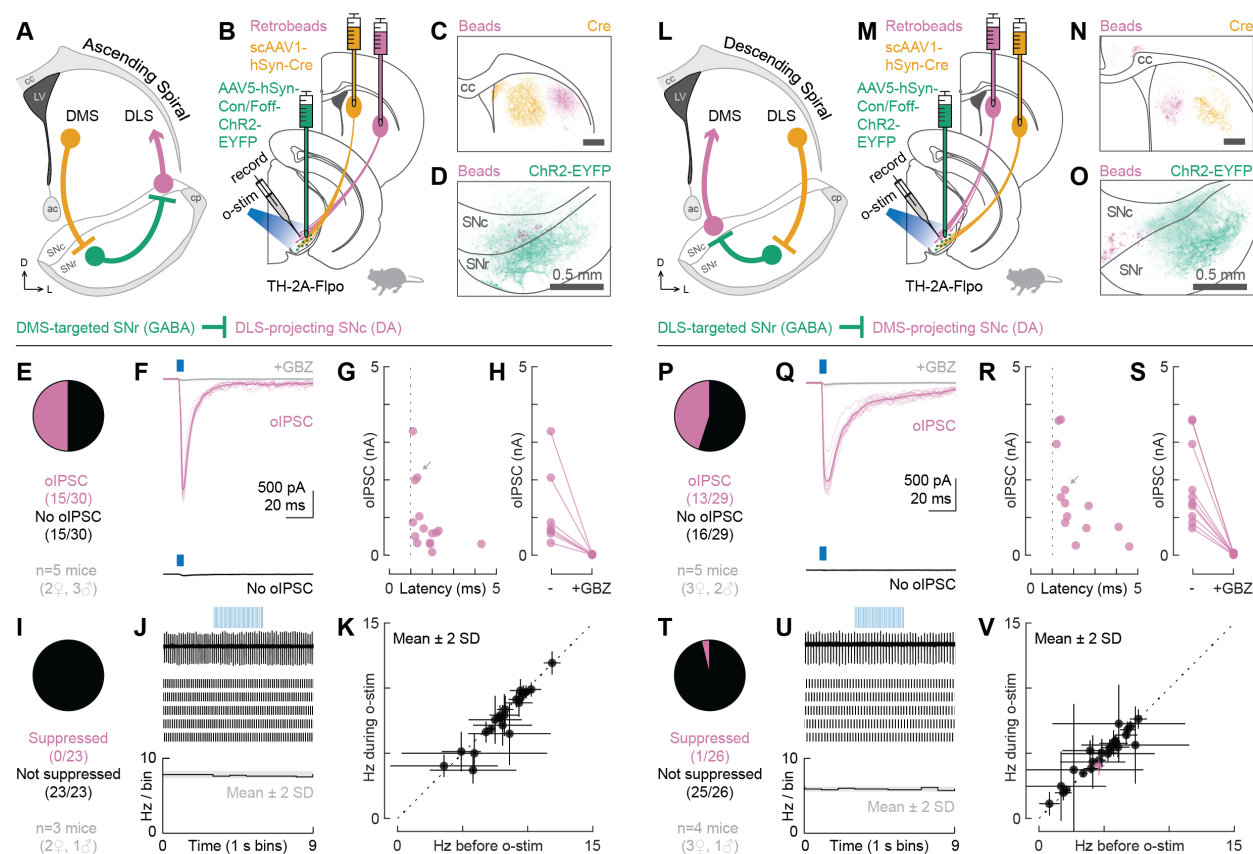
After employing our experimental strategy to test closed striato-nigro-striatal loops, we used a similar approach to test open-loop spiral circuits, beginning with the ascending spiral circuit (DMS→SNr→SNc→DLS). We injected the transsynaptic Cre virus (scAAV1-hSyn-Cre) into the DMS and red retrobeads into the DLS of TH-2A-Flpo mice (**Figure 7A**). We also injected AAV5-hSyn-Con/Foff-ChR2-EYFP into SNr. With this design, we could record from bead-labeled DLS-projecting DA neurons in SNc while optogenetically stimulating DMS-targeted GABAergic neurons in SNr (**Figure 7B**). We verified that all injections in striatum were contained within their target areas (**Figure 7C**, **Supplementary Figure 4A-B**). We also observed an overlap of bead-labeled cells and ChR2-EYFP<sup>+</sup> neuropil in SN (**Figure 7D**), consistent with the predictions of the ascending spiral hypothesis (Haber et al. 2000). Under recording conditions used to isolate monosynaptic inhibitory connections, we found that 50% (15/30) of the recorded DLS-projecting neurons were monosynaptically inhibited by DMS-targeted GABAergic cells in SNr (**Figure 7E-F**). The oIPSC amplitude ranged from 0.1 to 3.3 nA (mean±SD: 0.9±0.9 nA) and the onset latencies were 1.1–4.3 ms (mean±SD: 1.8±0.8 ms; **Figure 7G**). For all tested cells, the oIPSC was blocked by GBZ (**Figure 7H**). Under a loose seal configuration, however, suppression of tonic firing was NOT observed in any of the recorded DLS-projecting cells (0/23, **Figure 7I-K**). The striking mismatch between the percentage of cells whose firing was inhibited and the percentage in which oIPSCs were observed was unexpected and in stark contrast to the nearly perfect match between synaptic connectivity and effective inhibition for DLS-projecting cells in our previous experiments (**Figure 4A-K** and **Figure 6A-K**). Our findings suggest that there is a fundamental difference between the closed DLS loop and the ascending spiral connecting DMS to DLS. Although synaptic

connections exist at roughly similar rates in the two circuits (53% vs 50%), the ability of these circuits to control the tonic firing of DA neurons is remarkably different (50% vs 0%).

In previous work establishing the ascending spiral hypothesis, a lack of overlap between axons from lateral striatum and the cell bodies of SN neurons projecting to medial striatum was noted (Haber et al. 2000). This result led to the prediction that there is limited connectivity in a “descending” spiral (DLS→SNr→SNc→DMS), yet this prediction has not been tested. Indeed, such overlap is not necessary for the existence of a functional polysynaptic circuit. To examine the descending spiral circuit (**Figure 7L**), we injected the transsynaptic Cre virus (scAAV1-hSyn-Cre) into the DLS and red retrobeads into the DMS of TH-2A-Flpo mice. We also injected AAV5-hSyn-Con/Foff-ChR2-EYFP into SNr. With this design, we could record from bead-labeled DMS-projecting DA neurons in SNc while optogenetically stimulating DLS-targeted GABAergic neurons in SNr (**Figure 7M**). We verified that all injections in striatum were contained within their target areas (**Figure 7N**, **Supplementary Figure 4E-F**). We observed poor overlap of bead-labeled cells and ChR2-EYFP<sup>+</sup> neuropil in SN (**Figure 7O**), consistent with the predictions of Haber and colleagues work in non-human primates (Haber et al. 2000). However, despite the lack of overlap, we found that 45% (13/29) of the recorded DMS-projecting neurons were monosynaptically inhibited by DLS-targeted GABAergic cells in SNr (**Figure 7P-Q**). The oIPSC amplitude ranged from 0.2 to 3.6 nA (mean±SD: 1.5±1.1 nA) and the onset latencies were 1.2–4.6 ms (mean±SD: 2.1±1.1 ms; **Figure 7R**). For all tested cells, the oIPSC was blocked by GBZ (**Figure 7S**). The connectivity we observed was surprising. However, we did not observe inhibition of tonic firing through these synaptic connections. Under a loose seal configuration, suppression of tonic firing was observed in only 4% (1/26) of the recorded DMS-projecting cells (**Figure 7T-V**). The striking

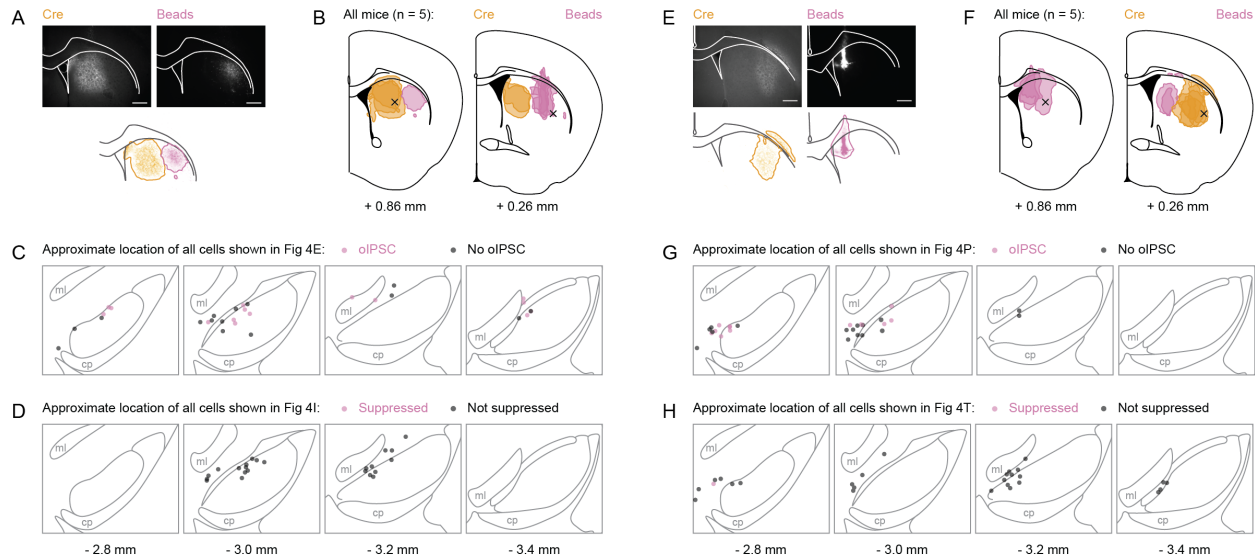
mismatch between synaptic connectivity and inhibition of tonic firing was once again unexpected, but not as surprising, given that some mismatch was previously observed for DMS-projecting cells (**Figure 4P-V** and **Figure 6P-V**). Together, our results from testing the ascending and descending spiral circuits suggest that these circuits are unlikely to support robust DA neuron disinhibition, at least in naïve mice.

**Figure 7. DMS-targeted and DLS-targeted GABAergic cells in SNr monosynaptically inhibit DLS-projecting and DMS-projecting DA neurons in SNc, respectively, but do not suppress their tonic firing.**



**(A)** Schematic of the Ascending Spiral. **(B)** Experimental design for probing the connection between DMS-targeted GABAergic cells in SNr and DLS-projecting DA neurons in SNc. **(C)** Distribution of retrobeads (magenta) and Cre (yellow) in a representative striatum slice. Scale bar: 0.5 mm. **(D)** Distribution of bead-labeled somas (magenta) and ChR2-EYFP-labeled neuropil (green) in a representative midbrain slice. **(E)** Proportion of DLS-projecting neurons that did (magenta) or did not (black) respond to o-stim with an oIPSC. **(F)** Example cells for E. **(G)** oIPSC amplitude and onset latency for all responding cells. Gray arrow: oIPSC shown in F. **(H)** oIPSC amplitude before and after GBZ perfusion. **(I)** Proportion of DLS-projecting neurons that did (magenta) or did not (black) have their tonic firing suppressed by o-stim. **(J)** Example cell for I. Top: data from a single sweep. Middle: raster plot showing action potentials from 5 sweeps. Bottom: average firing rate across all sweeps. The gray shaded area indicates mean±2SD of the baseline firing rate. **(K)** Average firing rate during vs before o-stim for all cells from I. Error bars represent ±2SD. Dotted line: unity. **(L-V)** Same as A-K but for testing the Descending Spiral. See also Supplementary Figure 4.

### Supplementary Figure 4. Injection spread in striatum and location of patched cells in midbrain slices for open spiral experiments.



**(A)** Example striatum slice. Scale bar: 0.5 mm. **(B)** Approximate spread of retrobeads in the striatum of all mice used for Figure 4A-K. A black x marks the approximate target location for DMS (left) and DLS (right) injections. The numbers below the atlas images indicate their AP position relative to bregma. **(C)** Approximate location of all DLS-projecting cells recorded in whole-cell mode used for Figure 4E-H. Each dot is a cell, color-coded in magenta (oIPSC) or black (no oIPSC). **(D)** Approximate location of all DLS-projecting cells recorded in loose seal mode used for Figure 4I-K. Each dot is a cell, color-coded in magenta (inhibited) or black (not inhibited). The numbers below the atlas images indicate their AP position relative to bregma. **(E-H)** Same as A-D but relative to experiments shown in Figure 4L-V with DMS-projecting cells instead of DLS-projecting.

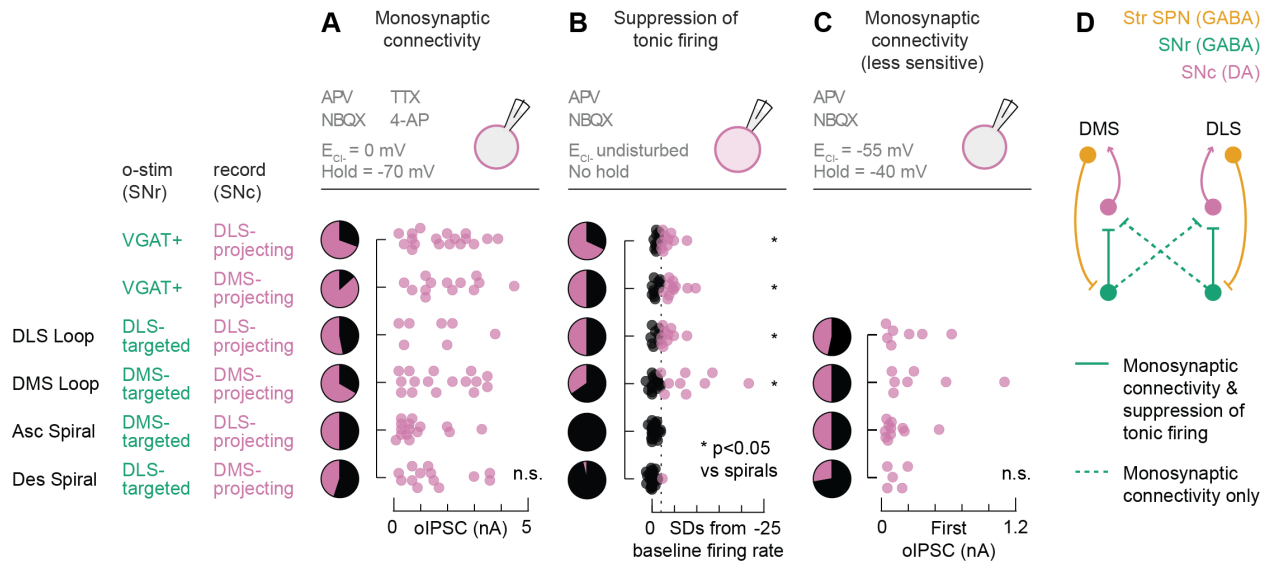
## 2.5 Strong GABAergic SNr Inputs Onto DA Neurons Do Not Predict Inhibition of Tonic Firing

In both open- and closed-loop striato-nigro-striatal circuits, we observed robust GABAergic connectivity from SNr neurons onto DA SNc neurons, mediated by GABA<sub>A</sub> receptor transmission. Given this connectivity, and the fact that the amplitude of the recorded oIPSCs was similar in all circuit configurations (**Figure 8A**), we expected to observe similar rates of suppression of DA neuron firing across conditions. Surprisingly, we found instead that the tonic firing of DA neurons was clearly inhibited in closed loops but not open spirals (**Figure 8B**).

The dissociation we observed between monosynaptic connectivity and firing suppression could be explained by technical differences between the testing conditions. During the detection of oIPSCs, we used 4-AP to boost neurotransmitter release probability from GABAergic SNr cells when action potentials were blocked by TTX, but a more physiological release probability was preserved during loose seal recordings. 4-AP could have masked oIPSC amplitude differences between low and high release probability synapses. Furthermore, the use of a high chloride internal during the detection of oIPSCs often resulted in large (>1nA) currents, which could have impaired our ability to voltage clamp. Thus, we repeated our monosynaptic connectivity experiments in the absence of TTX and 4-AP and used an internal solution with a lower chloride concentration to better mimic the physiological chloride reversal potential. Under these conditions, we observed smaller oIPSCs (most <1nA), yet we still found no differences in oIPSC amplitudes between circuit configurations (**Figure 8C**). We also reproduced the connection probabilities previously observed for DLS-projecting cells (47% vs 53% for DLS Loop and 50% vs 50% for Ascending Spiral) but found lower connection probabilities for DMS-projecting cells (50% vs 67% for DMS Loop and 28% vs

45% for Descending Spiral). Under these recording conditions, monosynaptic connectivity rates once again perfectly predict firing suppression rates for the DLS Loop but the dissociation for the other circuits - which is particularly stark for the ascending spiral - remains unexplained. Collectively, these findings support a model in which only closed striato-nigro-striatal loops induce strong firing suppression, although latent functional connectivity is present in open spirals (**Figure 8D**).

**Figure 8. Closed loops are supported by monosynaptic connectivity and suppression of tonic firing, while open spirals are supported by monosynaptic connectivity only.**



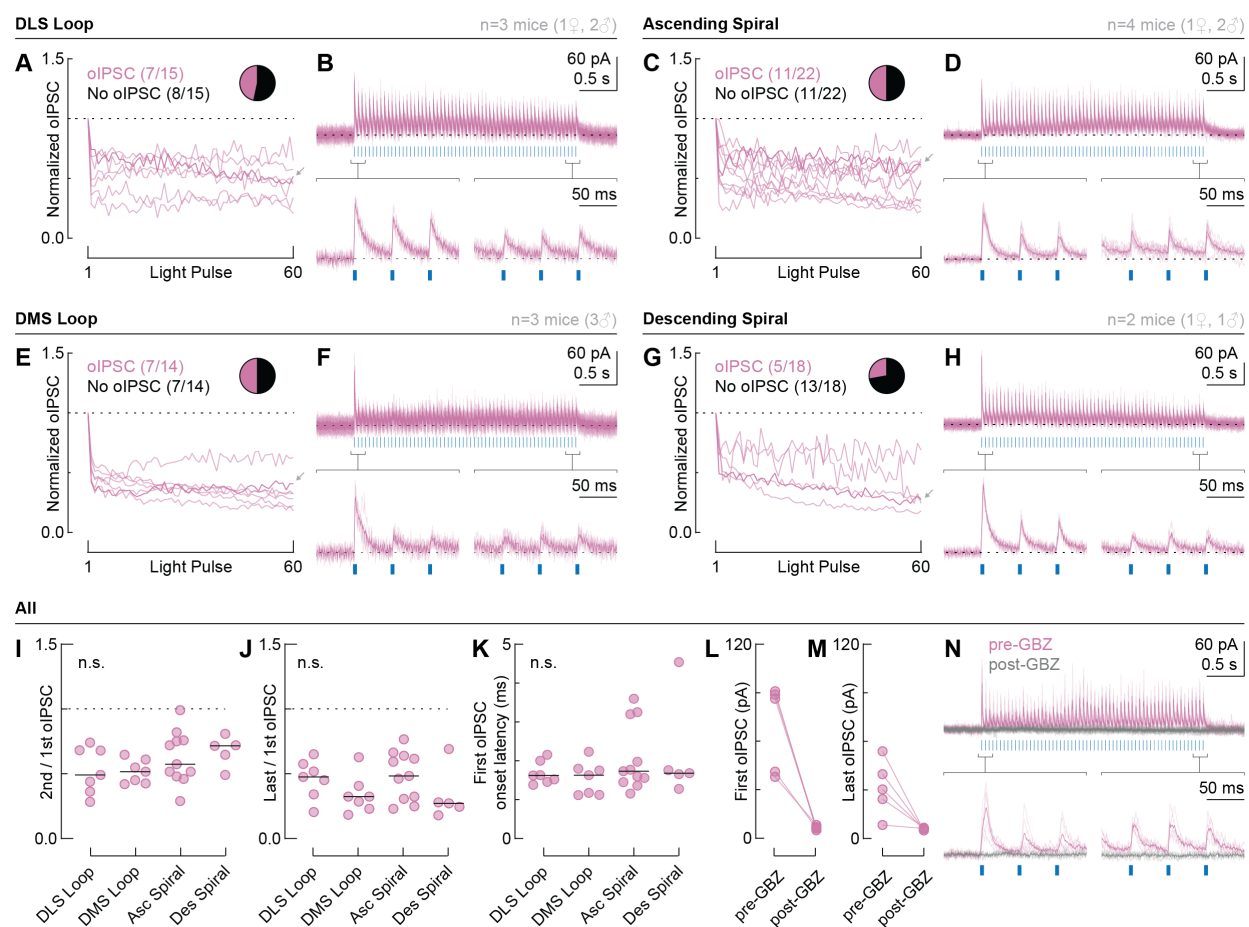
(A-C) Top: recording configuration. Pie charts: proportion of bead-labeled neurons that did (magenta) or did not (black) respond to o-stim. Scatter plots: (A,C) oIPSC amplitude or (B) change in tonic firing rate from baseline. Dotted line: -2SD. n.s.: not significant. \* $p < 0.05$  versus Ascending Spiral and versus Descending Spiral. (A,B) Data reproduced from Figure 4, Figure 6, and Figure 7. (C) For cell and mouse numbers, see Figure 9. (D) Circuit diagram supported by the data.

## 2.6 Differences Between Closed Loops and Open Spirals Are Not Explained by Differences in Short-Term Plasticity

One explanation for the dissociation between connectivity and firing suppression could be short-term plasticity. Given that firing suppression was assessed with a light train containing 60 pulses over 3 s, it could be that SNr→SNc synapses in open spirals are prominent initially but robustly depressing during the light train. If so, inhibition would not be sustained over the course of seconds.

To test this possibility, we stimulated the cells shown in **Figure 8C** with the same o-stim used for loose seal recordings (3 s, 20 Hz) and measured the amplitude of all oIPSCs relative to the first. We found that cells in all circuit configurations showed modest short-term depression (**Figure 9A-H**). A few cells displayed delayed facilitation relative to the second oIPSC (see **Figure 9C**, for example) but there were no clear differences between closed loops and open spirals. The paired-pulse ratio between the second and first oIPSC was not significantly different between groups (**Figure 9I**), and neither was the ratio between the last and first oIPSC (**Figure 9J**). Despite the lack of TTX in the bath, the detected oIPSCs are likely to be monosynaptic given their onset latency (**Figure 9K**). All cells tested displayed oIPSCs mediated entirely by GABA<sub>A</sub> receptors (**Figure 9L-N**). Collectively, these data show that the observed differences between closed loops and open spirals are not due to differences in short-term plasticity.

**Figure 9. Pre-synaptic release probability does not explain differences between closed loops and open spirals.**



(A-B) DLS Loop dataset. (A) Normalized oIPSC amplitude for bead-labeled neurons that responded to o-stim (20 Hz, 3 s). Dotted line: 1. Insert: proportion of bead-labeled neurons that did (magenta) or did not (black) respond to o-stim. Gray arrow: example cell shown in B. (B) Example cell with a zoom-in of the first and last three oIPSCs. Thin lines: individual sweeps. Thick lines: average across sweeps. Dotted line: baseline. (C-D) Same as A-B but for the Ascending Spiral. (E-F) Same as A-B but for the DMS Loop. (G-H) Same as A-B but for the Descending Spiral. (I) Ratio between the second and first oIPSCs. (J) Ratio between the last and first oIPSCs. (K) Onset latency of the first oIPSC. Black bars in I-K indicate the median. n.s.: not significant. (L) First and (M) last oIPSC amplitude before and after GBZ perfusion for all tested cells. (N) Example recording before (magenta) and after (gray) GBZ perfusion.

## 2.7 Discussion

### *Evidence For and Against the Ascending Spiral Hypothesis*

We tested multiple striato-nigro-striatal loops connecting two striatal subregions (DMS and DLS) via SNr and SNc (i.e., DMS/DLS→SNr→SNc→DMS/DLS). These loops have the potential to transform activity in a striatal subregion into DA release in the same or neighboring region of striatum by disinhibiting dopaminergic neurons in SNc. We were particularly interested in testing the predictions of the ascending spiral hypothesis, which argues that an open loop striato-nigro-striatal circuit permits the progressive disinhibition of DA neurons in a unidirectional, “ascending” (medio-lateral) direction (Haber et al. 2000). We focused on circuits involving the dorsal striatum given that the ascending spiral hypothesis is frequently invoked to explain changes in DMS and DLS that occur over the course of extended training, as animals become proficient in motor skill tasks or transition from goal-directed to habitual behavior.

Our data provide evidence both for and against the ascending spiral hypothesis. They support the existence of a DMS→SNr→SNc→DLS circuit but challenge the prediction that this circuit alone can support disinhibition in DA neurons. Instead, our data suggest that closed striato-nigro-striatal loops (i.e., DMS→SNr→SNc→DMS and DLS→SNr→SNc→DLS) are better suited to support disinhibition. Our findings are complemented by findings in ventral striatal circuits, which similarly suggest that disinhibition operates primarily in closed loops (Yang et al. 2018). Our findings further diverge from the ascending spiral hypothesis by documenting the existence of a descending spiral (DLS→SNr→SNc→DMS) of approximately equal strength to the ascending spiral, challenging the claim of unidirectional information flow.

These results are important because previous anatomical findings about the topography of striato-nigro-striatal circuits (Haber et al. 2000) have inspired the field to interpret behavioral and neural activity findings under the framework of an ascending spiral (Yin and Knowlton 2006; Lerner 2020; Lüscher et al. 2020). Indeed, the sequential recruitment of DMS and DLS during motor skill learning and habit formation fits nicely with the ascending spiral hypothesis (Yin et al. 2009; Thorn et al. 2010; Gremel and Costa 2013). So does the dependence of habit formation on DA projections to DLS (Faure et al. 2005) and the increasing recruitment of DLS DA activity with drug use (Belin and Everitt 2008; Willuhn et al. 2012). In addition, modeling studies point to striatonigral circuits in the form of Str→SNr→SNc as a robust means of disinhibition and burst firing in dopaminergic neurons (Lobb et al. 2011). Although no direct evidence exists for impaired DA release in DLS following DMS lesions, ventromedial striatum (VMS) lesions are reported to impair DLS DA release (Willuhn et al. 2012).

While these previous findings are consistent with the ascending spiral hypothesis, direct evidence for a continuous polysynaptic circuit connecting DMS→SNr→SNc→DLS was lacking, and other findings do not fit. For instance, if repeated activation of DMS is required to elicit DA release in DLS and drive motor learning and habit formation, one would expect DMS lesions to hinder these processes, but that is not the case. Instead, DMS lesions do not prevent motor skill learning (Yin et al. 2009) and are in fact reported to accelerate habit formation (Yin et al. 2004; Yin et al. 2005a; Yin et al. 2005b; Gremel and Costa 2013). It is also hard to reconcile the slow time course of habit formation and the associated changes in DLS (days to weeks) with a tri-synaptic circuit theoretically capable of regulating DA release in DLS within tens of milliseconds. One possible explanation is that a disinhibitory ascending spiral circuit is not fully functional in naïve animals

but develops slowly during training. The latent synaptic connections we observed in the DMS→SNr→SNc→DLS circuit could undergo plasticity and/or regulate the plasticity of other inputs onto DA neurons over the course of training even if they do not regulate DA neuron firing in naïve mice. Therefore, adjustments to the ascending spiral hypothesis that incorporate experience-dependent plasticity may be warranted.

#### *Potential Mechanisms for the Dissociation Between Connectivity and Firing Rate Modulation*

Presynaptic short-term plasticity mechanisms did not explain the dissociation we observed (**Figure 9**). Therefore, we suspect that a postsynaptic mechanism is involved. DA neurons, which do not express the chloride extruder KCC2 (potassium-chloride cotransporter 2), have a weakly hyperpolarizing chloride reversal potential (Gulácsi et al. 2003). Therefore, inhibition through GABA<sub>A</sub> receptor activity is primarily due to shunting inhibition and will be less effective at regulating firing rates if synapses are located far from the action potential generating mechanisms of the DA cell. In other words, one might expect lower rates of firing modulation as compared to rates of monosynaptic connectivity if synapses are located on distal dendrites. We hypothesize that preferential targeting of distal DA neuron dendrites is the key difference between open spiral and closed loop SNr→SNc synapses, a topic for future study.

Compartmentalization of synaptic inputs has been previously reported for midbrain DA neurons, as has heterogeneity in intrinsic properties (Lammel et al. 2008; Lammel et al. 2011; Crittenden et al. 2016; Tarfa et al. 2017; Evans et al. 2017; Farassat et al. 2019; Evans et al. 2020). Notably, striosome SPNs target the distal SNr dendrite of SNc DA neurons, in so-called striosome-dendron bouquets (Crittenden et al. 2016), while neurons of the globus pallidus external segment (GPe) target the soma and proximal dendrites of DA neurons (Evans et al. 2020). Moreover, striosomes

target ventral tier DA neurons, which have a prominent sag current and after-depolarization that support rebound firing (Evans et al. 2017; Evans et al. 2020). Interactions between intrinsic properties and preferential targeting could explain the differences we observed between closed and open loops. Additional layers of synaptic input integration would be possible if, like hippocampal and cortical neurons, DA cells maintain a compartmentalized responsiveness to GABAergic inputs due to subcellular variance in intracellular chloride (Khirug et al. 2008; Rahmati et al. 2021).

Activation of slow inhibitory conductances through GABA<sub>B</sub> receptors or other G-protein coupled receptors (GPCRs) might also explain the dissociation we observed. However, our data suggests that this is not the case. In the dataset shown in **Figure 9**, we identified a slow hyperpolarizing current in a subset of cells, but the relative number of cells with this current was comparable across circuit configurations, and therefore unlikely to explain the differences between closed and open loops (DLS Loop: 3/7 cells; DMS Loop: 4/7; Ascending Spiral: 7/11; Descending Spiral: 3/5). Furthermore, this slow current is dependent on GABA<sub>A</sub> receptors, given that it is sensitive to GBZ (see example in **Figure 9N**).

#### *Alternatives to the Ascending Spiral Hypothesis*

The ascending spiral hypothesis as formulated by Haber and colleagues is not the only means by which striatal subregions could influence each other. For example, VMS can modulate DLS activity via a long polysynaptic loop through SNr, thalamus and motor cortex (Aoki et al. 2019), bypassing not only DMS but also DA neurons. Other mechanisms might exist through lateral inhibition amongst SPNs (Burke et al. 2017), striatal interneuron networks (Xu et al. 2015; Fino et al. 2018; Cai and Ford 2018; Holly et al. 2019; Dorst et al. 2020), modulation of DA axon terminals (Mohebi et al. 2019; Kramer et al. 2020; Liu et al. 2021), or striatal astrocyte networks

(Khakh 2019). Thus, even if the ascending spiral circuit for DMS-DLS communication through the control of DA neuron activity is weak, other circuits may instead support information transfer between DMS and DLS.

### *Balancing Striatal Inhibition and Disinhibition of Dopamine Neurons*

Given the findings described here regarding the *indirect* connections between striatum and SNc via SNr, and previous research on the *direct* connections between striatum and SNc, it is hard to predict which patterns of striatal activity would support the disinhibition of DA neurons *in vivo*. Multiple rabies tracing studies have characterized the monosynaptic inputs onto projection-defined DA neurons and identified the striatum as a major source of direct inhibition to DA cells (Watabe-Uchida et al. 2012; Lerner et al. 2015; Menegas et al. 2015). However, these direct connections were excluded from computational models of striato-nigro-striatal circuits that predicted disinhibition of DA neurons following striatal activation (Lobb et al. 2011). Lerner and colleagues further dissected these *direct* striato-nigro-striatal circuits with slice electrophysiology and found that DMS preferentially targets DMS-projecting DA neurons, while DLS targets both DMS- and DLS-projecting DA neurons. Thus, monosynaptic connections between striatum and SNc support the existence of closed loops (DMS→SNc→DMS and DLS→SNc→DLS), as well as a descending circuit (DLS→SNc→DMS). Work in ventral striatal circuits also draws attention to the role of direct inhibition of DA neurons by striatal inputs, which can be mediated by GABA<sub>B</sub> as well as GABA<sub>A</sub> receptors (Yang et al. 2018). Further investigation is required to compare the relative strength of *direct* and *indirect* striato-nigro-striatal circuits on the activity of DA neurons and test the conditions that favor disinhibition over inhibition *in vivo*.

Finally, it is possible that the balance between inhibition and disinhibition of DA neurons is altered by training, either by synaptic plasticity or by the recruitment of additional circuits during learning. We and others have observed that the *in vivo* patterns of DA axon activity and DA release in DMS and DLS change with training (Willuhn et al. 2012; Hamid et al. 2021; Seiler et al. 2022). The reasons for training-induced changes in DA signaling are not yet clear, but with the approaches developed here, and with additional innovations to adapt them for *in vivo* investigations, we can begin to rigorously address this hypothesis and advance our mechanistic understanding of the complex process of habit formation.

#### *Limitations of the Study*

Two technical caveats could result in underestimation of the connectivity probabilities reported here: (1) incomplete penetrance of our labeling methods and (2) severing of the distal dendrites of DA neurons in midbrain slices. Although our labeling methods are not 100% penetrant, any underestimation due to this caveat should affect all tested circuits similarly since we used the same viruses and retrobeads in all experiments. The severing of distal dendrites, on the other hand, could disproportionately affect some circuit configurations. The substantia nigra has a complex 3D structure that is not fully preserved in coronal slices (Gerfen et al. 1987; Maurin et al. 1999). If a particular subpopulation of SNr cells targets the distal dendrites of DA neurons, then this connection is more likely to be underestimated. Additionally, if DA neurons projecting to DLS or DMS belong predominantly to ventral tier SNc and have a prominent distal dendrite in SNr (Gerfen et al. 1987), connections onto these cells are also more likely to be underestimated. Fortunately, these caveats do not seem to significantly bias our results, given that oIPSCs of similar amplitudes were detected in all circuit configurations (**Figure 8**). In addition, we assessed synaptic

connectivity and effects on tonic firing in slices from the same mice. DA cells that were not suppressed by optogenetic stimulation were often located adjacent to DA cells that exhibited robust oIPSCs. Hence, the dissociation between synaptic connectivity and effective inhibition we report is not due to variability in slicing and/or ChR2 expression across animals. We were also careful to sample bead-labeled cells across the entire volume of SN to avoid any biases regarding the location of DA neurons (**Supplementary Figure 1, Supplementary Figure 3 and Supplementary Figure 4**). We did not observe any correlations between cell location and likelihood of connection for any of the tested circuits.

## 2.8 Methods

### *Mice*

Male and female C57BL/6J mice were group housed under a conventional 12:12 h light/dark cycle with ad libitum access to food and water. The VGAT-IRES-Cre knock-in strain was obtained from The Jackson Laboratory (Jackson Stock #028862) and the TH-2A-Flpo line was a gift from Dr. Awatramani (Poulin et al., 2018; MMRRC Stock #050618-MU). Animals were bred in-house, and only heterozygous transgenic mice were used for experiments. WT mice used in **Figure 5** and **Supplementary Figure 2** were Flp- mice from our TH-2A-Flpo breeding. Littermates were randomly assigned to experimental groups. Adult mice at least 10 weeks of age were used in all experiments. All experiments were approved by the Northwestern University Institutional Animal Care and Use Committee. An analysis of the influence of sex on our results was not provided given that our study is underpowered to detect potential sex differences.

### *Stereotaxic surgery*

Surgery was performed on adult (7-20 weeks old) male and female mice. Briefly, anesthesia was induced and maintained with isoflurane 1-4% (Patterson Scientific Link 7). Buprenorphine SR (0.5 mg/kg, Zoopharm) and Carprofen (5 mg/kg, Zoetis) were administered subcutaneously for analgesia. Ophthalmic ointment (Puralube, Dechra) was used to prevent dehydration of the cornea. A far infrared heating pad (Kent Scientific) was placed on top of the stereotax (Stoelting 51733D) to keep body temperature at ~37°C. Fur was removed with Nair; 10% povidone-iodine and 70% isopropyl alcohol were used to disinfect the scalp. A small (~1 cm) scalp incision was made to expose the skull, which was later closed with non-absorbable sutures (Ethicon, 661H) and tissue adhesive (Vetbond, 3M). Bregma and lambda were used as landmarks to level the head and guide

injections. To drill skull holes, a micromotor drill (Stoelting, 51449) was moved to the appropriate coordinates with the aid of a digital stereotaxic display. Viruses and/or retrobeads were injected into the brain at 50-100 nl/min through a blunt 33-gauge needle using a syringe pump (World Precision Instruments). The needle was left in place for 5 min following the end of the injection, then slowly retracted to avoid leakage up the injection tract. The following coordinates were used (AP, ML, DV – in mm): DMS (0.8, 1.5, -2.8), DLS (0.3, 2.5, -3.3), and SNr (-3.3, 1.2, -4.7). Where indicated, we injected 250 nl of scAAV1-hSyn-Cre (2.81e13 vg/ml, WZ Biosciences) into DMS/DLS, and 250 nl of AAV5-hSyn-Con/Foff-EYFP (2.6e12 vg/ml, UNC, Addgene plasmid #55651) or AAV5-hSyn-Con/Foff-hChR2(H134R)-EYFP (5.3e12 vg/ml, UNC, Addgene plasmid #55646) into SNr. Red retrobeads (LumaFluor Inc) were diluted 1:4 (dilution factor) in sterile saline, and 100 nl were injected into DMS/DLS. When retrobeads were mixed with scAAV1-hSyn-Cre for investigation of closed loops, they were diluted 1:8 in a virus aliquot, and a total volume of 250 nl was injected into DMS or DLS. As a consequence, approximately the same amount of beads was injected into striatum (half the concentration at ~double the volume), and the transsynaptic Cre virus was only slightly diluted (7:8 dilution factor). After surgery, animals were placed on a warm recovery bin until ambulant. A moist nutritional supplement (DietGet 31M, Clear H<sub>2</sub>O) was placed on the floor of the homecage to aid recovery from surgery. 4-9 weeks after surgery, animals received a lethal intraperitoneal injection of Euthasol (1 mg/kg, Virbac), a combination of sodium pentobarbital (390 mg/ml) and sodium phenytoin (50 mg/ml), and underwent a transcardial perfusion for electrophysiology and/or histology experiments.

### *Electrophysiology*

We followed the methods described by Ting and colleagues (Ting et al., 2014) to prepare acute brain slices from adult mice. Following Euthasol injection, unresponsive mice were transcardially perfused with ice-cold N-Methyl-D-Glutamine (NMDG) artificial cerebrospinal fluid (ACSF) containing (in mM): 92 NMDG, 2.5 KCl, 1.2 NaH<sub>2</sub>PO<sub>4</sub>, 30 NaHCO<sub>3</sub>, 20 HEPES, 25 Glucose, 5 Na-Ascorbate, 2 Thiourea, 3 Na-Pyruvate, 10 MgSO<sub>4</sub>, 0.5 CaCl<sub>2</sub> (Millipore Sigma). All extracellular solutions used for electrophysiology were saturated with 95%O<sub>2</sub>/5%CO<sub>2</sub> and their pH and osmolarity were adjusted to 7.3-7.4 and 300±5 mOsm, respectively. After perfusion, the brain was quickly removed and cut coronally to separate the rostral half (containing striatum) from the caudal half (containing SN). The cut face of each brain half was glued (Loctite 454) to a specimen holder and immersed into ice-cold NMDG ACSF. Coronal slices (300 µm thick) were made using a vibratome (Leica, VT1200S) set to 0.08 mm/s speed and 1.00 mm amplitude. Striatal slices were saved to confirm injection sites, while midbrain slices were used for recordings. Slices were allowed to recover for 45 min in three 15 min baths: (1) warm (33°C) NMDG ACSF; (2) warm (33°C) recovery ACSF, containing (in mM): 92 NaCl, 2.5 KCl, 1.2 NaH<sub>2</sub>PO<sub>4</sub>, 30 NaHCO<sub>3</sub>, 20 HEPES, 25 Glucose, 5 Na-Ascorbate, 2 Thiourea, 3 Na-Pyruvate, 1 MgSO<sub>4</sub>, 2 CaCl<sub>2</sub>; and (3) room temperature (RT) recovery ACSF. Finally, slices were kept at RT in recording ACSF, containing (in mM): 125 NaCl, 26 NaHCO<sub>3</sub>, 1.25 NaH<sub>2</sub>PO<sub>4</sub>, 2.5 KCl, 1 MgCl<sub>2</sub>, 2 CaCl<sub>2</sub>, 11 Glucose. During recordings, fresh ACSF was continuously delivered to the slice chamber at ~1.5 ml/min and warmed to 30-32°C with an inline heater (Warner Instruments). Where indicated, the following drugs were added to the recording ACSF: D-AP5 (50 µM, Cayman Chemical), NBQX disodium (5 µM, Tocris Bioscience), TTX (1 µM, Tocris Bioscience), 4-AP (100 µM, Tocris Bioscience), and GBZ (10 µM, Tocris Bioscience). Three different internal solutions were used in

this study. For monosynaptic connectivity experiments, a high chloride internal solution was used, adjusted to  $290 \pm 5$  mOsm and pH 7.3-7.4, containing (in mM): 130 CsCl, 1 EGTA, 10 HEPES, 5 QX-314-Cl, 10 TEA-Cl, 2 Mg-ATP, 0.3 Na-GTP. For suppression of tonic firing experiments, a HEPES-buffered synthetic interstitial fluid solution (SIF) was used as internal solution, adjusted to  $300 \pm 5$  mOsm and pH 7.3-7.4, containing (in mM): 140 NaCl, 23 Glucose, 15 HEPES, 3 KCl, 1.5 MgCl<sub>2</sub>, 1.6 CaCl<sub>2</sub>. For pre-synaptic release probability experiments, a low chloride internal solution was used, adjusted to  $290 \pm 5$  mOsm and pH 7.3-7.4, containing (in mM): 130 CsMeSO<sub>3</sub>, 1 EGTA, 10 HEPES, 5 QX-314-Cl, 10 TEA-Cl, 2 Mg-ATP, 0.3 Na-GTP. Patch pipettes (3-5 M $\Omega$ ) were pulled (Narishige, PC-100) from borosilicate glass (Warner Instruments, G150TF-4) and moved with the assistance of a micromanipulator (Sensapex). Cells were visualized with a 40x water-immersion objective (NA 0.8, Olympus, #N2667700) on a microscope (Olympus, BX51WI) equipped with infrared-differential interference imaging (DIC) and a camera (QImaging, Retiga Electro Monochrome). An LED light source (CoolLED, pE-300<sup>white</sup>) was used to illuminate the slice through the objective for targeted patching and for optogenetic stimulation. With the aid of a power meter (Thor Labs, PM130D), the LED power was adjusted to deliver  $\sim 10$  mW/mm<sup>2</sup> at 475 nm to the slice during the o-stim. Signals were recorded at 10 kHz using Wavesurfer v0.945 (<https://wavesurfer.janelia.org/>), a National Instruments Digitizer (NIDAQ X series PCIe-6323) and BNC Breakout (BNC-2090A), and a Multiclamp 700B amplifier (Molecular Devices). Data analysis was performed offline using custom-written MATLAB scripts.

### *Histology*

The following protocol was used to slice, stain and image the tissue used exclusively for histology (**Figure 5** and **Supplementary Figure 2**). Following Euthasol injection, unresponsive mice were

transcardially perfused with ice-cold phosphate-buffered saline (PBS), followed by 4% paraformaldehyde (PFA) diluted in PBS. Brains were immersed in 4% PFA overnight, and then cryoprotected with 30% sucrose (diluted in PBS) at 4°C. Coronal slices (30-50 µm thick) were made using a freezing microtome (Leica, SM2010 R). Staining was performed on free floating slices, with 3x10 min PBS washes in-between incubations. Slices were blocked for 1-2 h at RT with 3% normal goat serum (NGS) diluted in 0.3% PBST (0.3% Triton X-100 in PBS). Then, slices were incubated overnight at 4°C with primary antibodies diluted in blocking solution. Striatum slices were incubated with guinea pig anti-Cre (1:500, Synaptic Systems, #257004) and rabbit anti-GFP (1:1000, Invitrogen, #A11122), while midbrain slices were incubated with chicken anti-TH (1:500, Aves Labs, #TYH) and rabbit anti-GFP (1:1000, Invitrogen, #A11122). Afterwards, slices were incubated for 2-3 h at RT in secondary antibodies diluted in a modified blocking solution (1% NGS in 0.3% PBST). Striatum slices were incubated with goat anti-guinea pig 647 (1:500, Invitrogen, #A21450) and goat anti-rabbit 594 (1:500, Invitrogen, #A11012), while midbrain slices were incubated with goat anti-chicken 647 (1:500, Invitrogen, #A21449) and donkey anti-rabbit 488 (1:500, Jackson Immuno Research, #711-546-152). Striatum slices were further stained for 1-2 h at RT with NeuroTrace 435/455 (1:100 diluted in PBS, Invitrogen, #N21479), a fluorescent Nissl staining. Fluoromount-G (Southern Biotech) was used as mounting media. Slides were imaged with an air-immersion 10x objective (NA 0.45, Nikon, #MRD70105) on an epifluorescence microscope (Keyence, BZ-X800).

A slightly different protocol was used to stain tissue derived from electrophysiology experiments (**Figure 4, Figure 6, Figure 7, Supplementary Figure 1, Supplementary Figure 3, Supplementary Figure 4**). Slices were fixed overnight at 4°C in 4% PFA and stored in PBS at

4°C. Staining was performed on free floating slices as described above, with some modifications – 0.3% PBST was replaced by 0.5% PBST, 10% NGS was used for blocking, and 1% NGS was used to dilute antibodies. Cre staining was performed in striatum slices using guinea pig anti-Cre and goat anti-guinea pig 647. TH staining was performed in midbrain slices using chicken anti-TH and goat anti-chicken 647. EYFP signal was enhanced in all slices with GFP immunolabeling, using rabbit anti-GFP and donkey anti-rabbit 488. Retrobeads did not require enhancement. A custom look-up table was applied in ImageJ to match our colorblind safe color-coding (Wong, 2011). For qualitative visualization of midbrain slices, we adjusted the brightness and contrast of the retrobeads and EYFP channel separately due to the brighter fluorescence of the beads. Analysis of injection spread in DMS/DLS was performed in ImageJ (Schneider et al. 2012), using the following tools: threshold, median filter, and binary outline. A lower threshold was used for outlining the spread of retrobeads due to their brighter fluorescence in comparison to Cre immunolabeling, but the same analysis parameters were used for all mice. Images were aligned to two striatum sections from the Mouse Brain Atlas (Franklin and Paxinos, 2008), and injection outlines were superimposed in Adobe Illustrator.

### *Monosynaptic connectivity*

Bead-labeled cells were held at -70 mV and exposed to the o-stim (5 ms blue light pulse) in 5-10 sweeps, with a 30 s interval between sweeps. Series resistance ( $R_s$ ) was monitored, but not compensated. Liquid junction potential was not corrected. Cells with  $R_s > 25 \text{ M}\Omega$  or with more than 30% change in  $R_s$  during the recording were excluded from the dataset. oIPSCs were characterized as fast-onset events (a monotonic decrease in current for 1.5 ms) that happened within 20 ms of the start of the light pulse. In rare sweeps, mIPSCs were mislabeled as oIPSCs.

Thus, a *cell* was labeled as “shows an oIPSC” only if oIPSCs were detected in more than 50% of the recorded sweeps. Cells that did not fit this criteria were labeled as “no oIPSC”. For a subset of cells that showed an oIPSC, GBZ was added to the bath for 4 min, and the response to the o-stim was reassessed. Before testing a new cell, GBZ was washed off for at least 20 min. These wash-in and wash-off times were sufficient to block and unblock mIPSCs, respectively (data not shown). The oIPSC amplitude and onset latency reported for each cell were averaged across sweeps. In experiments using the VGAT-IRES-Cre line, a total of 17 cells (4 DLS-projecting and 13 DMS-projecting) were excluded from the dataset due to Chr2 expression, as evidenced by GBZ-insensitive oIPSCs with onset latency  $< 1$  ms. A VGAT<sup>+</sup> subgroup of dopaminergic neurons has been previously described (Poulin et al. 2020).

#### *Suppression of tonic firing*

Bead-labeled cells were recorded in voltage clamp (no holding voltage was applied) with a loose seal (20-100 M $\Omega$ ) and exposed to the o-stim (5 ms pulses delivered at 20 Hz for 3 s) in 5-10 sweeps, with a 30 s interval between sweeps. 10 sweeps were recorded for 88% of the cells (126/142 cells). Cells that did not display tonic firing were excluded from the dataset. The baseline firing rate was calculated during the 3 s prior to the o-stim. Mean $\pm$ SD were calculated across sweeps. In our experiments using the VGAT-IRES-Cre line, a total of 16 cells (7 DLS-projecting and 9 DMS-projecting) were excluded from the dataset due to Chr2 expression, as evidenced by GBZ-insensitive light-evoked excitation.

#### *Pre-synaptic release probability*

Bead-labeled cells were held at -40 mV and exposed to the same o-stim used above (5 ms pulses delivered at 20 Hz for 3 s) in 5-10 sweeps, with a 30 s interval between sweeps. This holding

voltage was chosen to allow detection of oIPSCs while masking spontaneous IPSCs. Series resistance ( $R_s$ ) was monitored, but not compensated. Liquid junction potential was not corrected. Cells with  $R_s > 25 \text{ M}\Omega$  or with more than 30% change in  $R_s$  during the recording were excluded from the dataset. oIPSCs were characterized as fast-onset events (a monotonic increase in current for 0.5 ms) that happened within 5 ms of the start of the light pulse. For a subset of cells that showed oIPSCs, GBZ was added to the bath for 4 min, and the response to the o-stim was reassessed. Before testing a new cell, GBZ was washed off for at least 20 min. The oIPSC amplitude and onset latency reported for each cell (and light pulse) were averaged across sweeps.

#### *Approximate cell location*

Following each cell recording, a low magnification DIC image was taken with a 5x air-immersion objective (NA 0.15, Olympus, #N2181500) to show the relative position of the cell in the slice. Offline, images from the same slice were stitched in MATLAB for registration purposes. Stitched DIC images were later aligned to an MRI based atlas (Chon et al., 2019) in Adobe Illustrator and the relative coordinates of all cells was documented.

#### *Statistical analyses*

Most statistical analyses were performed in Prism (GraphPad) using the Kruskal-Wallis test, a non-parametric version of one-way ANOVA, followed by a Multiple Comparison Test.  $p < 0.05$  was considered statistically significant. The p values were adjusted for multiple comparisons by controlling the False Discovery Rate (two-stage step-up method of Benjamini, Krieger and Yekutieli). A Multinomial logistic regression was performed in MATLAB to predict the likelihood of connection based on the medio-lateral, dorsal-ventral and antero-posterior location of the

recorded cells. In all statistical tests, n represented the number of cells. The number of cells and mice used for each experiment is shown in the Figures.

*Key Resources Table*

<b>REAGENT or RESOURCE</b>	<b>SOURCE</b>	<b>IDENTIFIER</b>
<b>Antibodies</b>		
Guinea Pig anti-Cre	Synaptic Systems	Cat# 257004; RRID:AB_2782969
Rabbit anti-GFP	Invitrogen	Cat# A11122; RRID:AB_221569
Chicken anti-TH	Aves Labs	Cat# TYH; RRID:AB_10013440
Goat anti-Guinea Pig 647	Invitrogen	Cat# A21450; RRID:AB_2735091
Goat anti-Rabbit 594	Invitrogen	Cat# A11012; RRID:AB_2534079
Donkey anti-Rabbit 488	Jackson ImmunoResearch Labs	Cat# 711-546-152; RRID:AB_2340619
Goat anti-Chicken 647	Life Technologies	Cat# A-21449; RRID:AB_2535866
<b>Bacterial and virus strains</b>		
scAAV1-hSyn-Cre	WZ Biosciences (Zingg et al. 2020)	Lot# 20200729
AAV5-hSyn-Con/Foff-EYFP	UNC Vector Core	Lot# AV6151; RRID:Addgene_55651
AAV5-hSyn-Con/Foff-hChr2(H134R)- EYFP	UNC Vector Core	Lot# AV8475; RRID:Addgene_55646
<b>Chemicals, peptides, and recombinant proteins</b>		
Red retrobeads IX	LumaFluor Inc	CAS: 78R180
D-AP5: D-APV	Cayman Chemical	CAS: 79055-68-8
NBQX disodium	Tocris Bioscience	CAS: 479347-86-9
TTX: Tetrodotoxin citrate	Tocris Bioscience	CAS: 18660-81-6
4-AP: 4-Aminopyridine	Tocris Bioscience	CAS: 504-24-5
GBZ: Gabazine: SR 95531 hydrobromide	Tocris Bioscience	CAS: 104104-50-9
QX-314-Cl: Lidocaine N-ethyl chloride	Sigma	CAS: 5369-03-9
TEA-Cl: Tetraethylammonium chloride	Sigma	CAS: 56-34-8
NeuroTrace 435/455	Invitrogen	Cat# N21479
Normal Goat Serum	Jackson ImmunoResearch Labs	RRID:AB_2336990

Fluoromont-G	Southern Biotech	Cat# 0100-01
Isoflurane	Henry Schein	CAS: 26675-46-7
<b>Experimental models: Organisms/strains</b>		
Mouse: VGAT-IRES-Cre: B6J.129S6(FVB)-Slc32a1 <sup>tm2(cre)Lowl</sup> /MwarJ	The Jackson Laboratory	RRID:IMSR_JAX:028862
Mouse: TH-2A-Flpo: C57BL/6N- <i>Th</i> <sup>tm1Awar</sup> /Mmmh	Awatranami Lab (Poulin et al. 2018)	RRID:MMRRC_050618-MU
Mouse: WT: C57BL/6J	The Jackson Laboratory	RRID:IMSR_JAX:000664
<b>Software and algorithms</b>		
MATLAB R2020b	Mathworks	RRID:SCR_001622
Wavesurfer v0.945	HHMI Janelia	RRID:SCR_021529; <a href="https://wavesurfer.janelia.org">https://wavesurfer.janelia.org</a>
ImageJ, FIJI 1.53h	(Schneider et al. 2012)	RRID:SCR_003070; <a href="http://fiji.sc/">http://fiji.sc/</a>
Prism 9	GraphPad	RRID:SCR_002798

## 2.9 Additional Data Sent to Reviewers

This data was not included in the published version of the paper, but I decided to include it here, in case the reader shares these two questions from our reviewers.

Question 1: The authors posit that location of synapses on dopaminergic neurons may be responsible for the differential ability of synapses of similar size to modulate the tonic firing of dopamine neurons, with more proximal synapses having greater ability to directly alter firing. If this is the case, the authors may be able to see evidence of this in the timecourses of their IPSCs – more proximal synapses should have a faster rise and decay time (for example see Straub and Sabatini, Neuron 2016). There are of course caveats with this approach, but it may provide additional evidence for the underlying mechanism.

Our Answer: Thank you for this suggestion. We analyzed the kinetics of our oIPSCs but did not find consistent differences between open and closed loops. This result does not invalidate our hypothesis, however, given that our recording conditions were not ideal to differentiate between proximal and distal synapses based on the IPSC kinetics. We used Cs-based internals with Qx-314 and TEA to achieve the best possible voltage clamping and minimize the effects of dendritic filtering. A potassium-based internal would be more appropriate to detect the hypothesized differences. In our recordings, all circuit configurations have similar rise time and decay time constants (**Figure 10** and **Figure 11**).

Straub and colleagues (Straub et al. 2016) were able to detect significant differences in IPSC kinetics despite using a Cs-based internal with Qx-314 and TEA. However, they had the advantage of studying large differences between distinct presynaptic cell types: LTSIs and FSIs. In our work,

we are dealing with two presumably less distinct presynaptic cell types: DLS-targeted vs DMS-targeted GABAergic cells in SNr. These two “cell types” are not well-characterized subpopulations of the SNr. It is likely that the proximal vs distal targeting of these cells onto DA neurons is more subtle than that of LTSI and FSI inputs onto SPNs. It is also possible, since we are patching a distinct postsynaptic cell (here, SNc DA neurons; in Straub et al, SPNs), that we have less space clamp error in our voltage-clamp recordings.

A more definitive test of the proximal vs distal synapse location hypothesis is desirable. We are currently doing circuit mapping experiments with focal optogenetic stimulation to test our proximal vs distal hypothesis and we plan to include these findings in a subsequent publication.

Question 2: Another potential underlying mechanism for differential ability to modulate firing is that some SNr GABAergic neurons are activating GABAB  $\gamma$ -receptors, or alternatively are releasing a peptide that activates slow inhibitory conductances through GPCRs. This would likely have an effect on dopaminergic neuron firing when stimulated at 20 Hz, but would not be detectable when optically evoking single IPSCs. Experimentally testing this would be beyond the scope of the manuscript, but the authors may have seen evidence of this (or against it) in their data examining 20 Hz trains of IPSCs shown in Figure 9 and it would be worthy of discussion.

Our Answer: This is a great point. In the dataset shown in Figure 9 of the manuscript, we did notice a slow hyperpolarizing current in some of the cells with oIPSCs. There are two examples of such cells in the figure: Figure 9D and Figure 9N. The percentage of cells with this slow baseline shift was comparable across circuit configurations, and therefore unlikely to explain the differences between closed and open loops:

DLS Loop: 3/7 cells (~40%)

DMS Loop: 4/7 cells (~60%)

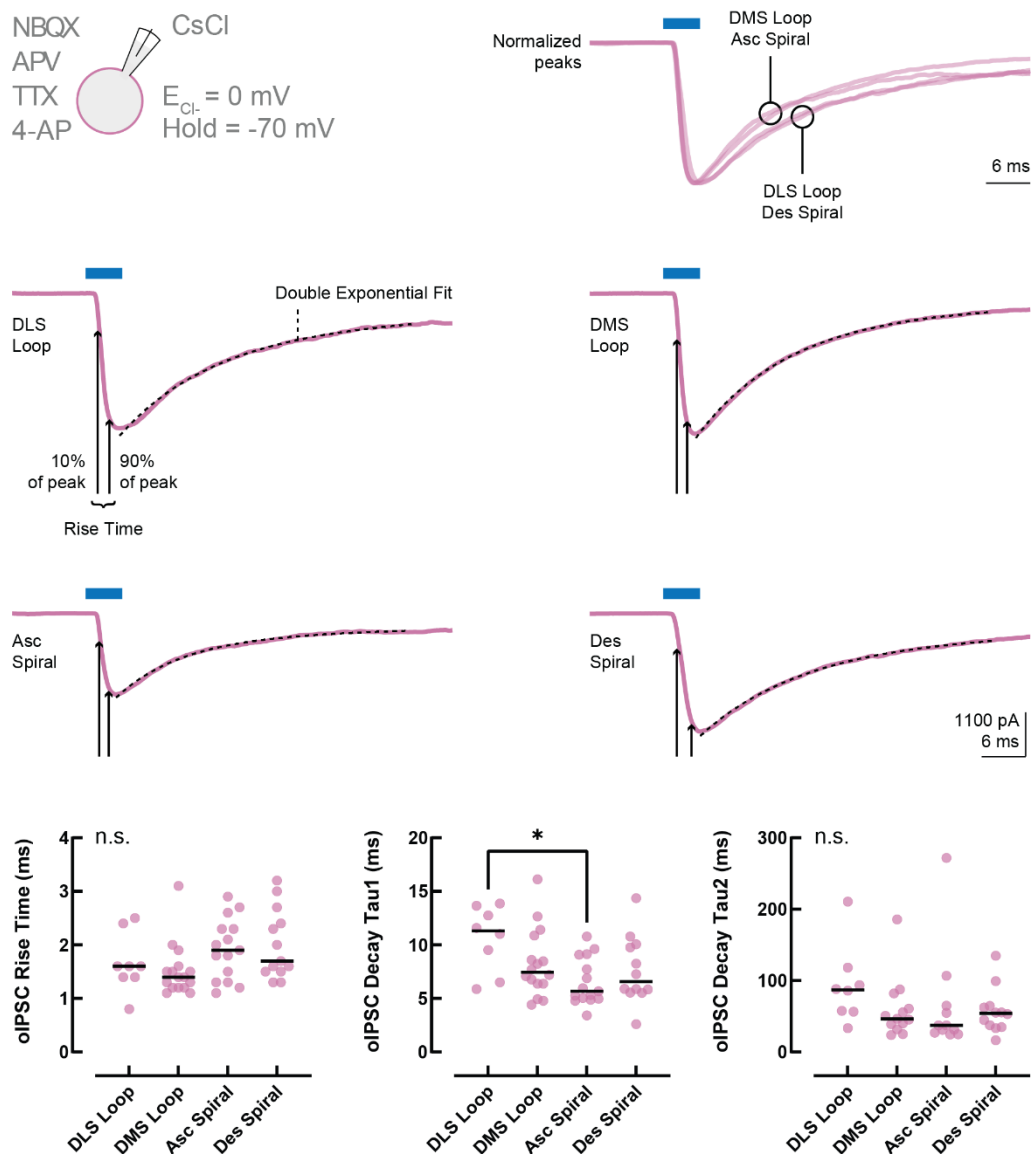
Ascending Spiral: 7/11 cells (~60%)

Descending Spiral: 3/5 (~60%)

Furthermore, this slow current does not seem to be GABAB mediated, given that it goes away with a gabazine wash (again, see example in Figure 9N). A few more example cells are shown in

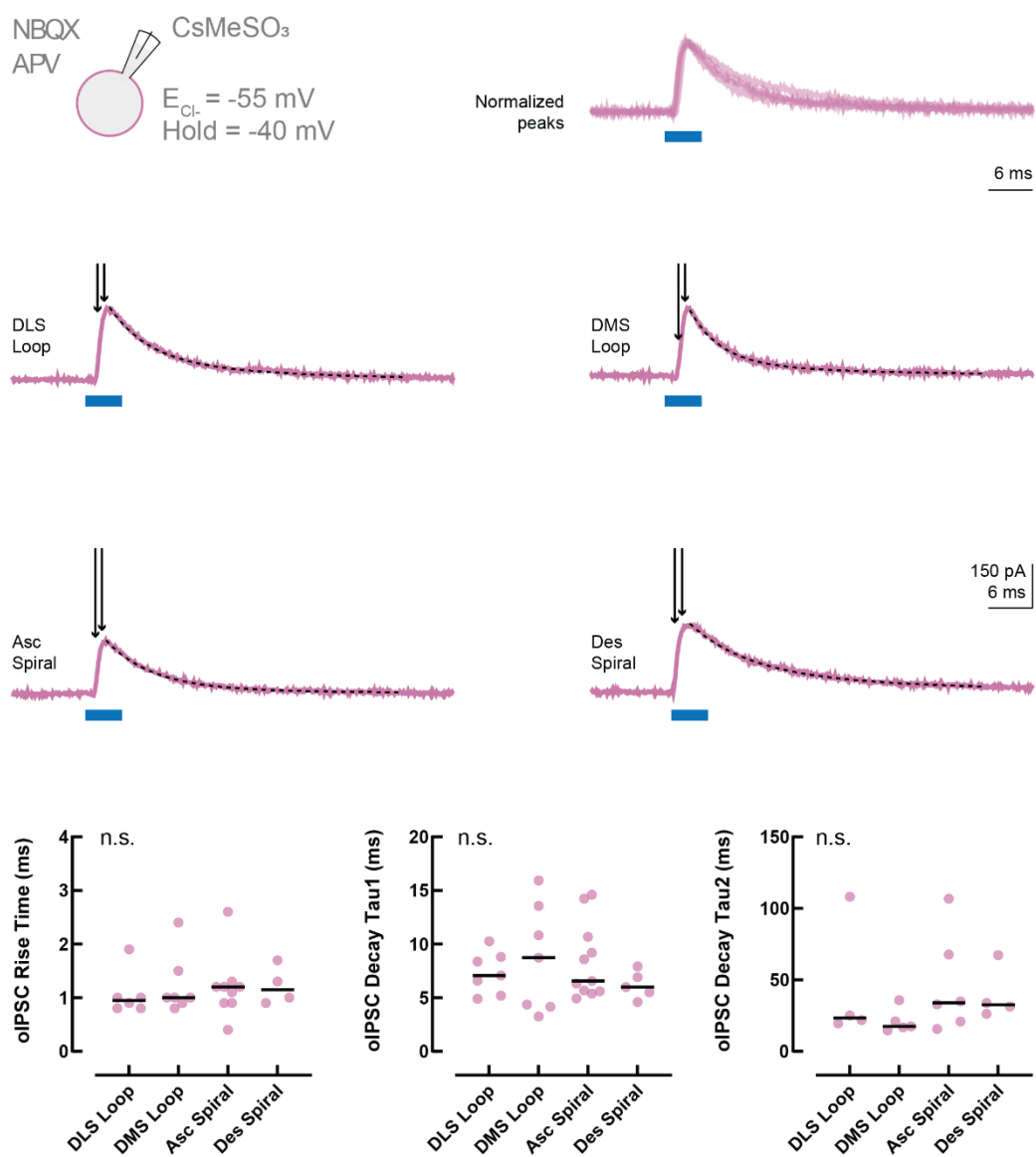
**Figure 12.**

**Figure 10. oIPSC kinetics are not consistently different between open and closed loops (CsCl recordings).**



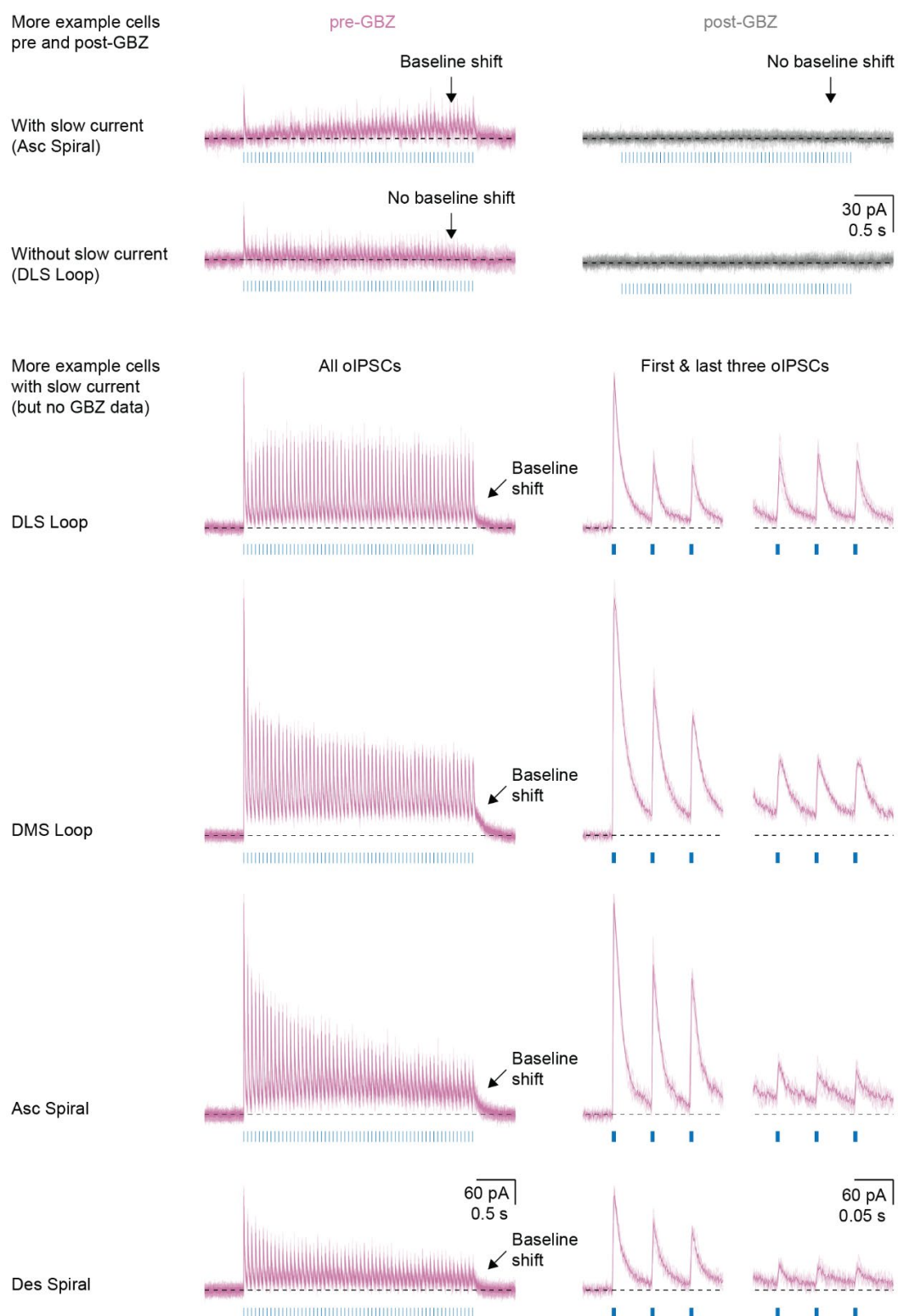
Example cells are shown overlaid on the top right corner. The same cells are shown individually below. Rise time was calculated as the time between 10% and 90% of the peak amplitude. Two decay time constants were calculated based on a double exponential fit (dotted lines). In the summary plots, each dot corresponds to a cell and the horizontal bar is the median. n.s.: not significant (Kruskal-Wallis test). \* $p < 0.05$ , Multiple Comparison Test after Kruskal-Wallis test ( $p < 0.05$ ). We consider the statistically significant difference found here to be physiologically irrelevant, given that it is inconsistent with the rest of the dataset, and it was not reproduced in

**Figure 11. oIPSC kinetics are not consistently different between open and closed loops (CsMeSO<sub>3</sub> recordings).**



Similar arrangement to Figure 10. Note the lack of statistically significant differences between the DLS Loop and the Ascending Spiral in this dataset.

**Figure 12. A GABAAR-mediated slow hyperpolarizing current was found in a subset of cells in all circuit configurations.**



## **Chapter 3 – Dopamine Disinhibition Cannot be Directly Assessed in Midbrain Slices**

In Chapter 2, we showed that closed, but not open, striato-nigro-striatal circuits support dopamine disinhibition. A skeptical reader might frown at the word “support” and ask for a more definite slice experiment testing dopamine disinhibition directly. You do not frown alone, fellow reader, for that was an experiment suggested by reviewers. But what reviewers did not know is that I attempted these experiments long before our paper submission, and they proved to be inadequate at assessing dopamine disinhibition. In this Chapter, I will describe these unpublished experiments.

### **3.1 Activation of DMS Terminals in Substantia Nigra Does NOT Disinhibit DLS-projecting Dopamine Neurons.**

One of the first experiments I did in the Lerner Lab was a direct test of a key ascending spiral prediction. If there is polysynaptic circuit in the form  $DMS \rightarrow SNr \rightarrow SNc \rightarrow DLS$ , then activation of DMS terminals in SN should lead to disinhibition of DLS-projecting dopamine neurons. To test this, I used optogenetics and slice electrophysiology. I injected a virus encoding ChR2 (AAV5-CamKIIa-ChR2-EYFP) into the DMS of adult mice and red retrobeads into the DLS of the same mice (**Figure 13A**). Then, I recorded the firing rate of bead-labeled cells in SNc while optogenetically stimulating neurotransmitter release from DMS terminals. Not surprisingly, many of the recorded cells had their firing rate suppressed by the o-stim (16/31 cells, **Figure 13C**). This result was expected given the known direct connection from striatum to dopamine neurons, although the percentage of connected cells was higher than previously reported (Lerner et al. 2015). This difference could be due to larger spread of the ChR2 virus in striatum, possibly

including some expression in DLS. However, disinhibition of tonic firing was NOT observed in any of the recorded DLS-projecting cells (0/31 cells, **Figure 13C**). As a first pass, this result could be interpreted as evidence against the ascending spiral, but we decided to investigate whether our methodology was appropriate to make such a claim.

### **3.2 Activation of DMS Terminals in Substantia Nigra Inhibits VGAT+ SNr Neurons.**

Our first control experiment was to verify that activation of DMS terminals could inhibit SNr cells in midbrain slices. For disinhibition of DA cells to occur via the circuit DMS→SNr→SNc→DLS, then inhibition of SNr cells must occur via the sub-circuit DMS→SNr. To test this, I injected a virus encoding cre-dependent EYFP (AAV5-hSyn-Con/Foff-EYFP-WPRE) into the SNr of the VGAT-Cre mice and a virus encoding ChrimsonR (AAV5-hSyn-ChrimsonR-tdTomato) into the DMS of the same mice (**Figure 13D**). Then, I recorded the firing rate of EYFP+ cells in SNr while optogenetically stimulating neurotransmitter release from DMS terminals. As expected, almost all of the recorded cells had their firing rate suppressed by the o-stim (13/15 cells, **Figure 13F**). Thus, the subcircuit DMS→SNr is working as expected and does not explain our failure to detect disinhibition of SNc neurons following activation of DMS terminals.

### **3.3 Silencing of SNr Neurons Does NOT Disinhibit DLS-projecting Dopamine Neurons.**

Our next control experiment was to assess the subcircuit SNr→SNc. As described in Chapter 2, optogenetic activation of VGAT+ SNr neurons leads to robust suppression of the tonic firing of DLS-projecting DA neurons (**Figure 4K**). But does the removal of this tonic inhibition from SNr allow DA neurons to fire at higher rates? To test this, I injected a virus encoding the inhibitory opsin NpHR in a cre-dependent basis into the SNr of VGAT-cre mice (AAV5-EF1a-DIO-

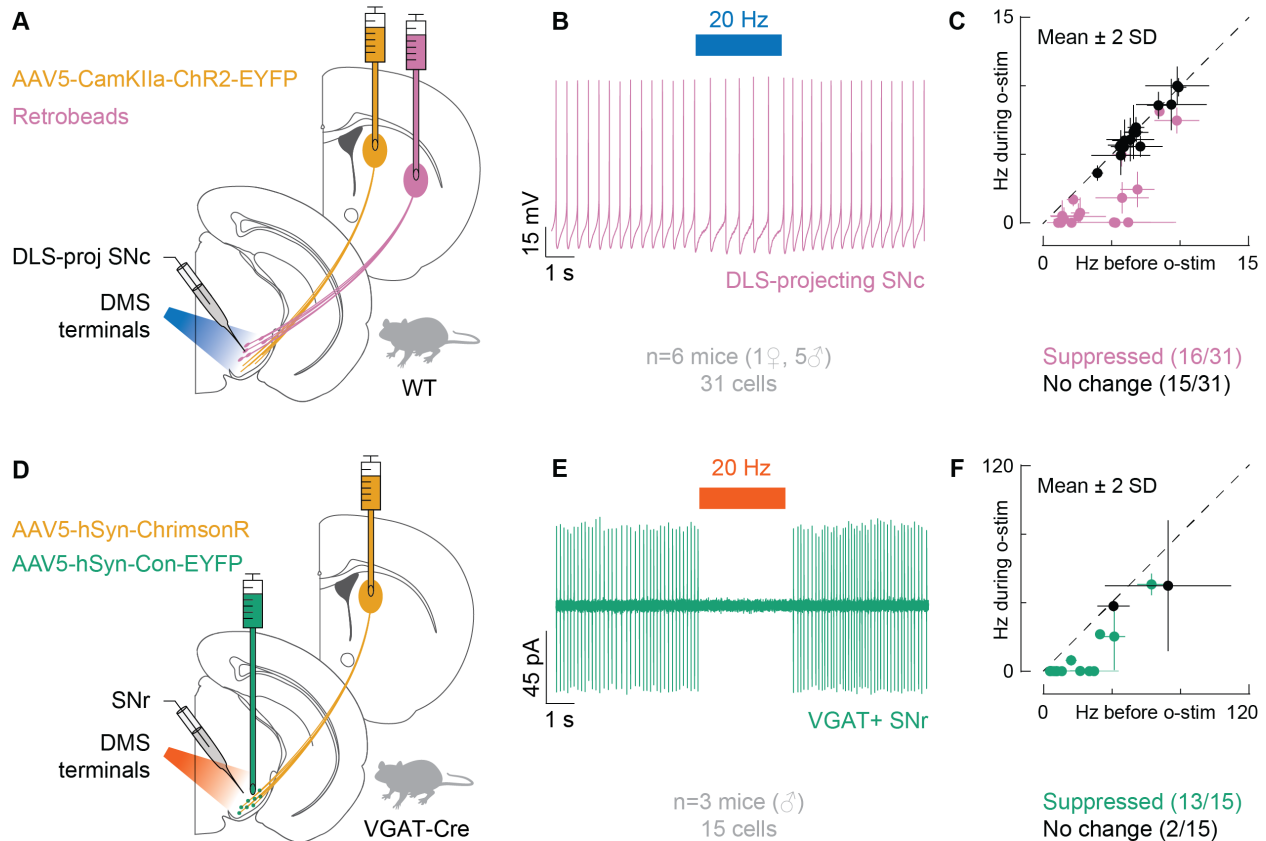
eNpHR3.0-EYFP). I also injected retrobeads into the DLS of the same mice, so I could record from DLS-projecting DA neurons in midbrain slices (**Figure 14A**). As expected, when I recorded from EYFP+ neurons in SNr (which express NpHR), the o-stim robustly suppressed the tonic firing of these cells (6/6 cells, **Figure 14C**). However, when I recorded from bead-labeled cells in the same slices, the tonic firing of these cells was undisturbed (4/4 cells, **Figure 14E**). This led us to consider the possibility that the SNr→SNc subcircuit is not preserved in our slices. While ChR2-expressing terminals can be readily excited to increase neurotransmitter release, NpHR-expressing terminals are not so easily manipulated to reduce neurotransmitter release (Mahn et al. 2016). We hypothesized that SNr axons are severed in our slices and therefore SNr terminals are disconnected from their cell bodies. If that was the case, the tonic activity we recorded from SNr cell bodies is not a good proxy for the rate of neurotransmitter release from SNr terminals. In the absence of action potentials, it is likely that SNr terminals were mostly silent and NpHR activation did not significantly reduce GABA release from these terminals. Thus, the lack of disinhibition of DLS-projecting DA neurons after SNr inhibition or after activation of DMS terminals cannot be interpreted as evidence against the ascending spiral.

### **3.4 Blockage of Inhibitory Transmission Does NOT Disinhibit Dopamine Neurons in Midbrain Slices.**

To further test the SNr→SNc subcircuit in our slices, we opted for a global pharmacological approach. We added gabazine (GBZ) to our ACSF while recording the tonic firing of DA neurons. Notably, we did not record from projection-defined DA neurons in this experiment, but rather from DAT+ neurons in SNc by using the reported line Ai14 crossed to DAT-cre mice (**Figure 15A**).

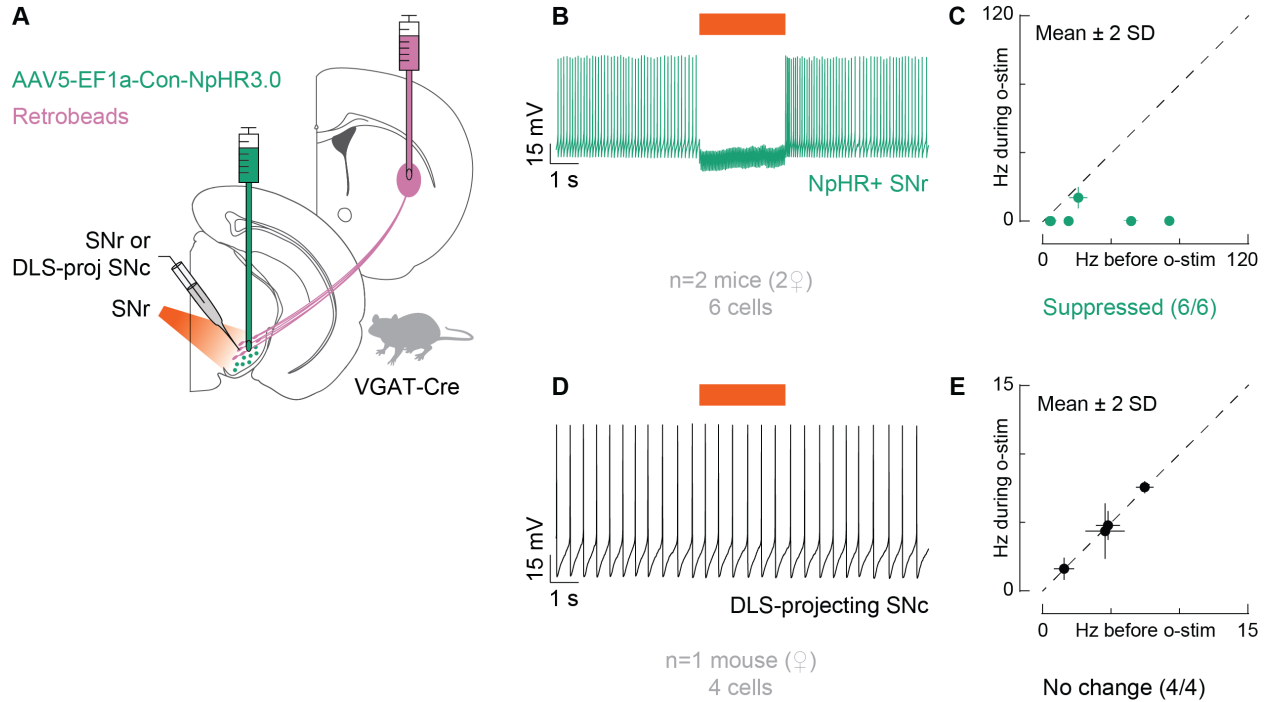
If the SNr→SNc subcircuit is preserved in slice and the tonic firing of DA neurons is constantly suppressed by incoming inhibition, we would expect that GBZ treatment would lead to an increase in the firing rate of DA neurons. Surprisingly, the firing of DA neurons was undisturbed by GBZ treatment (**Figure 15E**), even though mIPSCs were completely abolished (**Figure 15C**). These results strongly suggest that the SNr→SNc subcircuit is NOT preserved in coronal midbrain slices.

**Figure 13. Optogenetic activation of DMS terminals in midbrain slices suppresses the tonic firing of VGAT+ cells in SNr, but does not disinhibit DLS-projecting SNc neurons.**



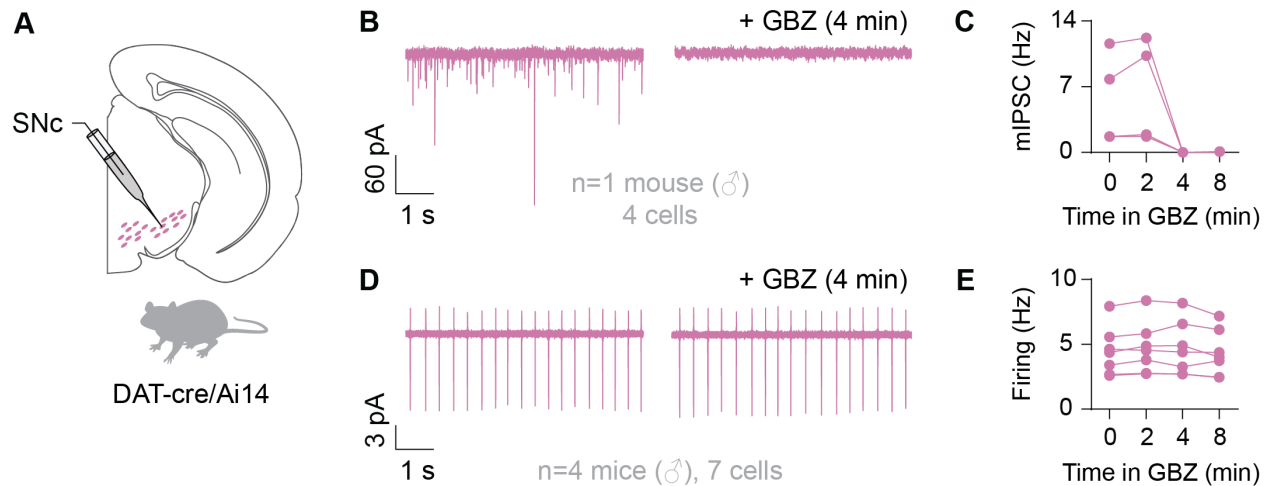
(A) Experimental design for testing a polysynaptic circuit of disinhibition from DMS to DLS-projecting DA neurons. In WT mice, AAV5-CamKIIa-ChR2-EYFP was injected into DMS to deliver the excitatory opsin ChR2 to spiny projection neurons. Retrobeads were injected into DLS to label DLS-projecting DA neurons in SNc for recording. Optogenetic stimulation (o-stim) was delivered via the objective (5 ms at 20 Hz for 3 s, 475 nm,  $\sim$ 10 mW/mm<sup>2</sup>). (B) Example cell (1 out of 10 recorded sweeps). (C) Average firing rate during vs before o-stim for all cells (suppressed cells: magenta; no change: black). Error bars represent  $\pm$ 2SD. Dotted line: unity. (D) Experimental design for assessing the DMS $\rightarrow$ SNr subcircuit. In VGAT-cre mice, AAV5-hSyn-Con/Foff-EYFP-WPRE was injected into the SNr to label VGAT+ cells for recording. AAV5-hSyn-ChrimsonR-tdTomato was injected into DMS to deliver the excitatory opsin ChrimsonR to spiny projection neurons. Optogenetic stimulation (o-stim) was delivered via the objective (5 ms at 20 Hz for 3 s, 572 nm,  $\sim$ 10 mW/mm<sup>2</sup>). (E) Example cell. (F) Average firing rate during vs before o-stim for all cells (suppressed cells: green; no change: black). Error bars represent  $\pm$ 2SD. Dotted line: unity.

**Figure 14. Optogenetic silencing of VGAT+ SNr cells in midbrain slices does not disinhibit DLS-projecting SNc neurons.**



(A) Experimental design for assessing the SNr→SNc subcircuit. In VGAT-cre mice, AAV5-EF1a-DIO-eNpHR3.0-EYFP was injected into SNr to label VGAT+ cells with the inhibitory opsin NpHR. Retrobeads were injected into DLS to label DLS-projecting DA neurons in SNc for recording. Optogenetic stimulation (o-stim) was delivered via the objective (continuous 3 s pulse, 572 nm,  $\sim 10$  mW/mm<sup>2</sup>). (B) Example recording from a VGAT+ cell in SNr (NpHR+). (C) Average firing rate during vs before o-stim for all cells (suppressed cells: green; no change: black). Error bars represent  $\pm 2$ SD. Dotted line: unity. (D) Example recording from a bead-labeled cell in SNc (DLS-projecting). (E) Average firing rate during vs before o-stim for all cells (no change: black). Error bars represent  $\pm 2$ SD. Dotted line: unity.

**Figure 15. Pharmacological blockage of inhibitory transmission does not disinhibit dopamine neurons in midbrain slices.**



(A) Experimental design for assessing the effect of the GABAAR blocker gabazine (GBZ) on the tonic firing of dopamine neurons in SNc. (B) Example recording showing the blockage of all mIPSC by GBZ. (C) mIPSC frequency for all cells after GBZ treatment. (D) Example recording showing the lack of effect of GBZ on the tonic firing of DA neurons. (E) Firing frequency for all cells after GBZ treatment.

### 3.5 Discussion

Given that the SNr→SNc subcircuit is not preserved in midbrain slices, we propose that slice experiments are not appropriate for assessing DA disinhibition mediated by disruptions in SNr activity. Furthermore, the lack of disinhibition of DLS-projecting DA neurons after DMS terminal activation cannot be interpreted as evidence against the ascending spiral hypothesis.

This data is consistent with the complete lack of pair recording data between SNr and SNc cells in the literature. It is also consistent with previous studies reporting great difficulty in finding connected pairs of SNr neurons in slice. SNr axons have long and complex 3-dimensional trees that move across the anterior-posterior axis and follow the onion-like organization of the SNr (Maurin et al. 1999; Maily et al. 2003). All data shown in this chapter was recorded in coronal slices, but similar results were found when slices were cut at different parasagittal angles. It is possible that an ideal slicing configuration exists that would better preserve the SNr→SNc subcircuit, but we decided to further address the question of disinhibition *in vivo*.

### 3.6 Methods

#### *Electrophysiology*

We followed the same methods described in Chapter 2, but firing data from different recording configurations were pooled together, since there were no obvious differences between configurations. Some cells were recorded in cell attached or whole cell mode with a potassium gluconate internal, adjusted to  $290\pm 5$  mOsm and pH 7.3-7.4, containing (in mM): 135 K-gluconate, 10 HEPES, 5 KCl, 4 Mg-ATP, 2 MgCl<sub>2</sub>, 0.1 EGTA, 0.3 Na-GTP. Other cells were recorded in cell attached mode with a HEPES-buffered synthetic interstitial fluid solution (SIF) used as internal solution, adjusted to  $300\pm 5$  mOsm and pH 7.3-7.4, containing (in mM): 140 NaCl, 23 Glucose, 15 HEPES, 3 KCl, 1.5 MgCl<sub>2</sub>, 1.6 CaCl<sub>2</sub>. In some recordings, D-AP5 and NBQX disodium were added to the recording ACSF. Where indicated, GBZ was also added to the ACSF.

For mIPSC recordings, a high chloride internal solution was used, adjusted to  $290\pm 5$  mOsm and pH 7.3-7.4, containing (in mM): 130 CsCl, 1 EGTA, 10 HEPES, 5 QX-314-Cl, 10 TEA-Cl, 2 Mg-ATP, 0.3 Na-GTP. Cells were held at -70 mV and recorded continuously for 8+ min in 30 s sweeps. D-AP5, NBQX disodium and TTX were added to the recording ACSF. Where indicated, GBZ was also added to the ACSF. The data shown in **Figure 15** represents the average mIPSC frequency recorded during 30 s. mIPSCs were detected using a custom-written Python code written by Venus Sherathiya.

## Chapter 4 – *in vivo* Assessment of Open and Closed Striato-Nigro-Striatal Circuits

Besides predicting the existence of a polysynaptic circuit of disinhibition from DMS to DLS-projecting DA neurons, the ascending spiral hypothesis also predicts that DMS activation leads to dopamine release in DLS. Although the data from Chapter 2 suggests that open striato-nigro-striatal circuits are unlikely to support DA disinhibition, the question of whether DMS activation leads to dopamine release in DLS *in vivo* remains unanswered. To start answering this question, we used *in vivo* fiber photometry and optogenetics in awake, freely behaving mice. This chapter includes unpublished data collected by me and my mentee, Ellen C. Coleman. All data are from naïve mice.

### 4.1 Activation of Dopamine Neurons in SNc Leads to Dopamine Release in DLS

To assess dopamine release *in vivo*, we used the dopamine sensor dLight (Patriarchi et al. 2018). To validate our approach, we performed a positive control experiment in which we tested the subcircuit SNc→DLS. First, I injected a virus encoding the excitatory opsin ChrimsonR in a cre-dependent manner (AAV5-hSyn-Flex-ChrimsonR-tdTomato) into the SNc of DAT-cre mice. Then, I placed a fiber optic implant over SN to optogenetically stimulate DA neurons. I also injected a virus encoding dLight (AAV9-CAG-dLight1.3b) into the DLS and implanted a fiber optic over DLS to record dopamine transients in this area in response to the optogenetic stimulation (**Figure 16A**). Mice were placed in an open field box during recordings and received 30-40 1 s light trains (5 ms at 20 Hz, 625 nm, 20 mW) every 30-60 s. As expected, we detected dopamine

release in DLS in response to optogenetic stimulation of DA neurons in SNc (**Figure 16B**), validating our setup.

#### **4.2 Inhibition of SNr Neurons Leads to Dopamine Release in DMS and DLS**

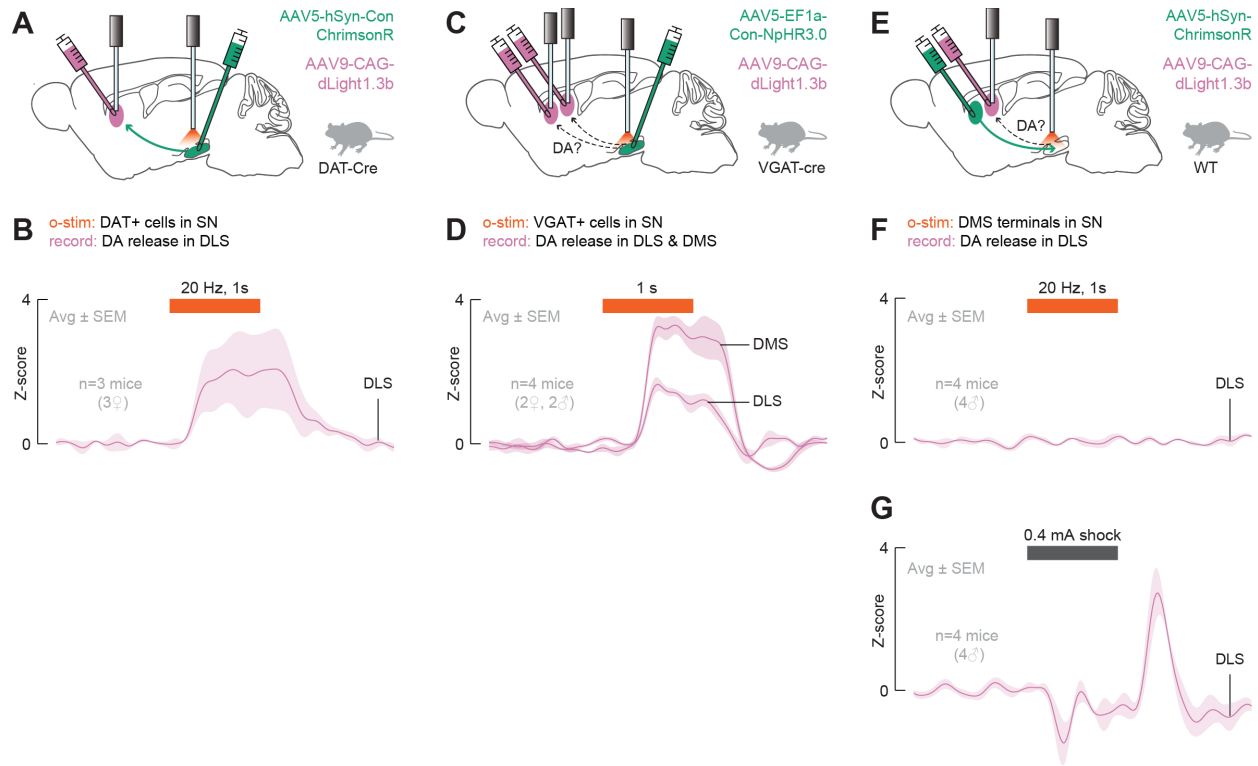
If a circuit in the form DMS→SNr→SNc→DLS mediates dopamine release in DLS, then global inhibition of SNr (not-projection defined) should also lead to dopamine release in DLS. To test this, Ellie injected a virus encoding the inhibitory opsin NpHR (AAV5-EF1a-DIO-eNpHR3.0-EYFP) into the SNr of VGAT-cre mice and she implanted a fiber optic over SNr to optogenetically inhibit VGAT<sup>+</sup> cells in SNr. Ellie also injected a virus encoding dLight (AAV9-CAG-dLight1.3b) into the DLS and DMS of the same mice, and placed fiber optic implants over these areas (**Figure 16C**). Mice were again placed in an open field box during recordings and received 20-30 1 s light pulses (625 nm, 10 mW) every 30-60 s. As expected, we detected dopamine release in DLS and DMS in response to optogenetic inhibition of VGAT<sup>+</sup> neurons in SNr (**Figure 16B**).

#### **4.3 Activation of DMS Terminals in Substantia Nigra is Not Sufficient to Cause Dopamine Release in DLS**

After validating our setup and confirming that a SNr→SNc→DLS circuit is capable of mediating dopamine release in DLS, we set out to test the ascending spiral hypothesis in vivo. If a circuit in the form DMS→SNr→SNc→DLS mediates dopamine release in DLS, then activation of DMS terminals in SN should lead to dopamine release in DLS. To test this, I injected a virus encoding the dopamine sensor dLight (AAV9-CAG-dLight1.3b) into the DLS of adult mice and a virus encoding the excitatory opsin ChrimsonR (AAV5-hSyn-ChrimsonR-tdTomato) into the DMS of the same mice. Then, I placed a fiber optic implant over SN to optogenetically stimulate axon

terminals from DMS in SNr. I also implanted a fiber optic above DLS to measure dopamine transients in this area in response to the optogenetic stimulation (**Figure 16E**). Surprisingly, the activation of terminals from DMS in SN did NOT lead to dopamine transients in DLS (**Figure 16F**). This result is consistent with our ex vivo data and challenges a key prediction from the ascending spiral hypothesis. To rule out the possibility of a negative result due to poor dLight expression in DLS, I tested whether I could detect dopamine transients in DLS in response to a salient stimulus like a foot shock. Mice were placed in an operant chamber in which 10 1 s shocks (0.4 mA) were delivered every 45-90 s. As expected, dopamine transients were detected in all mice in response to the shock (**Figure 16G**), validating our approach.

**Figure 16. *in vivo* fiber photometry controls and test of the ascending spiral hypothesis.**



(A) Experimental design for a positive control experiment. (B) dLight transient in DLS in response to the o-stim (625 nm, 20 mW, 5 ms pulses at 20 Hz for 1 s). (C) Experimental design for testing the SNr→SNc subcircuit. (D) dLight transients in DLS and DMS in response to the o-stim (625 nm, 10 mW, continuous 1 s pulse). (E) Experimental design for testing the ascending spiral hypothesis. (F) dLight transient in DLS in response to the o-stim (625 nm, 20 mW, 5 ms pulses at 20 Hz for 1 s). (G) Control experiment for mice shown in (F) – dLight transient in DLS in response to foot shocks (0.4 mA for 1 s). All data were averaged across mice and across trials (20-40 o-stims/mouse and 10 shocks/mouse). Shaded areas represent  $\pm$  SEM. Data in (D) was collected by Ellen C. Coleman.

#### 4.4 Discussion

Our *in vivo* results are consistent with our *ex vivo* results shown in Chapter 2, but more experiments are required to complete this *in vivo* story. We showed that optogenetic activation of DMS terminals in SN is not sufficient to cause DA release in DLS, challenging the ascending spiral hypothesis. But what about closed loops? According to our *ex vivo* data, activation of DMS or DLS terminals in SN should lead to DA release in DMS and DLS, respectively. Future experiments should test both open and closed loops in the same mice.

More control experiments are also required to further validate our approach. Are our results robust to small changes in fiber optic locations? DMS fibers in SN are relatively ventral, while the cell bodies of SNc neurons are more dorsally located. It is possible that, to reach the DMS fibers, the implant damages the DA neurons that project to DLS. Our positive control experiment shown in **Figure 16A** suggests that the SN implant does not completely damage the SNc→DLS subcircuit, but it could damage the DMS→SNr or the SNr→SNc subcircuit.

One caveat of our experiments testing the SNr→SNc→Striatum subcircuit is that we used VGAT-cre mice to limit opsin expression to VGAT<sup>+</sup> cells in SNr, but some DA neurons in SNc also express VGAT. Thus, it is possible that some DA release in DMS and DLS is not mediated by disinhibition but rather by direct opsin expression. NpHR activation can have paradoxical effects on neuronal firing and lead to excitation of VGAT<sup>+</sup> DA neurons. To account for this caveat, future experiments could use an intersectional approach to limit opsin expression to VGAT<sup>+</sup>, TH-neurons. For instance, a virus encoding NpHR in a CreON, FlpOFF manner could be injected into the SNr of VGAT-cre; TH-Flpo mice.

The robust difference between DMS and DLS dopamine release in response to SNr inhibition was not expected. As previously discussed, it is important to check whether this result is physiologically meaningful or just a consequence of our implant locations. Given the medio-lateral organization of DMS- and DLS-projecting DA neurons, it is possible that moving our optogenetics probe more laterally would lead to larger DA transients in DLS and smaller transients in DMS. If the results are robust, however, they could be explained by local release dynamics in striatum (like heterogeneous expression of the dopamine transporter DAT) or by circuit dynamics in SN. Indeed, our previous *ex vivo* data revealed differences between the SNr→SNc→DMS and SNr→SNc→DLS subcircuits (**Figure 4**). A study using dLight1.3b in rats also showed differences between DA transients in DMS and DLS, with DMS transients having slower kinetics (Wei et al. 2022).

One alternative explanation to our results in **Figure 16F** is that the disinhibitory effects of DMS activation were masked by parallel inhibitory effects. Besides the indirect effect of DMS on DLS-projecting DA neurons via the DMS→SNr→SNc→DLS circuit, DMS also directly inhibits DLS-projecting DA neurons via a DMS→SNc→DLS circuit (**Figure 13C**). Thus, additional experiments are required to fully dissect the effects of DMS activation on DLS dopamine release.

## 4.5 Methods

### *Stereotaxic surgery*

Surgeries were performed as described in Chapter 2 with the following changes. Fiber optics were implanted over the injection sites and secured with Metabond (Parkell) and Flow-it ALC blue light-curing dental epoxy (Pentron). Probes used for optogenetics were assembled in house using fiber optics from Prizmatix (250  $\mu\text{m}$  core, 0.66 NA), while probes used for fiber photometry were from Doric Lenses (400  $\mu\text{m}$ , 0.48 NA). All injections and implants were made unilaterally, on the same hemisphere, and hemispheres were counterbalanced between mice.

### *in vivo fiber photometry and optogenetics*

All recordings were done using components from Doric lenses controlled by a real-time processor from Tucker Davis Technologies (TDT; RZ5P). TDT Synapse was used for data acquisition. 465 nm and 405 nm LED currents were adjusted independently for each mouse and recording session to return a signal between 150-200 mV. Noldus or Synapse were used to trigger optogenetic stimulation from LED drivers (Prizmatix) every  $\sim 1$  min (interval range: 30-90 s). LED power was adjusted to deliver 10-20 mW from the tip of the fiber optic implant. Timestamps for optogenetic stimulation were fed into the real-time processor as TTL pulses for alignment with the photometry data. Data was analyzed using custom-written MATLAB code.

## Chapter 5 – Conclusions and Future Directions

In my thesis proposal from 2019, I planned to answer the following questions:

1 - Is there a polysynaptic circuit of disinhibition from DMS to DLS-projecting DA neurons?

2 - Does activation of DMS lead to DA release in DLS *in vivo*?

3 - Does habit training change the activity and/or synaptic connections of DLS-projecting DA neurons?

Question 1 grew far beyond its humbling beginnings, and it was really where the bulk of my time and energy were spent. Instead of characterizing one circuit, I characterized four – two spirals and two loops. And I did it twice, because a new, better version of the Cre virus I was using was published in 2020 (Zingg et al. 2020), and I repeated my experiments with this virus. The answer? It's complicated.

A polysynaptic circuit in the form DMS→SNr→SNc→DLS exists in the naïve mouse brain, but this circuit does not support disinhibition of DA neurons. Thus, one of the key predictions of the ascending spiral hypothesis is only half-right. Closed striato-nigro-striatal circuits, on the other hand, support disinhibition. From these observations, a new question emerged:

4 – What explains the differences between open and closed loops?

With the experiments shown in Chapter 2, we ruled out many possible explanations, including intrinsic properties and presynaptic release probabilities, but we did not answer this new question. We hypothesized that the sub-cellular organization of SNr synapses onto DA neurons could

explain these differences and we are currently testing this hypothesis with ChR2-Assisted Circuit Mapping (CRACM). Our results are still preliminary and did not make it into a full chapter in this dissertation, but I am excited to dig into this new data (**Figure 17**).

Question 2 is also under further investigation. Many unexpected issues with viruses slowed down our progress in answering this question, but this project is now in the very talented hands of my mentee, Ellie Coleman. As shown in Chapter 4, our preliminary *in vivo* results are consistent with the *ex vivo* data from Chapter 2. Although inhibition of SNr neurons leads to DA release in DLS (confirming a disinhibitory effect from the subcircuit SNr→SNc→DLS), activation of DMS terminals in SN does not (challenging the disinhibitory effect of the ascending spiral). Future experiments will use a similar viral approach from the one used in Chapter 2 to test open and closed loops *in vivo* in the same mice (**Figure 18A**).

What about question 3? I attempted to start answering question 3 using the techniques described in Chapter 3. More specifically, I tested if DLS-projecting DA neurons were disinhibited by the activation of DMS terminals in midbrain slices from both naïve and habit-trained mice. Unfortunately, as discussed in chapter 3, the SNr→SNc subcircuit is not preserved in midbrain slices. Thus, this technique is inadequate for assessing the full DMS→SNr→SNc→DLS circuit. Not surprisingly, I did not observe disinhibition in habit-trained mice, but this data is not a valid answer to question 3. One could repeat the experiments from Chapter 2 in habit-trained mice, but that would be a very time-consuming endeavor. In the short term, we are planning to answer question 3 with *in vivo* fiber photometry experiments, which allow us to assess striato-nigrostriatal circuits before and after habit training in the same mice (**Figure 18BC**). The results of these

in vivo experiments will guide a more focused search for underlying synaptic mechanisms using slice electrophysiology.

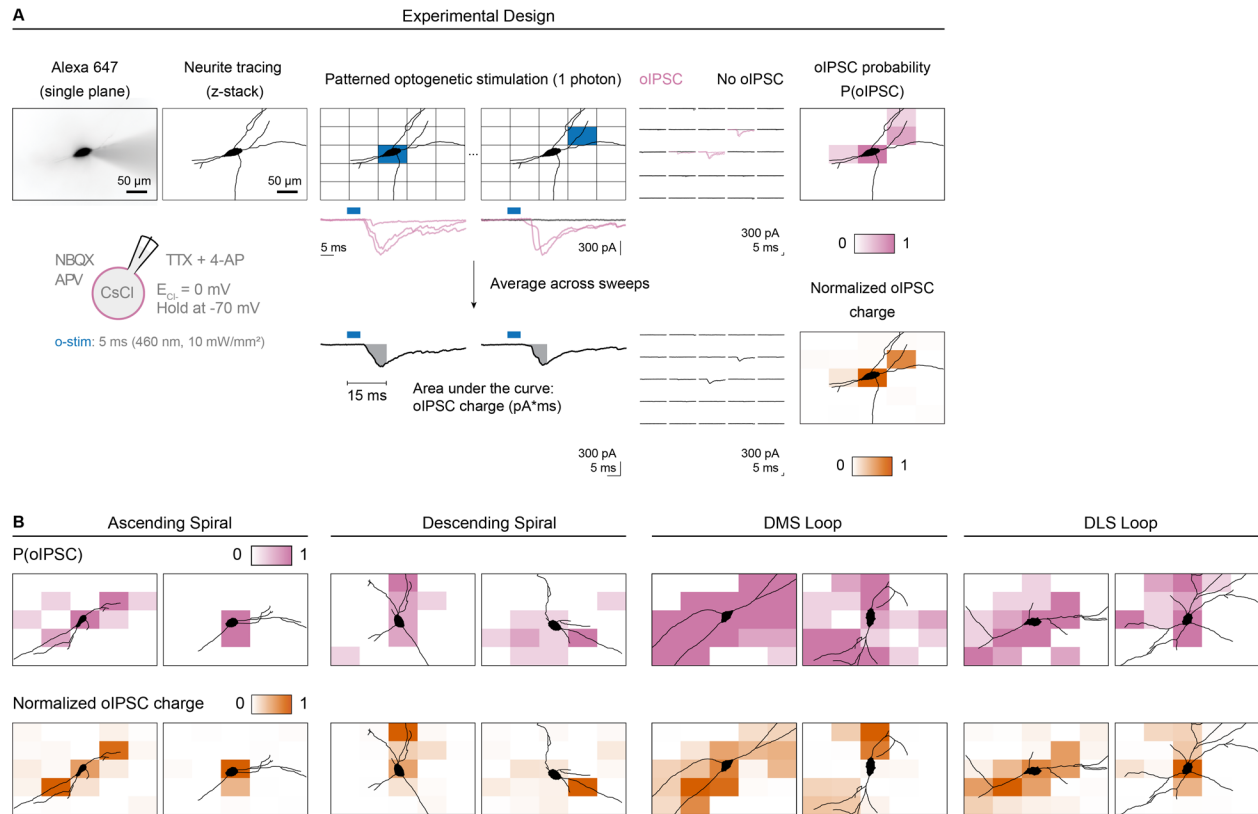
Many other questions emerged from this project, but there is one question in particular I need to address: what are the implications of our findings to the habit formation literature? Briefly, we confirmed the existence of a long hypothesized basal ganglia circuit – the ascending spiral – which is thought to connect activity in DMS to dopamine release in DLS, and promote habit formation. Although we confirmed the existence of a DMS→SNr→SNc→DLS circuit, we also showed that this circuit *per se* does NOT connect activity in DMS to dopamine release in DLS. Thus, our data challenges this putative mechanism of habit formation.

If DA-dependent plasticity in DLS is required for habit formation, the underlying mechanisms controlling this DA release in DLS remain unknown. One exciting possibility is that the ascending spiral works together with other circuits to regulate the activity of DLS-projecting DA neurons. The removal of shunting inhibition via the ascending spiral could be the deciding factor that allows these DA neurons to burst in response to excitatory inputs. The need for excitatory inputs could also explain our negative results in Chapter 4 (**Figure 16F**), since we activated DMS terminals at random, while mice were exploring an open field box, and not coincidentally with a salient stimulus or action that might be required to trigger excitatory inputs onto DLS-projecting DA neurons. Future experiments will address whether open striato-nigro-striatal circuits contribute to the integration of synaptic inputs onto DA neurons.

Another key contribution of this project to the literature is the confirmation of the existence of a descending spiral in the form DLS→SNr→SNc→DMS. This circuit can no longer be ignored by

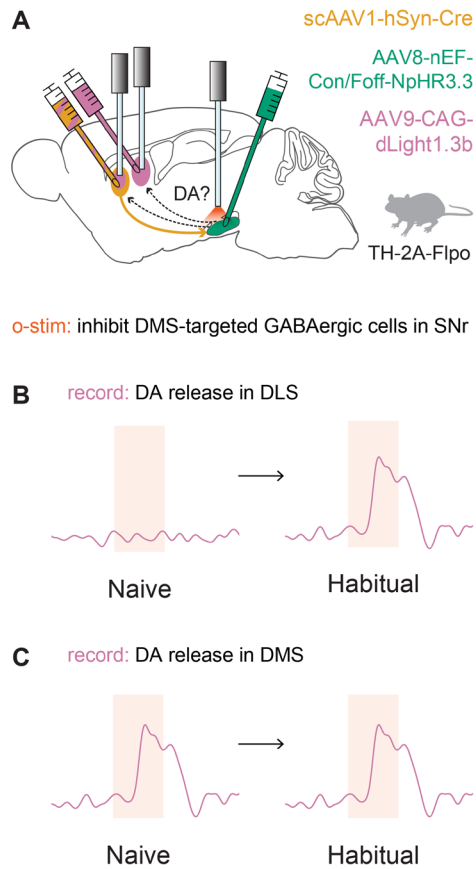
studies investigating information transfer between DMS and DLS, since it is as strong as the ascending spiral in naïve mice.

**Figure 17. Testing if synapse location explains the differences between closed and open striato-nigro-striatal circuits using sCRACM.**



(A) Experimental design. A digital mirror device (DMD) was used to illuminate a small sub-cellular compartment of the recorded cell instead of the whole field of view. The organization of the SNr inputs onto the DA neuron is represented by the spatial pattern of optogenetically-evoked inhibitory postsynaptic currents (oIPSCs). (B) Example cells from different striato-nigro-striatal circuits.

**Figure 18. Testing closed and open striato-nigro-striatal circuits in vivo.**



(A) Experimental design. (B-C) Predicted results for open (B) and closed (C) loops.

## References

- Alexander GE, DeLong MR, Strick PL (1986) Parallel Organization of Functionally Segregated Circuits Linking Basal Ganglia and Cortex. *Annual Review of Neuroscience* 9(1):357–381. <https://doi.org/10.1146/annurev.ne.09.030186.002041>
- Ambrosi P, Lerner TN (2022) Striatonigrostriatal circuit architecture for disinhibition of dopamine signaling. *Cell Reports* 40(7). <https://doi.org/10.1016/j.celrep.2022.111228>
- Aoki S, Smith JB, Li H, Yan X, Igarashi M, Coulon P, Wickens JR, Ruigrok TJ, Jin X (2019) An open cortico-basal ganglia loop allows limbic control over motor output via the nigrothalamic pathway. *eLife* 8:e49995. <https://doi.org/10.7554/eLife.49995>
- Belin D, Everitt BJ (2008) Cocaine Seeking Habits Depend upon Dopamine-Dependent Serial Connectivity Linking the Ventral with the Dorsal Striatum. *Neuron* 57(3):432–441. <https://doi.org/10.1016/j.neuron.2007.12.019>
- Braitenberg Valentino (1986) *Vehicles : experiments in synthetic psychology*, 1st MIT Press pbk. ed. MIT Press, Cambridge, Mass
- Brown HD, McCutcheon JE, Cone JJ, Ragozzino ME, Roitman MF (2011) Primary food reward and reward-predictive stimuli evoke different patterns of phasic dopamine signaling throughout the striatum. *Eur J Neurosci* 34(12):1997–2006. <https://doi.org/10.1111/j.1460-9568.2011.07914.x>
- Burke DA, Rotstein HG, Alvarez VA (2017) Striatal Local Circuitry: A New Framework for Lateral Inhibition. *Neuron* 96(2):267–284. <https://doi.org/10.1016/j.neuron.2017.09.019>
- Cai Y, Ford CP (2018) Dopamine Cells Differentially Regulate Striatal Cholinergic Transmission across Regions through Corelease of Dopamine and Glutamate. *Cell Reports* 25(11):3148–3157.e3. <https://doi.org/10.1016/j.celrep.2018.11.053>
- Chevalier G, Vacher S, Deniau JM, Desban M (1985) Disinhibition as a basic process in the expression of striatal functions. I. The striato-nigral influence on tecto-spinal/tecto-diencephalic neurons. *Brain Research* 334(2):215–226. [https://doi.org/10.1016/0006-8993\(85\)90213-6](https://doi.org/10.1016/0006-8993(85)90213-6)
- Corbit LH, Nie H, Janak PH (2012) Habitual alcohol seeking: time course and the contribution of subregions of the dorsal striatum. *Biol Psychiatry* 72(5):389–395. <https://doi.org/10.1016/j.biopsych.2012.02.024>
- Crittenden JR, Tillberg PW, Riad MH, Shima Y, Gerfen CR, Curry J, Housman DE, Nelson SB, Boyden ES, Graybiel AM (2016) Striosome–dendron bouquets highlight a unique

- striatonigral circuit targeting dopamine-containing neurons. *Proceedings of the National Academy of Sciences* 113(40):11318–11323. <https://doi.org/10.1073/pnas.1613337113>
- Derusso AL, Fan D, Gupta J, Shelest O, Costa RM, Yin HH (2010) Instrumental uncertainty as a determinant of behavior under interval schedules of reinforcement. *Front Integr Neurosci* 4. <https://doi.org/10.3389/fnint.2010.00017>
- Dickinson A (1985) Actions and Habits: The Development of Behavioural Autonomy. *Philosophical Transactions of the Royal Society of London Series B, Biological Sciences* 308(1135):67–78
- Dickinson A, Nicholas DJ, Adams CD (1983) The effect of the instrumental training contingency on susceptibility to reinforcer devaluation. *The Quarterly Journal of Experimental Psychology Section B* 35(1):35–51. <https://doi.org/10.1080/14640748308400912>
- Dorst MC, Tokarska A, Zhou M, Lee K, Stagkourakis S, Broberger C, Masmanidis S, Silberberg G (2020) Polysynaptic inhibition between striatal cholinergic interneurons shapes their network activity patterns in a dopamine-dependent manner. *Nature Communications* 11(1):5113. <https://doi.org/10.1038/s41467-020-18882-y>
- Drummond N, Niv Y (2020) Model-based decision making and model-free learning. *Current Biology* 30(15):R860–R865. <https://doi.org/10.1016/j.cub.2020.06.051>
- Evans RC, Twedell EL, Zhu M, Ascencio J, Zhang R, Khaliq ZM (2020) Functional Dissection of Basal Ganglia Inhibitory Inputs onto Substantia Nigra Dopaminergic Neurons. *Cell Reports* 32(11):108156. <https://doi.org/10.1016/j.celrep.2020.108156>
- Evans RC, Zhu M, Khaliq ZM (2017) Dopamine Inhibition Differentially Controls Excitability of Substantia Nigra Dopamine Neuron Subpopulations through T-Type Calcium Channels. *J Neurosci* 37(13):3704–3720. <https://doi.org/10.1523/JNEUROSCI.0117-17.2017>
- Farassat N, Costa KM, Stojanovic S, Albert S, Kovacheva L, Shin J, Egger R, Somayaji M, Duvarci S, Schneider G, Roeper J (2019) In vivo functional diversity of midbrain dopamine neurons within identified axonal projections. *eLife* 8:e48408. <https://doi.org/10.7554/eLife.48408>
- Faure A, Haberland U, Condé F, Massioui NE (2005) Lesion to the Nigrostriatal Dopamine System Disrupts Stimulus-Response Habit Formation. *J Neurosci* 25(11):2771–2780. <https://doi.org/10.1523/JNEUROSCI.3894-04.2005>
- Fenno LE, Mattis J, Ramakrishnan C, Hyun M, Lee SY, He M, Tucciarone J, Selimbeyoglu A, Berndt A, Grosenick L, Zalocusky KA, Bernstein H, Swanson H, Perry C, Diester I, Boyce FM, Bass CE, Neve R, Huang ZJ, Deisseroth K (2014) Targeting cells with single vectors using multiple-feature Boolean logic. *Nat Methods* 11(7):763–772. <https://doi.org/10.1038/nmeth.2996>

- Ferster CB, Skinner BF (1957) Schedules of reinforcement. Appleton-Century-Crofts, East Norwalk, CT, US
- Fino E, Vandecasteele M, Perez S, Saudou F, Venance L (2018) Region-specific and state-dependent action of striatal GABAergic interneurons. *Nature Communications* 9(1):3339. <https://doi.org/10.1038/s41467-018-05847-5>
- Freeze BS, Kravitz AV, Hammack N, Berke JD, Kreitzer AC (2013) Control of Basal Ganglia Output by Direct and Indirect Pathway Projection Neurons. *J Neurosci* 33(47):18531–18539. <https://doi.org/10.1523/JNEUROSCI.1278-13.2013>
- Gerfen CR, Herkenham M, Thibault J (1987) The neostriatal mosaic: II. Patch- and matrix-directed mesostriatal dopaminergic and non-dopaminergic systems. *J Neurosci* 7(12):3915–3934. <https://doi.org/10.1523/JNEUROSCI.07-12-03915.1987>
- Grace AA, Bunney BS (1983) Intracellular and extracellular electrophysiology of nigral dopaminergic neurons—1. Identification and characterization. *Neuroscience* 10(2):301–315. [https://doi.org/10.1016/0306-4522\(83\)90135-5](https://doi.org/10.1016/0306-4522(83)90135-5)
- Gremel CM, Costa RM (2013) Orbitofrontal and striatal circuits dynamically encode the shift between goal-directed and habitual actions. *Nature Communications* 4(1):2264. <https://doi.org/10.1038/ncomms3264>
- Gulácsi A, Lee CR, Sík A, Viitanen T, Kaila K, Tepper JM, Freund TF (2003) Cell Type-Specific Differences in Chloride-Regulatory Mechanisms and GABAA Receptor-Mediated Inhibition in Rat Substantia Nigra. *J Neurosci* 23(23):8237–8246. <https://doi.org/10.1523/JNEUROSCI.23-23-08237.2003>
- Haber SN, Fudge JL, McFarland NR (2000) Striatonigrostriatal Pathways in Primates Form an Ascending Spiral from the Shell to the Dorsolateral Striatum. *J Neurosci* 20(6):2369–2382. <https://doi.org/10.1523/JNEUROSCI.20-06-02369.2000>
- Hamid AA, Frank MJ, Moore CI (2021) Wave-like dopamine dynamics as a mechanism for spatiotemporal credit assignment. *Cell* 184(10):2733–2749.e16. <https://doi.org/10.1016/j.cell.2021.03.046>
- Hollis ER, Kadoya K, Hirsch M, Samulski RJ, Tuszynski MH (2008) Efficient Retrograde Neuronal Transduction Utilizing Self-complementary AAV1. *Molecular Therapy* 16(2):296–301. <https://doi.org/10.1038/sj.mt.6300367>
- Holly EN, Davatolhagh MF, Choi K, Alabi OO, Vargas Cifuentes L, Fuccillo MV (2019) Striatal Low-Threshold Spiking Interneurons Regulate Goal-Directed Learning. *Neuron* 103(1):92–101.e6. <https://doi.org/10.1016/j.neuron.2019.04.016>

- Ikemoto S (2007) Dopamine reward circuitry: Two projection systems from the ventral midbrain to the nucleus accumbens–olfactory tubercle complex. *Brain Research Reviews* 56(1):27–78. <https://doi.org/10.1016/j.brainresrev.2007.05.004>
- Joel D, Weiner I (2000) The connections of the dopaminergic system with the striatum in rats and primates: an analysis with respect to the functional and compartmental organization of the striatum. *Neuroscience* 96(3):451–474. [https://doi.org/10.1016/S0306-4522\(99\)00575-8](https://doi.org/10.1016/S0306-4522(99)00575-8)
- Khakh BS (2019) Astrocyte-Neuron Interactions in the Striatum: Insights on Identity, Form, and Function. *Trends Neurosci* 42(9):617–630. <https://doi.org/10.1016/j.tins.2019.06.003>
- Khirug S, Yamada J, Afzalov R, Voipio J, Khiroug L, Kaila K (2008) GABAergic Depolarization of the Axon Initial Segment in Cortical Principal Neurons Is Caused by the Na-K-2Cl Cotransporter NKCC1. *Journal of Neuroscience* 28(18):4635–4639. <https://doi.org/10.1523/JNEUROSCI.0908-08.2008>
- Kramer PF, Twedell EL, Shin JH, Zhang R, Khaliq ZM (2020) Axonal mechanisms mediating  $\gamma$ -aminobutyric acid receptor type A (GABA-A) inhibition of striatal dopamine release. *eLife* 9:e55729. <https://doi.org/10.7554/eLife.55729>
- Lammel S, Hetzel A, Häckel O, Jones I, Liss B, Roeper J (2008) Unique Properties of Mesoprefrontal Neurons within a Dual Mesocorticolimbic Dopamine System. *Neuron* 57(5):760–773. <https://doi.org/10.1016/j.neuron.2008.01.022>
- Lammel S, Ion DI, Roeper J, Malenka RC (2011) Projection-Specific Modulation of Dopamine Neuron Synapses by Aversive and Rewarding Stimuli. *Neuron* 70(5):855–862. <https://doi.org/10.1016/j.neuron.2011.03.025>
- Lee J, Wang W, Sabatini BL (2020) Anatomically segregated basal ganglia pathways allow parallel behavioral modulation. *Nature Neuroscience* 23(11):1388–1398. <https://doi.org/10.1038/s41593-020-00712-5>
- Lerner TN (2020) Interfacing behavioral and neural circuit models for habit formation. *Journal of Neuroscience Research* 98(6):1031–1045. <https://doi.org/10.1002/jnr.24581>
- Lerner TN, Shilyansky C, Davidson TJ, Evans KE, Beier KT, Zalocusky KA, Crow AK, Malenka RC, Luo L, Tomer R, Deisseroth K (2015) Intact-Brain Analyses Reveal Distinct Information Carried by SNc Dopamine Subcircuits. *Cell* 162(3):635–647. <https://doi.org/10.1016/j.cell.2015.07.014>
- Lipton DM, Gonzales BJ, Citri A (2019) Dorsal Striatal Circuits for Habits, Compulsions and Addictions. *Front Syst Neurosci* 13. <https://doi.org/10.3389/fnsys.2019.00028>
- Liu C, Goel P, Kaeser PS (2021) Spatial and temporal scales of dopamine transmission. *Nature Reviews Neuroscience* 22(6):345–358. <https://doi.org/10.1038/s41583-021-00455-7>

- Lobb CJ, Troyer TW, Wilson CJ, Paladini CA (2011) Disinhibition Bursting of Dopaminergic Neurons. *Front Syst Neurosci* 5. <https://doi.org/10.3389/fnsys.2011.00025>
- Lüscher C, Robbins TW, Everitt BJ (2020) The transition to compulsion in addiction. *Nature Reviews Neuroscience* 21(5):247–263. <https://doi.org/10.1038/s41583-020-0289-z>
- Mahn M, Prigge M, Ron S, Levy R, Yizhar O (2016) Biophysical constraints of optogenetic inhibition at presynaptic terminals. *Nat Neurosci* 19(4):554–556. <https://doi.org/10.1038/nn.4266>
- Mailly P, Charpier S, Menetrey A, Deniau J-M (2003) Three-Dimensional Organization of the Recurrent Axon Collateral Network of the Substantia Nigra Pars Reticulata Neurons in the Rat. *J Neurosci* 23(12):5247–5257. <https://doi.org/10.1523/JNEUROSCI.23-12-05247.2003>
- Mandelbaum G, Taranda J, Haynes TM, Hochbaum DR, Huang KW, Hyun M, Umadevi Venkataraju K, Straub C, Wang W, Robertson K, Osten P, Sabatini BL (2019) Distinct Cortical-Thalamic-Striatal Circuits through the Parafascicular Nucleus. *Neuron* 102(3):636-652.e7. <https://doi.org/10.1016/j.neuron.2019.02.035>
- Matsuda W, Furuta T, Nakamura KC, Hioki H, Fujiyama F, Arai R, Kaneko T (2009) Single Nigrostriatal Dopaminergic Neurons Form Widely Spread and Highly Dense Axonal Arborizations in the Neostriatum. *J Neurosci* 29(2):444–453. <https://doi.org/10.1523/JNEUROSCI.4029-08.2009>
- Maurin Y, Banrezes B, Menetrey A, Mailly P, Deniau JM (1999) Three-dimensional distribution of nigrostriatal neurons in the rat: relation to the topography of striatonigral projections. *Neuroscience* 91(3):891–909. [https://doi.org/10.1016/S0306-4522\(98\)00681-2](https://doi.org/10.1016/S0306-4522(98)00681-2)
- McElvain LE, Chen Y, Moore JD, Brigidi GS, Bloodgood BL, Lim BK, Costa RM, Kleinfeld D (2021) Specific populations of basal ganglia output neurons target distinct brain stem areas while collateralizing throughout the diencephalon. *Neuron* 109(10):1721-1738.e4. <https://doi.org/10.1016/j.neuron.2021.03.017>
- Menegas W, Bergan JF, Ogawa SK, Isogai Y, Umadevi Venkataraju K, Osten P, Uchida N, Watabe-Uchida M (2015) Dopamine neurons projecting to the posterior striatum form an anatomically distinct subclass. *eLife* 4:e10032. <https://doi.org/10.7554/eLife.10032>
- Mohebi A, Pettibone JR, Hamid AA, Wong J-MT, Vinson LT, Patriarchi T, Tian L, Kennedy RT, Berke JD (2019) Dissociable dopamine dynamics for learning and motivation. *Nature* 570(7759):65–70. <https://doi.org/10.1038/s41586-019-1235-y>
- Oyama Susan (1985) *The ontogeny of information : developmental systems and evolution.* Cambridge University Press, Cambridge ;

- Patriarchi T, Cho JR, Merten K, Howe MW, Marley A, Xiong W-H, Folk RW, Broussard GJ, Liang R, Jang MJ, Zhong H, Dombeck D, von Zastrow M, Nimmerjahn A, Gradinaru V, Williams JT, Tian L (2018) Ultrafast neuronal imaging of dopamine dynamics with designed genetically encoded sensors. *Science* 360(6396):eaat4422. <https://doi.org/10.1126/science.aat4422>
- Petreanu L, Mao T, Sternson SM, Svoboda K (2009) The subcellular organization of neocortical excitatory connections. *Nature* 457(7233):1142–1145. <https://doi.org/10.1038/nature07709>
- Poulin J-F, Caronia G, Hofer C, Cui Q, Helm B, Ramakrishnan C, Chan CS, Dombeck DA, Deisseroth K, Awatramani R (2018) Mapping projections of molecularly defined dopamine neuron subtypes using intersectional genetic approaches. *Nature Neuroscience* 21(9):1260–1271. <https://doi.org/10.1038/s41593-018-0203-4>
- Poulin J-F, Gaertner Z, Moreno-Ramos OA, Awatramani R (2020) Classification of Midbrain Dopamine Neurons Using Single-Cell Gene Expression Profiling Approaches. *Trends in Neurosciences* 43(3):155–169. <https://doi.org/10.1016/j.tins.2020.01.004>
- Rahmati N, Normoyle KP, Glykys J, Dzhala VI, Lillis KP, Kahle KT, Raiyyani R, Jacob T, Staley KJ (2021) Unique actions of GABA arising from cytoplasmic chloride microdomains. *J Neurosci*. <https://doi.org/10.1523/JNEUROSCI.3175-20.2021>
- Robbins TW, Costa RM (2017) Habits. *Current Biology* 27(22):R1200–R1206. <https://doi.org/10.1016/j.cub.2017.09.060>
- Schneider CA, Rasband WS, Eliceiri KW (2012) NIH Image to ImageJ: 25 years of image analysis. *Nat Methods* 9(7):671–675. <https://doi.org/10.1038/nmeth.2089>
- Seiler JL, Cosme CV, Sherathiya VN, Schaid MD, Bianco JM, Bridgemohan AS, Lerner TN (2022) Dopamine signaling in the dorsomedial striatum promotes compulsive behavior. *Current Biology* 32(5):1175–1188.e5. <https://doi.org/10.1016/j.cub.2022.01.055>
- Sommer WH, Costa RM, Hansson AC (2014) Dopamine systems adaptation during acquisition and consolidation of a skill. *Front Integr Neurosci* 8:87. <https://doi.org/10.3389/fnint.2014.00087>
- Straub C, Saulnier JL, Bègue A, Feng DD, Huang KW, Sabatini BL (2016) Principles of Synaptic Organization of GABAergic Interneurons in the Striatum. *Neuron* 92(1):84–92. <https://doi.org/10.1016/j.neuron.2016.09.007>
- Tarfa RA, Evans RC, Khaliq ZM (2017) Enhanced Sensitivity to Hyperpolarizing Inhibition in Mesoaccumbal Relative to Nigrostriatal Dopamine Neuron Subpopulations. *J Neurosci* 37(12):3311–3330. <https://doi.org/10.1523/JNEUROSCI.2969-16.2017>

- Tepper JM, Lee CR (2007) GABAergic control of substantia nigra dopaminergic neurons. In: Tepper JM, Abercrombie ED, Bolam JP (eds) *Progress in Brain Research*. Elsevier, pp 189–208
- Tepper JM, Martin LP, Anderson DR (1995) GABAA receptor-mediated inhibition of rat substantia nigra dopaminergic neurons by pars reticulata projection neurons. *J Neurosci* 15(4):3092–3103. <https://doi.org/10.1523/JNEUROSCI.15-04-03092.1995>
- Thompson RF (2005) In Search of Memory Traces. *Annu Rev Psychol* 56(1):1–23. <https://doi.org/10.1146/annurev.psych.56.091103.070239>
- Thorn CA, Atallah H, Howe M, Graybiel AM (2010) Differential Dynamics of Activity Changes in Dorsolateral and Dorsomedial Striatal Loops during Learning. *Neuron* 66(5):781–795. <https://doi.org/10.1016/j.neuron.2010.04.036>
- Tsutsui-Kimura I, Matsumoto H, Akiti K, Yamada MM, Uchida N, Watabe-Uchida M (2020) Distinct temporal difference error signals in dopamine axons in three regions of the striatum in a decision-making task. *eLife* 9:e62390. <https://doi.org/10.7554/eLife.62390>
- Watabe-Uchida M, Zhu L, Ogawa SK, Vamanrao A, Uchida N (2012) Whole-Brain Mapping of Direct Inputs to Midbrain Dopamine Neurons. *Neuron* 74(5):858–873. <https://doi.org/10.1016/j.neuron.2012.03.017>
- Wei W, Mohebi A, Berke JD (2022) A Spectrum of Time Horizons for Dopamine Signals. 2021.10.31.466705
- Willuhn I, Burgeno LM, Everitt BJ, Phillips PEM (2012) Hierarchical recruitment of phasic dopamine signaling in the striatum during the progression of cocaine use. *PNAS* 109(50):20703–20708. <https://doi.org/10.1073/pnas.1213460109>
- Xu M, Kobets A, Du J-C, Lenington J, Li L, Banasr M, Duman RS, Vaccarino FM, DiLeone RJ, Pittenger C (2015) Targeted ablation of cholinergic interneurons in the dorsolateral striatum produces behavioral manifestations of Tourette syndrome. *PNAS* 112(3):893–898. <https://doi.org/10.1073/pnas.1419533112>
- Yang H, de Jong JW, Tak Y, Peck J, Bateup HS, Lammel S (2018) Nucleus Accumbens Subnuclei Regulate Motivated Behavior via Direct Inhibition and Disinhibition of VTA Dopamine Subpopulations. *Neuron* 97(2):434–449.e4. <https://doi.org/10.1016/j.neuron.2017.12.022>
- Yin HH, Knowlton BJ (2006) The role of the basal ganglia in habit formation. *Nat Rev Neurosci* 7(6):464–476. <https://doi.org/10.1038/nrn1919>
- Yin HH, Knowlton BJ, Balleine BW (2004) Lesions of dorsolateral striatum preserve outcome expectancy but disrupt habit formation in instrumental learning. *European Journal of Neuroscience* 19(1):181–189. <https://doi.org/10.1111/j.1460-9568.2004.03095.x>

- Yin HH, Knowlton BJ, Balleine BW (2005a) Blockade of NMDA receptors in the dorsomedial striatum prevents action–outcome learning in instrumental conditioning. *European Journal of Neuroscience* 22(2):505–512. <https://doi.org/10.1111/j.1460-9568.2005.04219.x>
- Yin HH, Knowlton BJ, Balleine BW (2006) Inactivation of dorsolateral striatum enhances sensitivity to changes in the action–outcome contingency in instrumental conditioning. *Behavioural Brain Research* 166(2):189–196. <https://doi.org/10.1016/j.bbr.2005.07.012>
- Yin HH, Mulcare SP, Hilário MRF, Clouse E, Holloway T, Davis MI, Hansson AC, Lovinger DM, Costa RM (2009) Dynamic reorganization of striatal circuits during the acquisition and consolidation of a skill. *Nature Neuroscience* 12(3):333–341. <https://doi.org/10.1038/nn.2261>
- Yin HH, Ostlund SB, Knowlton BJ, Balleine BW (2005b) The role of the dorsomedial striatum in instrumental conditioning. *European Journal of Neuroscience* 22(2):513–523. <https://doi.org/10.1111/j.1460-9568.2005.04218.x>
- Zingg B, Chou X, Zhang Z, Mesik L, Liang F, Tao HW, Zhang LI (2017) AAV-Mediated Anterograde Transsynaptic Tagging: Mapping Corticocollicular Input-Defined Neural Pathways for Defense Behaviors. *Neuron* 93(1):33–47. <https://doi.org/10.1016/j.neuron.2016.11.045>
- Zingg B, Peng B, Huang J, Tao HW, Zhang LI (2020) Synaptic Specificity and Application of Anterograde Transsynaptic AAV for Probing Neural Circuitry. *J Neurosci* 40(16):3250–3267. <https://doi.org/10.1523/JNEUROSCI.2158-19.2020>

## Short Vita

### Education

- 2023 **Ph.D. in Neuroscience**, Northwestern University, Chicago  
2014 **B.S. in Biomedicine**, Universidade Federal do Rio Grande do Sul, Brazil

### Research

- 2021 **Junior Scientist Workshop on Mechanistic Cognitive Neuroscience**, Janelia Farms  
2017 **Zebrafish Development and Genetics Course**, Marine Biological Laboratory  
2013 **Summer Research Fellow**, École Polytechnique Fédérale de Lausanne  
2012 **Brazil Science Without Borders Fellow**, Case Western Reserve University  
2010 **Psychobiology Summer Course**, Universidade Federal de São Paulo  
2009 **Topics in Comparative Physiology Winter Course**, Universidade de São Paulo  
2008 – 2011 **Research Assistant**, Universidade Federal do Rio Grande do Sul

### Other

- 2019 **Management for Scientists and Engineers**, Kellogg School of Management  
2016 – 2020 **Science Club Mentor**, Pedersen-McCormick Boys & Girls Club  
2011 & 2013 **Science Outreach Fellow**, Universidade Federal do Rio Grande do Sul

### Awards

- 2021 **Houk Scholar Award**, Northwestern University  
2020 – 2022 **T32 Award**, General Motor Control Mechanisms and Disease Training Grant

### First-Author Publications

- 2022 **Ambrosi** and Lerner, Cell Reports (PMID: 35977498)  
2014 **Ambrosi et al**, PLoS Computational Biology (PMID: 25165818)